SNOW G B

SHEAR ZONE HOSTED GOLD MINERALIZATION IN THE MOODIES GROUP AT SHEBA GOLD MINE, BARBERTON GREENSTONE BELT

MSc UP 1991

Shear zone hosted gold mineralization in the Moodies Group at Sheba Gold Mine, Barberton Greenstone Belt.

by

Gary Bruce Snow

Submitted in partial fulfilment of the requirements for the degree of

Master of Science

Faculty of Natural Sciences
University of Pretoria

October 1991

ABSTRACT

The Barberton Sequence of Archaean age rocks exposed at Sheba Gold Mine, Barberton, are amongst the oldest auriferous rocks in the world. Rocks of the Onverwacht, Figtree and Moodies Groups outcrop with the mine claims area, while the study area consists entirely of meta-arkoses of the Clutha Formation, Moodies Group. Gold mineralization within this group of rocks is restricted to narrow shear zones, where it is hosted by both arsenopyrite and pyrite mineralization. Several ages of both pyrite and arsenopyrite mineralization exist within each shear zone.

Individual shear zones are characterized by a strongly developed sericitic cleavage, which strikes parallel to bedding within the meta-arkose, but dips steeply to the north while bedding dips steeply south. Several ages of quartz and quartz-carbonate veins occur within the shear zone. These veins are highly sheared and boudinaged, indicative of post emplacement shearing and extension along the shear zone.

Kinematic indicators from the Mamba Shear Zone, which include bedding rotation due to shearing, and lineation plunges on shear planes, identify the deformation to be dominated by a dip-slip movement component, with a reverse sense of motion. The deformation style is consistent with that of a brittle-ductile shear environment.

The Mamba Shear Zone has undergone hydrothermal alteration which has been dominated by the breakdown of feldspar to sericite, and an enrichment in silica, arsenic and gold within the shear zones. Elevated gold values and sulphide concentrations in association with tourmaline mineralization, suggests a granitic fluid influence in the shear zones. These zones of tourmaline occurrence exhibit minor deformation only, suggesting emplacement at a late stage into the shear zones.

The Eureka and Cat's Cave Shear Zones exhibit similar deformation environments, movement directions, mineralization styles and hydrothermal alteration to that seen in the Mamba Shear Zone. From this evidence it is concluded that the Eureka, Mamba and Cat's Cave Shear Zones form a north dipping thrust imbricate stack.

This thrust imbricate is bounded to the south by the south dipping Sheba fault, which exhibits a north-westerly directed thrust sense of movement, and is clearly the dominant structure within the study area. To accommodate the Eureka, Mamba and Cat's Cave thrust imbricate pile within the north-westerly directed thrust environment, they are interpreted as back thrusts in the footwall of the Sheba Fault Zone.

OPSOMMING

Die Barberton Opeenvolging van Argeiese gesteentes, blootgele in die Sheba Goudmyn, Barberton, is van die oudste gouddraende gesteentes in die wereld. Gesteentes van die Onverwacht, Fig Tree en Moodies Groepe dagsoom in die Sheba Myn-kleimarea, maar die studie gebied bestaan heeltemal uit meta-arkose van die Clutha Formasie, Moodies Groep. Goudmineralisasie in hierdie gesteentegroep is beperk tot nou skuifskeursones, waar dit saam met arsenopiriet- en pirietmineralisasie voorkom. Verskeie ouderdomme van beide piriet- en arsenopirietmineralisasie bestaan in elke skuifskeursone.

Individuele skuifskeursones word gekenmerk deur 'n goed ontwikkelde serisitiese kliewing, parallel aan die strekking van die gelaagdheid van die meta-arkoos, maar wat steil na die noorde hel terwyl die gelaagdheid steil suid hel. Verskeie ouderdomme kwarts- en kwartskarbonaatare kom in die skuifskeursone voor. Hierdie are vertoon 'n hoe mate van skuifskeuring en "boudinage", wat skuifskeuring en verlenging langs die skuifskeursone na inplasing aandui.

Kinematiese aanwysers van die Mamba-skuifskeursone, ingeslote mineraalverlengingslineasies en die rotasie van gelaagdheid, dui aan dat die deformasie gedomineer is deur 'n hellingsglipbewegingsrigting, met 'n opwaartse bewegingssin. Die deformasiestyl is in ooreenstemming met 'n bros-buigbare skuifskeuromgewing.

Die Mamba-skuifskeursone het hidrotermale verandering ondergaan wat gedomineer is deur die afbreek van veldspaat na serisiet en 'n verryking in silika, arseen en goud. Plaaslik bevat die skuifskeursone verhoogde goudwaardes en sulfiedkonsentrasies geassosieerd met toermalynmineralisasie, wat moontlik die invloed van 'n granitiese vloeistof aandui. Die sones met toermalynvoorkomste toon slegs geringe deformasie, wat moontlik 'n laat stadium van inplasing van toermalyn in die skuifskeursones aandui.

Die Eureka- en Cat's Cave-skuifskeursones vertoon soortgelyke deformasieomgewings, bewegingsrigtings, mineralisasiestyl en

hidrotermale veranderings as die Mamba-skuifskeursone. Hieruit word afgelei dat die Eureka-, Mamba- en Cat's Cave-skuifskeursones 'n noordhellende geskubbe oorskuiwingsone vorm.

Die oorskuiwingskubsone word in die suide begrens deur die suidhellende Sheba-verskuiwingsone, wat 'n noordwestelik gerigte stootbeweging vertoon en duidelik die dominante struktuur in die studiegebied is. Om die Eureka-, Mamba- en Cat's Caveoorskuiwingskubbe in die noordwestelik-gerigte stootverskuiwingomgewing te akkommodeer, word hulle geinterpreteer as terugwaartse stootverskuiwings in die vloer van die Sheba-verskuiwingsone.

CONTENTS

CHAPTER 4

MINERALOGY AND ORE MICROSCOPY

CHAPTER 5

GEOCHEMISTRY OF THE MAMBA SHEAR ZONE

List of Figures

List of Plates

List of Tables

List of Maps

[All maps displayed in back cover]

CHAPTER 1

INTRODUCTION

1.1 Locality of Study Area

The Barberton Sequence of Archaean supracrustal remnants crop out in a roughly tabular north-east to south-westerly orientated pattern (the Barberton Belt), on the eastern edge of the Kaapvaal Craton south-eastern Transvaal, South Africa (Figure 1). The rocks of the Barberton Sequence are characterized by a low grade of metamorphism combined with a complex tectonic history. Some of the rocks have a marked positive weathering profile which has resulted in the formation of a rugged and often spectacular topography. The study area is located within the outcrop of Moodies Group sediments (Barberton Sequence), within the Sheba Gold Mine claims area, approximately 14km north-east of Barberton (Figure 1).

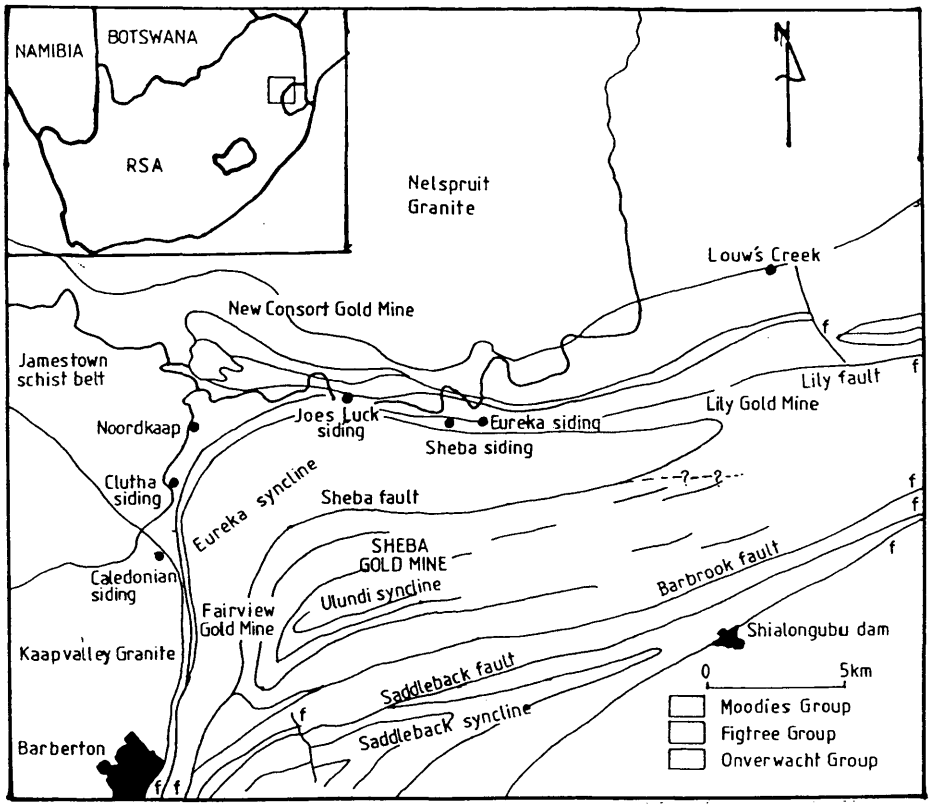

Figure 1. The surface outcrop of a portion of the Barberton Sequence (after Anhaeusser, 1979).

1.2 Aim and Methods

The principal aim of the present study was to document, primarily by detailed mapping, the geology and geometry of auriferous structures within the clastic sediments of the Moodies Group, in the Sheba Mine area. The geology in the Sheba Gold Mine area is dominated by the presence of two large synclines in an apparent "back-to-back" relationship, namely the Eureka and Ulundi synclines (Figure 1). The two synclines are separated by the Sheba Fault Zone (Figure 1) which is arcuate and dips both south and south-east. The southern limb of the Eureka Syncline has been overturned. All structures investigated lie in the footwall of the Sheba Fault zone. Particular attention was paid to the structural settings of gold-associated sulphide minerals and the deformation style (brittle or ductile) of these settings. In this way it was hoped to gain insight into the structural controls, if any, on gold mineralisation within the Sheba Mine area. Based on these observations an attempt was then made to place the Sheba structures into a local and regional deformation model, and hence predict potential new areas of mineralisation.

The initial approach was to consult the literature, in particular internal reports written over the last fifty years. In addition to the internal reports, attention was also paid to papers and theses published on the north-western portion of the mountainland (Anhaeusser, 1969, 1976b; Ramsay, 1963; Robertson, 1989; Roering, 1965; Schouwstra, 1988; Steyn, 1976). The literature study was followed by reconnaissance investigations in the Eureka, Mamba, Margaret, and Cat's Cave workings (Figure 2).

The reconnaissance survey indicated that detailed mapping would be restricted to 1 and 6 levels at Eureka, and 10 and 11 levels Mamba. The Margaret shears were completely inaccessible, while the Cat's Cave shear had only limited access.

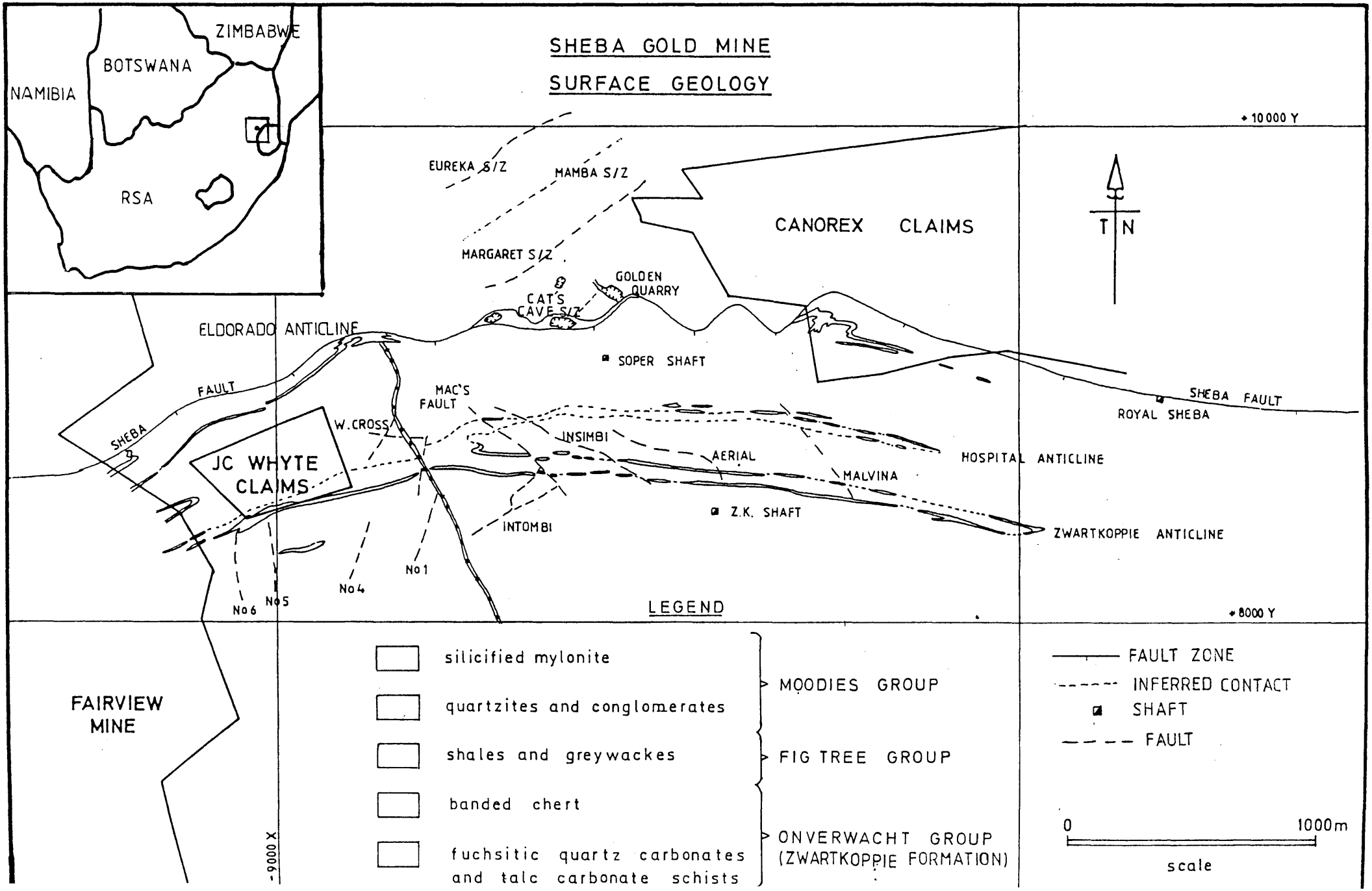

Within the Mamba and Eureka Shear Zones mapping was conducted at a scale of 1:200, and all sites were offset to exactly 1 metre above footwall elevation, by making use of existing and additional survey pegs.

In addition to the mapping exercise, a mineralogical and geochemical study of a mineralized and unmineralized shear zone was conducted. In the mineralogical study use was made of X-ray diffraction techniques and conventional transmitted and reflected light microscopy to identify mineral phases as well as textural and alteration features associated with the host and shear zone rocks. The samples for the geochemical study were taken from diamond drill core and analysed by X-ray fluorescence spectroscopy. The aim of the geochemical study was to investigate if the whole rock geochemistry could be used as a guide to mineralisation. The absolute values obtained from this process were handled by means of the "isocon method" proposed by Grant (1986), and discussed in detail in Chapter 5.

Gold mineralisation within the Barberton Sequence supracrustal remnants has long been recognized to be closely associated with major strike-persistent faults, of which the Sheba Fault is one. In view of this, several sites along the Sheba Fault were investigated with the aim of identifying the deformation styles at these sites and incorporating them into a larger regional model for the north-western portion of the Barberton supracrustal remnant.

1.3 Previous Work

In view of both their importance to models dealing with early crustal evolution and their economic potential, Precambrian supracrustal remnants have long been the subject of intense research worldwide. Archaean supracrustal remnants (greenstone belts and cratonic basin successions older than 2 500 Ma), because of their close association with gold mineralisation, have been particularly well studied.

The Barberton supracrustal sequence is amongst the oldest and largest of these remnants, and is considered by many researchers to be a classic example of a "greenstone-type" Archaean supracrustal remnant. Unlike many other remnants the Barberton Sequence (SACS, 1980) contains volumetrically significant amounts of clastic sediments, as well as the thick mafic successions recognised elsewhere in the world. The low grade of metamorphism throughout the area has resulted in the preservation of numerous primary igneous as well as sedimentary textures, making the area ideal for research.

Unique elements of the research history will be dealt with in the following chapters. However, a brief overview is appropriate at this stage. The earliest documentation of the geology of the Barberton area is by Schenk in 1888. Between the period 1888 to the early 1960's all descriptions of the geology of the Barberton supracrustal remnant were dominated by lithological descriptions and attempts at stratigraphic classification. During the period 1960 to 1980 the emphasis of the research changed considerably, with the first decisive attempts at a structural interpretation of the mountainland being made. These efforts were dominated by Ramsay (1963), Anhaeusser (1965, 1969), and Roering (1965). The result of these studies was the proposal of a four-event deformational history for the mountainland. During the same period considerable research was also conducted into the granitic-gneissic terranes surrounding the supracrustal remnant, as well as into the genesis of the ultramafic component of the remnant, this line of research being dominated by Robb (1977 a, b) and Viljoen and Viljoen (1969 a, b; 1979). The result of work during this period was a genetic model for the formation of the mountainland based on gravity induced tectonism intimately related to granite emplacement.

The post-1980 research period has been characterised by a spate of papers dealing with the ages of the various units within the mountainland (de Wit, 1981; Kroner and Compston, 1988; Kroner and Todt, 1988; Kroner et al.,

1989), and the mechanism responsible for the preserved deformation history. De Wit has successfully shown the deformation in the southern portion of the mountainland to be dominated by crustal shortening processes related to horizontal tectonics, a possibility which, to date, has not been documented for the northern mountainland. During this research period several small scale studies were also conducted with an economic bias, particularly in the Sheba Gold Mine area. Schouwstra (1988) reported the existence of a structurally controlled hydrothermal orebody at the Main Reef Complex (Sheba Gold Mine), while Robertson (1989) related the deformation features there to a regional strike-slip system.

CHAPTER 2

STRATIGRAPHY

2.1 Historical Development

The first reference to "Swaziland" age rocks in the Barberton area is by Schenk (1888), a mere six years after the discovery of gold in the area. Schenk (1888) proposed the name "Swasischichten" for these remnants and grouped them with the "Sudafrikanische Primarformation" (SACS, 1980). This early classification was followed by the "Barberton-formatie" or "oude lei-formatie" of Molengraaf (1898), which held favour until the term Swaziland System was introduced by Hatch and Corstorphine in 1905 (in SACS, 1980).

The first formal classification of the Swaziland supracrustal sequence was by Hall (1918). Hall recognised the existence of 3 major units in the area, namely (1) the Jamestown Series, (2) the Moodies Series, and (3) the Onverwacht Volcanic Series. He also recognised the existence of basic intrusions into the Moodies Series, which he grouped with the Jamestown Series, as well as the existence of an "older granite", which was subdivided into a younger Nelspruit type and an older De Kaapvalley type.

During the period 1937-1948, the Barberton Mountain Land was remapped by the Geological Survey of South Africa. In the subsequent memoir van Eeden (1941), quoted in S.A.C.S. (1980), suggested that the Moodies Sequence could be subdivided into a lower Fig Tree Series and an upper Moodies Series on the basis of the existence of an unconformable contact between the two. A further subdivision occurred when Truter (1950) and Visser et al., (1956) suggested that the Swaziland System comprised a lower Onverwacht Series and a conformably overlying Fig Tree Series, with the Moodies Series being a separate entity. This exclusion of the Moodies Series from the Swaziland Sequence was not accepted by either the Geological Survey of Swaziland, or the majority of post-1959 researchers.

Table 1. Lithostratigraphy Of The Barberton Sequence (after SACS, 1980).

Group	Subgroup	Formation	Bed	Informal Unit	Description	Thickness	Dated Field	Age (Ma)
		Baviaanskop			Sandstones, grits, conglomerates, shales, subgreywackes, sandstone, grits, conglomerate, quartzite, phyllites	685		
MOODIES		Joe's Luck			Shales, subgreywackes, sandstone, quartzite, phyllites, jaspilites, ferruginous shales, basaltic lavas.	740		
		Clutha			Shales, quartzites, conglomerates, jaspilites.	1600	Single zircon	3570
		?			Trachytic tuffs, agglomerates, lavas, tuffaceous greywackes and greywacke conglomerates.	550	Shale	3460
FIG TREE		Belvue Road		Ulundi Bar	Siltstone, shale and subordinate greywackes with banded ferruginous cherts and a trachytic tuff	600	Shale	
		Sheba	Granville Grove Oolite		Greywackes with some shales and interlayers of chert and ferruginous chert	1000	Shale	2980
		Zwart-koppie			Felsic volcanics and interlayered chert	915 900	Acid volcanics	3360 3340
	Geluk	Kromberg			Mafic and felsitic lavas, pyroclastics and agglomerates Banded chert and carbonate rocks, mainly metamorphosed	1920 1900		3290
		Hoogge-noeg		Middle marker	Mafic and felsic and pyroclastics. Banded cherts. Mainly metamorphosed	4850		3355
		Komati			Mafic and ultramafic komatiites, lavas, chert, metamorphosed		Middle marker Single zircon	3350 3450
	Tjakastad	Theespruit			Mafic and subordinate ultramafic lavas and felsic tuffs, schists, carbonaceous cherts, mainly metamorphosed	1890 1900	Whole rock	3430 3560 3510
		Sandspruit			Ultramafic and subordinate mafic lavas, mainly metamorphosed	2130 2100		

Allsopp et al. (1968)
de Witt et al. (1987)

Ramsay (1963) in his study of the Sheba Gold Mine area, proposed a two-fold classification of the stratigraphy based on structural relationships. The lower division comprises the Onverwacht Series and the upper division the Fig Tree and Moodies series. Steyn (1976) further refined the stratigraphy when he recognized an unconformable contact between the Fig Tree Series and the underlying Onverwacht Series, in the Steynsdorp and Fairview areas. From this age relationship Steyn (1976), Truswell (1967), Viljoen and Viljoen (1969a), and Anhaeusser (1975) all concluded that the Swaziland succession should comprise rocks of the Onverwacht, Fig Tree, and Moodies series.

The Swaziland succession in the Barberton area has since been defined by SACS (1980) to be of sequence rank, and is called the Barberton Sequence, comprising the Onverwacht, Fig Tree, and Moodies Groups. The lithostratigraphy of the sequence is summarised in Table 1 and the surface outcrop in Figure 1. For detailed descriptions of the lithostratigraphic units comprising this sequence the reader is referred to SACS (1980) and the references therein.

The granitoid rocks associated with the supracrustal rocks together with their currently accepted ages are listed in Table 2.

2.2 Stratigraphic Considerations

Although traditionally regarded as structurally simple features, recent research (Barley et al., 1989; Groves et al., 1988; Harris, 1987; Nesbitt, 1988) has shown greenstone sequences to be characterised by complex tectonic histories. Major fault or shear zone systems are common in most sequences and although locally conformable they typically crosscut stratigraphy on a regional scale. Displacements on these shear systems are both horizontal and vertical and often polyphase. The overall result is that stratigraphy within greenstone sequences is both locally and regionally eliminated or duplicated (Figure 3). Figure 3a illustrates the elimination of stratigraphy due to extensional (normal) faulting (cf. profiles 1 and 2) and Figure 3b duplication of stratigraphy as a result of contractional (reverse) faulting (cf.profile 3 and 4). Figures 3c and 3d illustrate complication due to local reverse (3c)

and normal (3d) faulting in the overlap zones between en echelon strike slip faults.

Table 2. Intrusives into the Barberton Sequence (after SACS, 1980).

Intrusives	Age (Ma)	Remarks
Ushushwana Complex	2874	Intrusive into the Lochiel gneisses and migmatites.
Young Plutons	2875	
Mpangeni Granite	2810	
Salisbury Kop Granodiorite	3060	
Dalmein Granodiorite	3290	
Bosmanskop Syenite	3130	
Lochiel gneisses and migmatites	3075	Granitoid rocks of various ages, intrusive into the Barberton Sequence
Nelspruit gneisses and migmatites	3075	
Tonalitic Diapiric Plutons	3170	
Lekkerloop gneisses and migmatites	3220	
Nelshoogte tonalitic gneisses	3310	
Kaap Valley tonalitic gneiss	3223	

de Wit et al. (1987)
Oosthuizen (1976)

Large scale regional structures have long been recognized in the Barberton supracrustal remnant (Hall, 1918; van Eeden, 1941; Hearn, 1943; Visser et al., 1956; Ramsay, 1963; Anhaeusser, 1965; Anhaeusser and Viljoen, 1965; Roering, 1965; Viljoen and Viljoen, 1979; Williams and Furnell, 1979; de Wit, 1981; Anhaeusser, 1986; Wagener and Wiegand, 1986). The effect these large scale structures have had on the classical stratigraphy has, however, largely been ignored. Notable exceptions are Williams and Furnell (1979), de Wit (1981), and de Wit et al., (1987). Williams and Furnell (1979) drew attention to the presence of "wrench" faulting in the Onverwacht Group type-section, and suggested that sections of the Komati and Hooggenoeg Formations are not represented in the section (effectively tectonic thinning due to strike-slip faulting). De Wit (1981) identified a period of thrusting responsible for

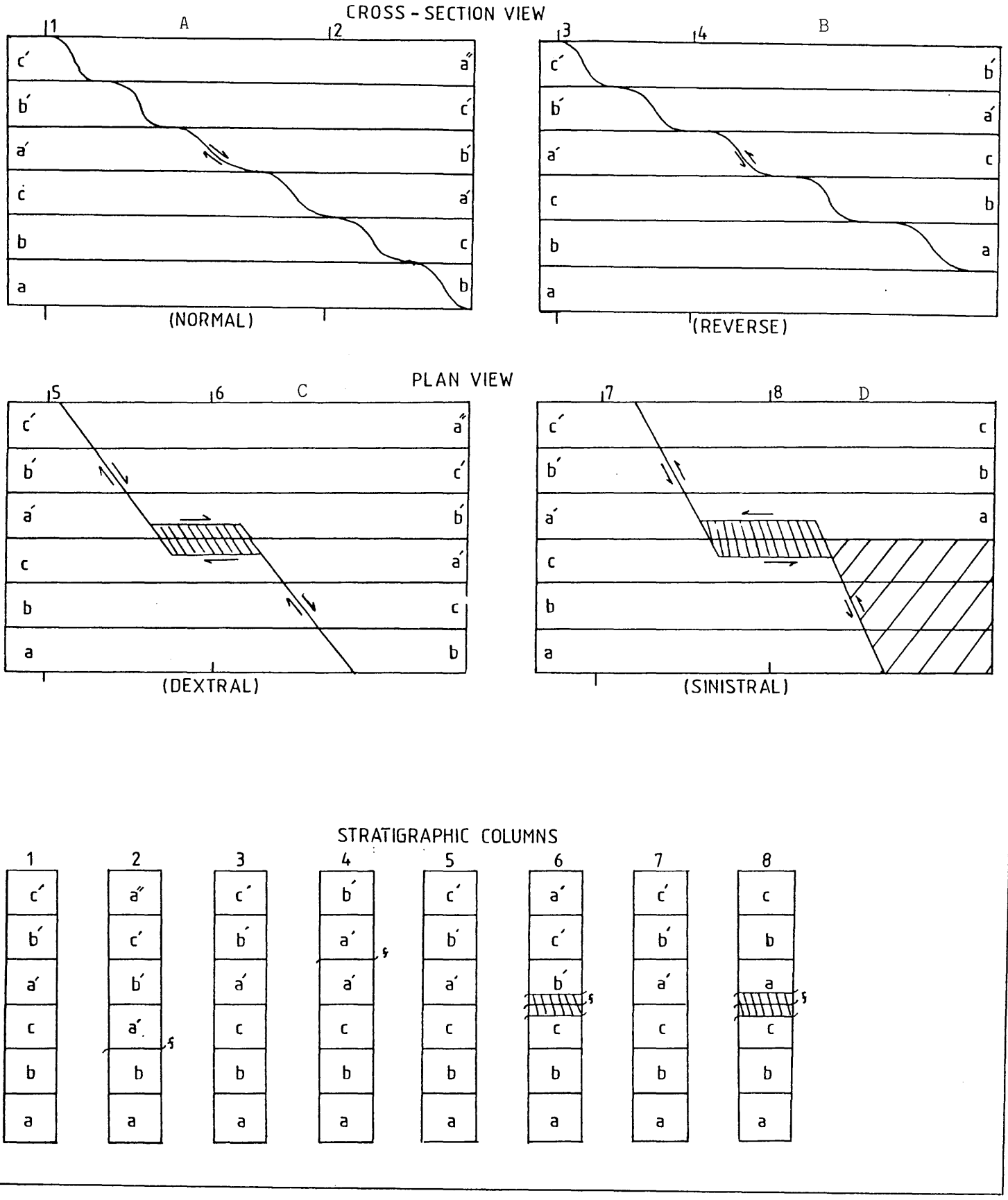

Figure 3. The effect of faulting on stratigraphy (a=normal faulting; b=reverse faulting; c=normal faulting with compression zone; d=reverse faulting with extension zone).

horizontal shortening in excess of 80%, which had previously been attributed to stratigraphic thinning by Viljoen and Viljoen (1969b). Although both the examples cited were from research in the southern part of the Barberton supracrustal remnant, they are important considerations as there is abundant evidence for vertical and horizontal tectonism in the northern areas as well (Anhaeusser, 1976; Ramsay, 1963; Fripp et al., 1980; H.G.Philpot pers. comm., 1989; Robertson, 1989). Additional evidence for horizontal shortening will be presented in this thesis, which further emphasizes the lack of an accurate stratigraphy. As suggested by Ramsay (1963) any description of the stratigraphy of the Barberton Sequence would best be achieved by considering it in terms of a tectonostratigraphy rather than a lithostratigraphy.

CHAPTER 3

STRUCTURAL GEOLOGY

3.1 Structures in the Moodies Group

i) The Mamba Shear Zone

a) Introduction

The Mamba Shear Zone is located immediately south of the Eureka Shear Zone (Figure 2) and forms part of the Margaret Section. The Mamba Shear Zone is locally referred to simply as Margaret. The exact date of commencement of mining activities on the Mamba Shear Zone is not known, although it probably coincided with or followed shortly after the discovery of the Golden Quarry shoot in 1884.

No figures exist as to the exact tonnages or grades mined from the individual shears within the Margaret Section, but the section as a whole has yielded approximately 250 000 tonnes of rock from an average stope width of 1.1 metres, and at an average grade of 6.4 grams gold per tonne. This has resulted in the production of approximately 1 592 kilograms of gold.

Prior to this study no detailed geological work had been conducted in the Margaret Section.

b) Geology of the Mamba Shear Zone

The Mamba Shear Zone strikes 035^{o} and dips between 70-80^{o} north, has a strike persistence in excess of 250 metres, and can be traced downdip for 11 levels (approximately 350 metres). The shear

zone is developed in meta-arkoses of the Clutha Formation, Moodies Group and is macroscopically defined by concentrations of sericite (foliation) related to localised high strain. This foliation dips $77^{o}/335^{o}$ (Figure 4) and is inclined at a low angle to bedding. Bedding dips at 71^{o} to 151^{o} (Figure 5) and youngs north.

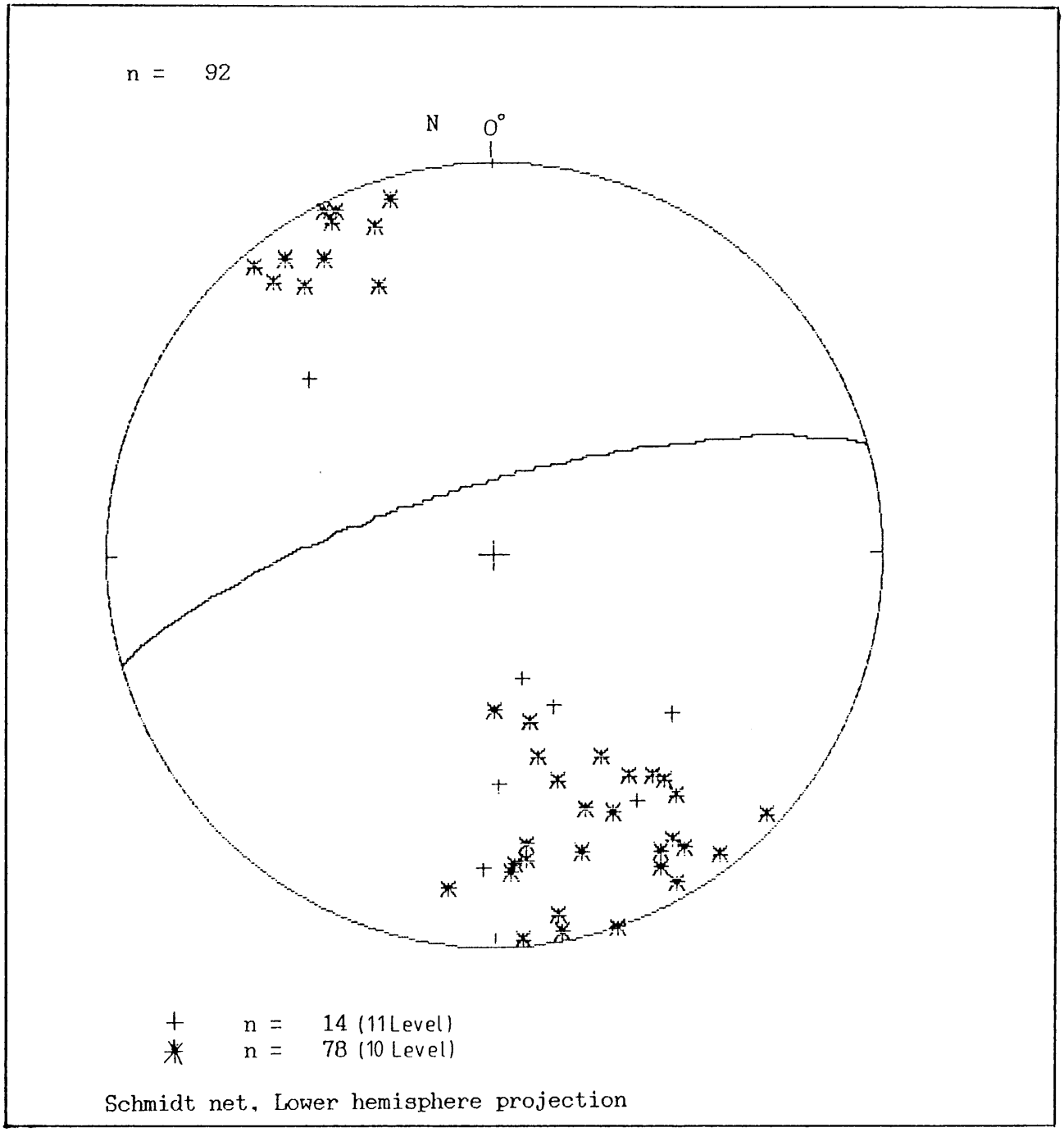

Figure 4. Stereographic projection of poles to shear planes in the Mamba Shear Zone (average plane is $75^{o}/335^{o}$).

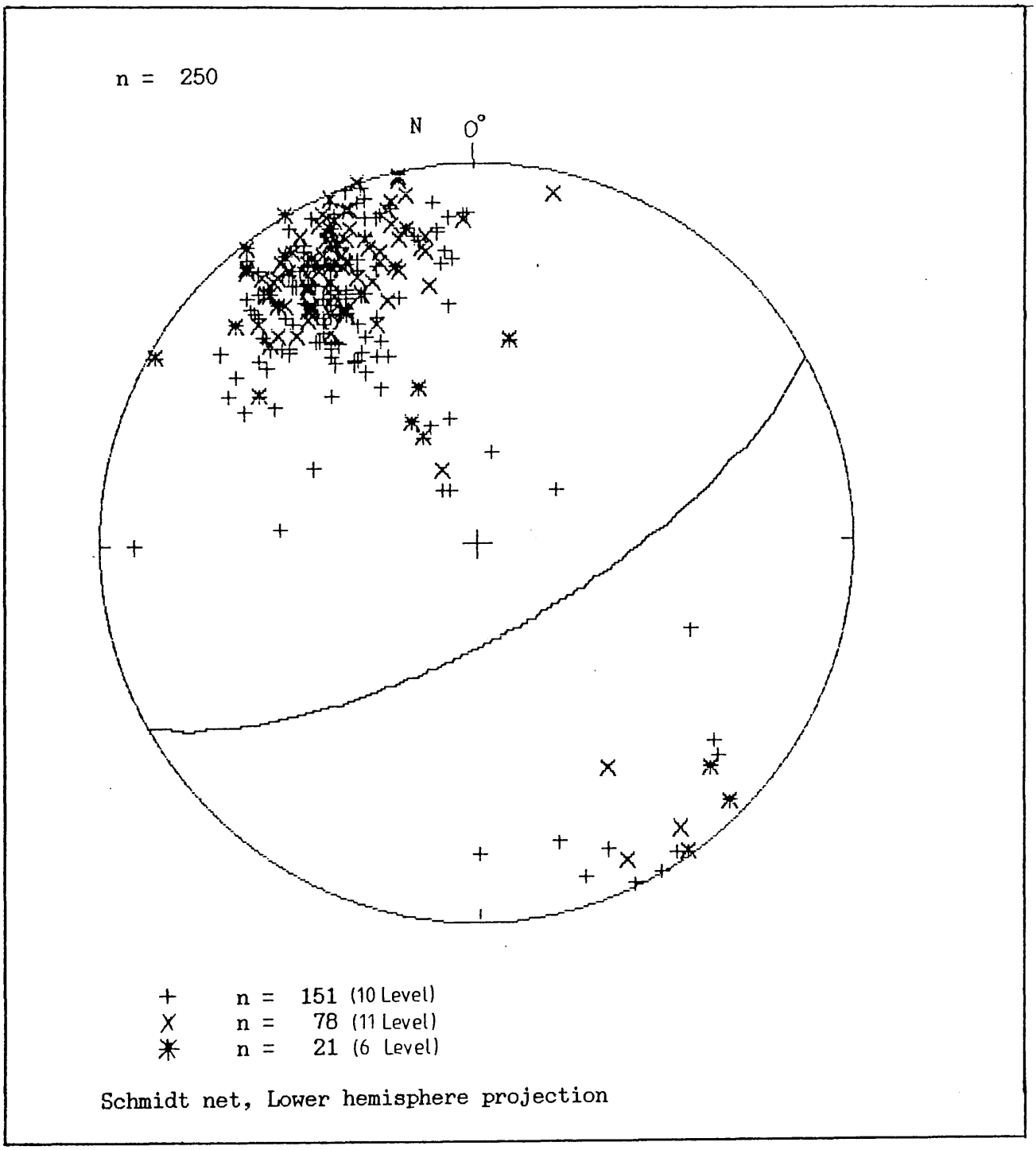

Figure 5. Stereographic projection of poles to bedding in the Mamba Shear Zone (average plane is $70^{o}/151^{o}$).

The concentration of sericitic shears increases toward an approximately central quartz vein, as does the concentration of sulphide minerals, silicification and carbonatization. Discrete satellite shears of short strike length also occur.

The central quartz vein shows considerable variation in width and persistence parallel to both dip and strike. The maximum thickness is in the order of 20cm. This central quartz vein has historically been the target for mining activities although it is now clear that the major portion of the mineralisation is in fact hosted by the encompassing shear zones and/or discrete, highly deformed quartz and quartz-carbonate veins within the shear zones. The central quartz vein at Mamba locally crosscuts the sericitic fabric at very shallow angles, but has a dominantly sub-parallel orientation. The crosscutting nature of the central quartz vein is particularly evident from the formation of kindred structures (Price and Hancock, 1972) off the main quartz vein which cut the fabric at a steep angle (Figure 6). These kindred structures have a similar composition to the main quartz vein and are considered to have formed simultaneously. The kindred structures are themselves cut by sericitic shears, sub-parallel to the central quartz vein and the older sericitic fabric. There is only minor displacement along these younger sericitic shears.

In addition to the main quartz vein, several earlier quartz and quartz-carbonate vein arrays are present in the Mamba shears, and are discussed below (Chapter 3, Section c).

The shear zones anastomose along strike (Maps 1 and 2), while in cross section they bifurcate up dip. Evidence of this bifurcation is the presence of two shears on 11 Level Mamba (Map 1) which can be followed up dip into four shears on 10 Level (Map

2). The point of bifurcation is subtle and is best recognized by a marked change in dip (either steepening or flattening), which returns to the original orientation after bifurcation. A further indication of the point of bifurcation is the presence of above average arsenopyrite concentrations. Bedding planes are rotated into the shear zones and alter from a south dipping orientation to sub-vertical or even north dipping (Figure 7; Plate 1). The "drag" on bedding clearly indicates a reverse sense of movement on the Mamba shear zone, i.e. north block up.

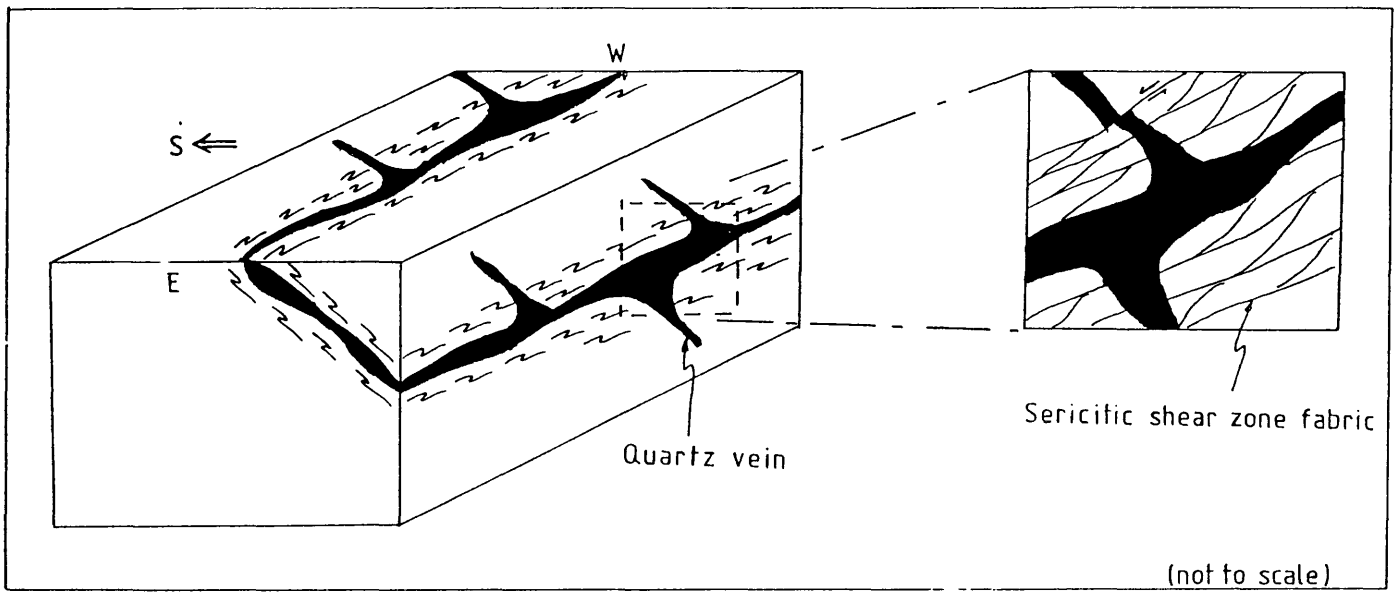

Figure 6. The formation of kindred structures within a shear zone, Mamba Shear Zone. (Shearing is syn-, pre- and post-kindred formation).

The central quartz vein terminates along strike by either boudinaging, horsetailing or hydraulically brecciating the host rock. Reworking of the hydraulically brecciated fragments is minimal with individual fragments being easily matched. Both the breccia and the host rock may themselves be hydraulically brecciated by a late intrusive calcite phase (Plate 2), which strikes and dips parallel to the shear zone.

This brecciation again shows little evidence of reworking.

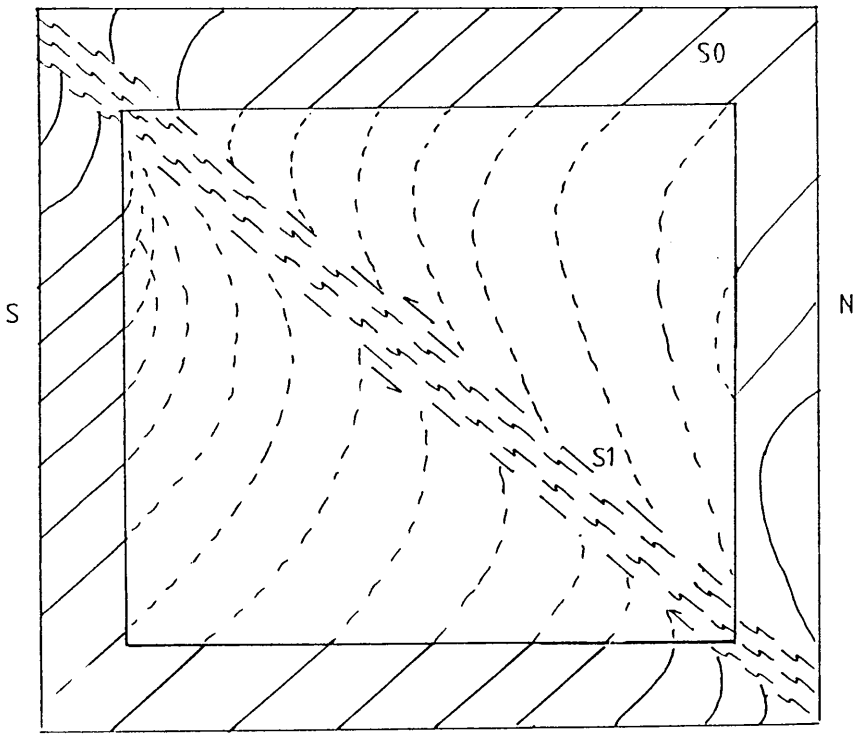

Figure 7. The rotation of bedding due to shear zone deformation (S0=bedding, S1=shear zone foliation).

In addition to the dominant east-west shear orientation, there is a late north-south striking fault event, which dips steeply to the west. Faults of this age are marked by a 2-3cm gouge and an S-C-like fabric development (Lister and Snoke, 1984), and display dextral displacements in the order of 5 to 10 metres. These faults clearly cut all previous vein and shear orientations. It was not possible to determine a vertical displacement component on these structures.

c) Vein Ages and Relationships

The microscopic investigation of the Mamba Shear Zone revealed the existence of at least nine different quartz, quartz-carbonate, or Fe-oxide vein ages. Distinction between the various vein ages was achieved by making use of such features as

Plate 1. Shear zone drag on bedding, Mamba Shear Zone looking west (Shear dips from top left corner to bottom right corner).

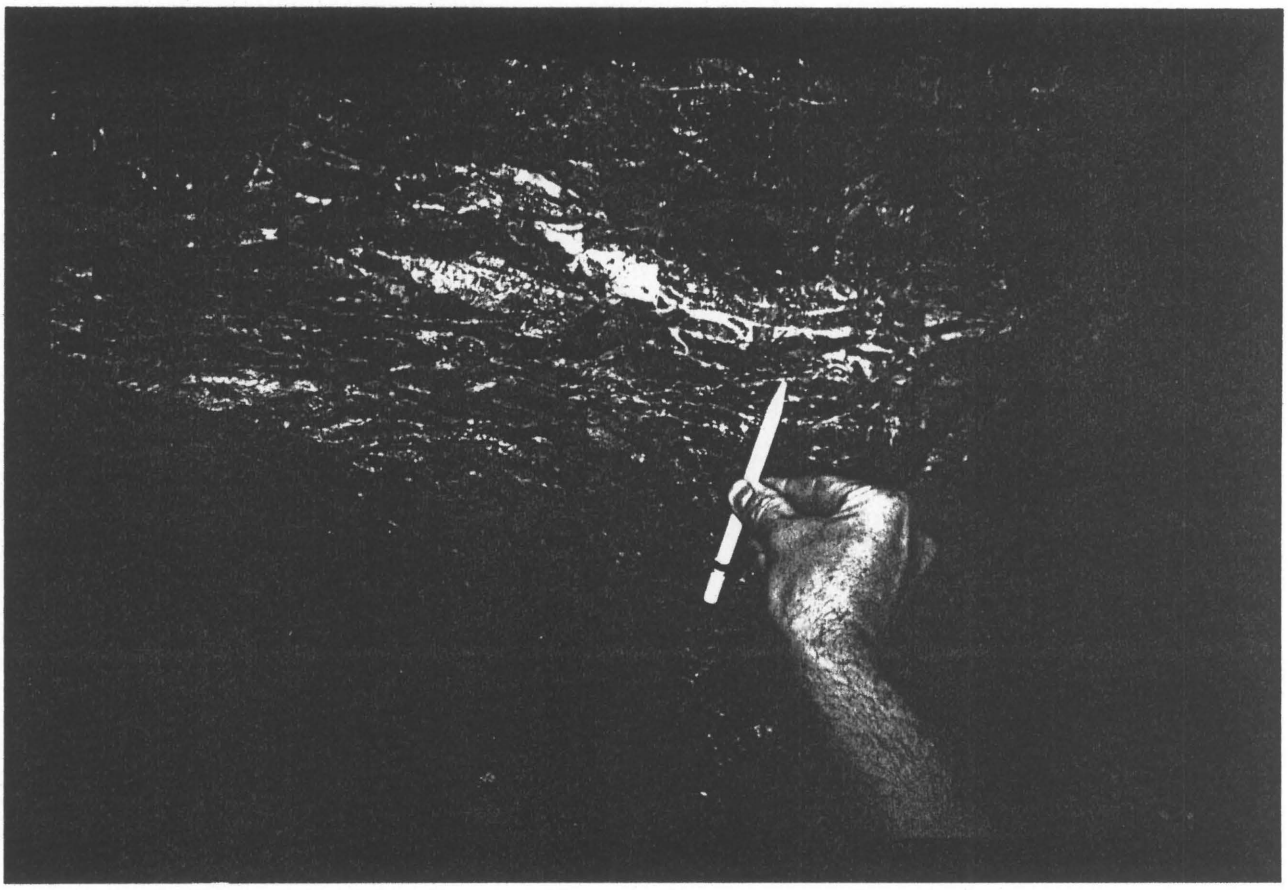

Plate 2. Calcite fill in late stage breccia, Mamba Shear Zone (11 level Mamba Shear Zone; peg 6563).

associated minerals, the dominant mineral/s present, the presence or absence of sulphide minerals, crosscutting relationships, and their relationship to the encompassing shear zone fabric (Haynes, 1987). In all cases the veins or vein remnants are orientated parallel to the sericitic fabric, or are crosscut by the fabric at a shallow angle.

The various veins are presented in order of decreasing age in Table 3. It should be noted that from vein age 5-8 no conclusive age relationships could be established. The iron oxide veins (vein age 9) crosscut both the pre-existing fabric and all other vein remnants, and are clearly late (i.e. post mineralization).

ii) The Eureka Shear Zone

a) Introduction

The Eureka Shear Zone (Figure 2) is the most northerly shear zone presently being worked at Sheba Gold Mine. Historical records of production from this shear zone are non-existent. However, from current mining activities an average grade of 5 g/t can be assumed. At the time of mapping this area only two of the three existing levels were accessible, viz. 1 and 6 levels. Although the lowest level is called 6 Level it is in fact the third working level in the mine. The spacing between levels is in the order of 37 to 40m vertically. All three levels are now accessed by adits, although until recently the 2 Level Adit was collapsed. Mining operations are assumed to have commenced in the same general period as the rest of the Margaret Section, which was probably around 1886.

b) Geology of the Eureka Shear Zone

Mapping of the Eureka Shear Zone was conducted at a scale of 1:200 and is presented on Map 3. The shear zone is characterized by the presence of an approximately central quartz vein hosted by a 1-1.5 metre thick sericitic ductile shear zone. The central quartz vein is dominantly dark in colour but may be altered to a lighter quartz locally (Plate 3). The quartz vein along with its host sericitic shear zone dips north at between 60° and 75 and strikes 050° (Figure 8). The host rock is dominantly quartzite and has been correlated with the Clutha Formation.

Table 3. Microscopic characteristics and relative vein ages of veins from the Mamba Shear Zone (sizes are relative to each other).

Vein Age	*Characteristics*	*Comments*
1	Small crystal size quartz veins Transposed & sheared Remnants only	Cross-cuts and cut by fabric
2	Small crystal size quartz veins Opaque rich	Cross-cuts and cut by fabric
3	Large crystal size quartz veins Opaque rich selvages Large euhedral pyrite crystals	Cross-cuts and cut by fabric
4	Quartz-carbonate veins Dolomitic-like growths Minor opaque minerals	Cross-cuts and cut by fabric Intense carbonate alteration
5	Large crystal size quartz veins Intense brecciation No opaque minerals	Cross-cuts and cut by fabric
6	Carbonate veins Minor opaque minerals	
7	Sulphide veins Tourmaline bearing	
8	Sulphide veins Tourmaline absent	
9	Iron-oxide veins	Cross-cut all other structures and pre-existing alteration

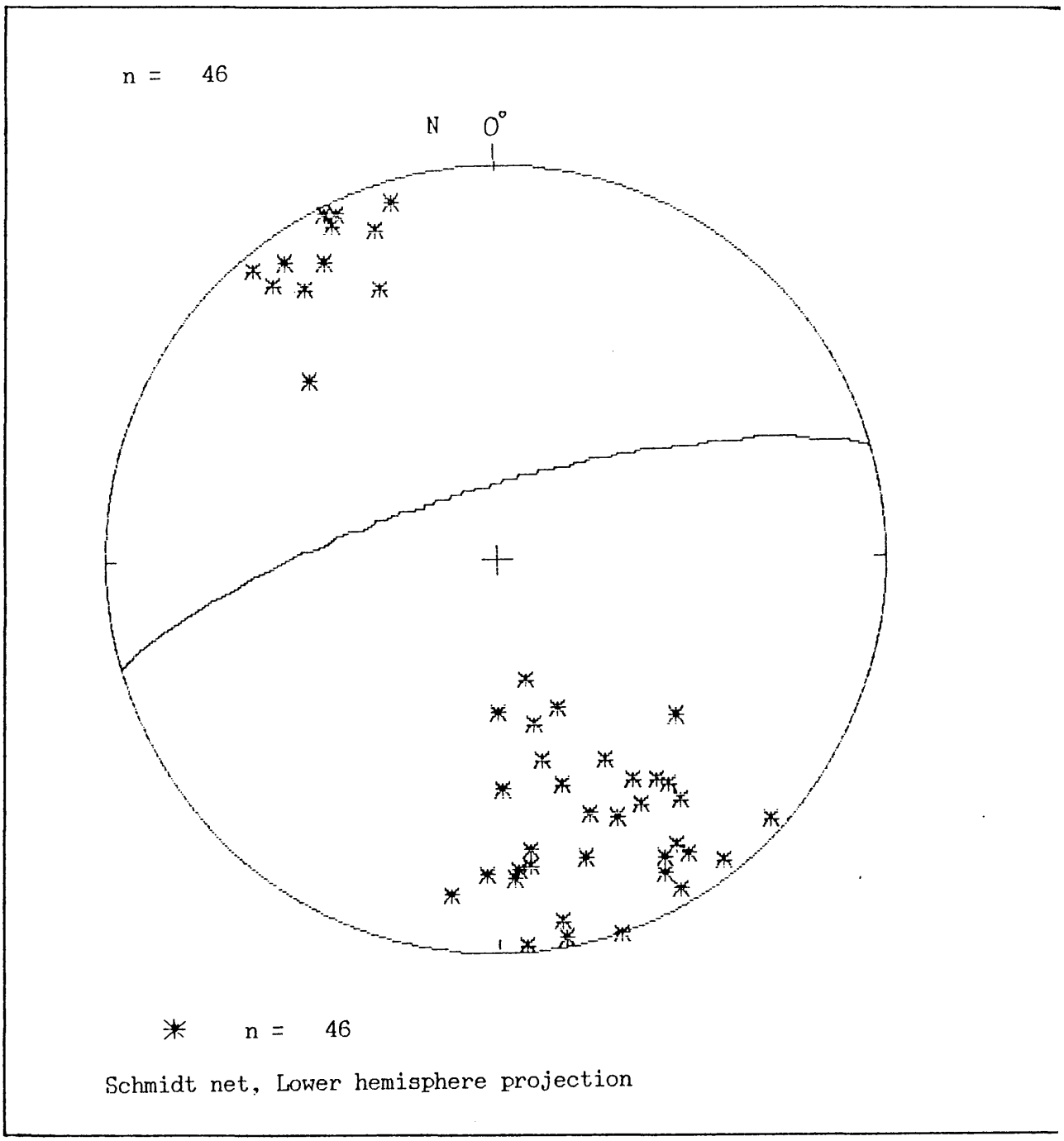

Figure 8. Stereographic projection of poles to shear fabric for the Eureka Shear Zone (average plane is $57^{o}/321^{o}$).

The shear zone is defined by the presence of discontinuous sericitic shears planes, sericitic shear bands, and transposed and sheared quartz veins. These features are regarded as evidence for deformation due

to simple shear under ductile conditions. The shear zone is seldom wider than 1 metre and may thin to a few millimetres. The dominant movement within the shear zone appears to have been dip-slip and reverse, as evidenced by the drag on bedding, with a minor dextral component. No attempt was made to quantify the displacement on this thrust zone. The horizontal movement component was identified from the rotation of bedding (Map 3) as well as from the orientation of quartz vein remnants, i.e. the vein remnants are assumed to have rotated into parallelism with the local movement direction. The central quartz vein at Eureka varies in thickness from less than 1cm up to 15cm, and has a highly irregular shape along strike. This irregular strike persistence is attributed to post-emplacement shearing along the host shear zone resulting in boudinaging of the quartz vein.

These lens shaped boudins have an irregular up and downdip persistence, which is ascribed to the thrusting event. Several ages of thin (less than 3mm) quartz and quartz-carbonate veins characterize both the shear zone and the adjacent quartzites. Within the shear zone these veins are arranged sub-parallel to the shear zone fabric, while equivalent veins outside the shear zone appear to be irregular in orientation. This orientation of veins within the shear zone is attributed to progressive rotation of the quartz veins into parallelism with the principal direction of shear (Figure 9). Age relationships between veins and sericitic fabric within the shear zone are confused.

Individual veins and vein remnants can either crosscut the sericitic fabric, or be crosscut themselves, always at low angles. The central quartz vein may also be crosscut by the sericitic fabric, although there is little obvious displacement along these planes. Superimposed on both the

shearing and the boudinaging events is an age of calcite veining, orientated parallel to shear fabric. The calcite-filled brittle shear planes have a sinistral sense of displacement in profile, as evident from local drag effects. From these age relationships it is tentatively suggested that the initial ductile shearing was followed closely by several ages of vein emplacement, with synchronous and post-emplacement shearing, implying an overall ductile to brittle deformation zone.

The shear zone on 6 Level Eureka is offset by a late north-west south-east trending fault, which dips steeply westward. This fault does not appear on Map 3 due to lack of control on outcrop. The vertical component of displacement on this fault is not known, however the horizontal movement component is dextral, with a displacement of approximately two metres. Individual textures within the fault zone itself are obscured by calcite and iron-oxide residues, formed in the fault plane by ground water movement.

iii) Cat's Cave Shear Zone

a) Introduction

The Cat's Cave workings are located immediately west of the 6 Level Eureka adit (Figure 2), and are the least developed of all the Margaret Section workings. Development is limited to a 50m reef drive on 1 Level (equivalent to 6 Level Margaret) which has been stoped to surface, a narrow winze to 2 Level (equivalent to 4 Level Eureka) with approximately 40m of reef drive west of the winze. The Cat's Cave shear, like many others in the Margaret Section, has no records of either production history or development history, and it is presumed that mining operations commenced in the late 1880's. The average stoping width was in the order of 1.5m over a strike of 30m. A grab sample taken from the adit

mouth on 1 Level yielded a grade of 32 g/t which is extremely high in comparison to other Moodies Group shear zones.

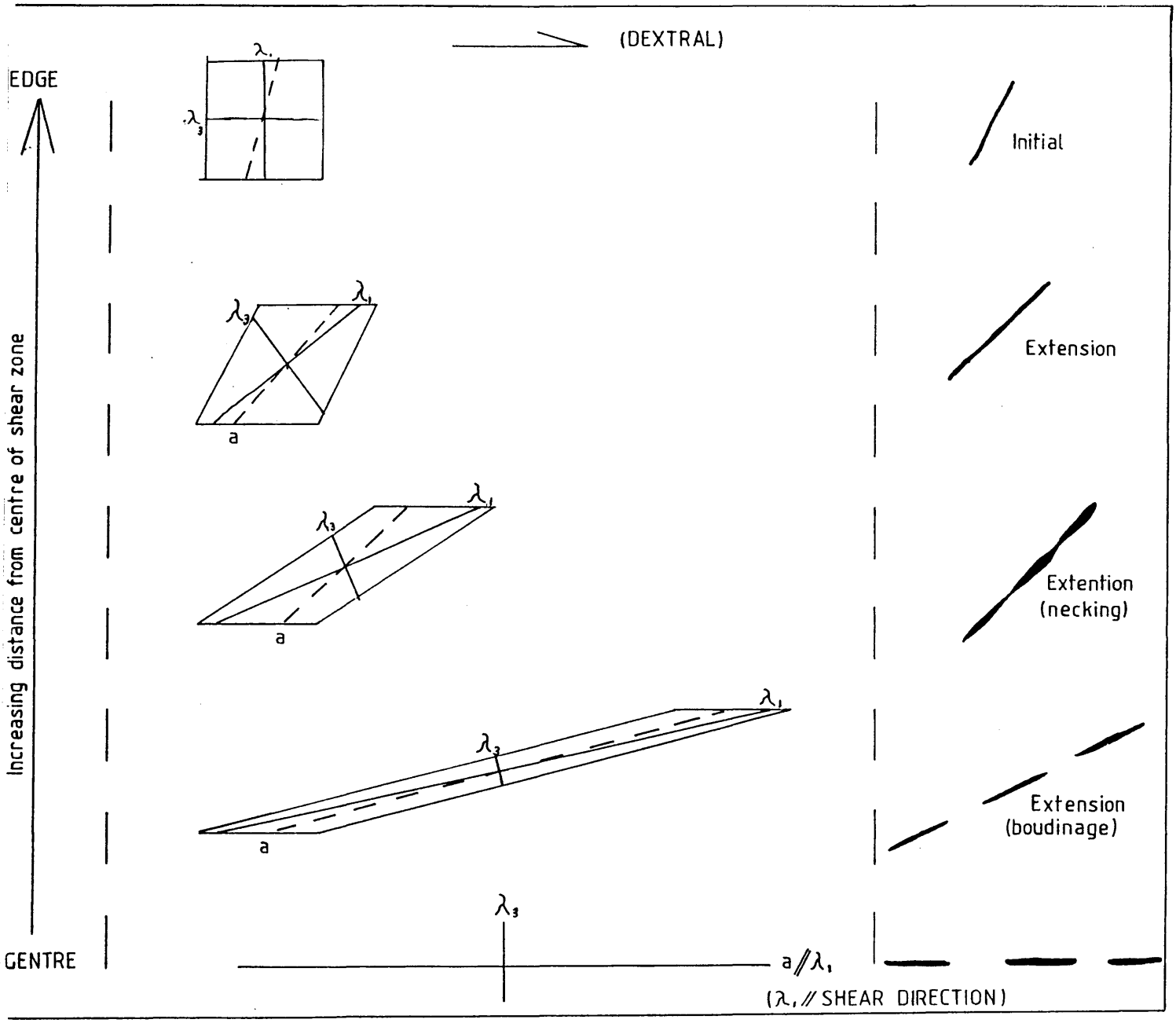

Figure 9. Strain axes associated with progressive simple shear (=direction of maximum shortening, =direction of maximum extension, a=initial finite strain marker, eg. quartz vein).

b) Geology of Cat's Cave Shear Zone

A description of the Cat's Cave Shear Zone is particularly difficult due to the fact that the major economic portion has been stoped out. In addition to this, the lack of both air and water services made it impossible to even attempt to clean the available exposure. The Cat's Cave Shear Zone is approximately 1m wide at its widest point and seldom thins to less than 30cm. It strikes 063° and dips north at between 43° and 58°. Several ages of quartz and quartz-carbonate veining accompany the shear zone, and are orientated sub-parallel to the margins of the structure. All these veins dip north at approximately the same angle as the host shear zone, but have limited strike extent. Where fresh exposure could be found the shear zone was clearly bounded by sericitic shears which increased in intensity towards an approximately central dark quartz vein. Mineralisation is in the form of fine to massive disseminated arsenopyrite with minor associated euhedral pyrite. Extensive oxidation of the ore minerals has occurred.

The host rock to the shear zone is dominantly quartzite, dipping at between 45° and 60° towards the south. The close proximity of the Cat's Cave Shear Zone to the base of the Moodies Group suggests that the host rock is part of the Clutha Formation. Although bedding and the shear zone have the same strike they dip south and north respectively. On approaching the shear zone, however, bedding steepens considerably, and may locally dip north. This reversal in bedding dip is attributed to rotation into the shear zone, suggesting a reverse sense of movement along the Cat's Cave Shear Zone (Plate 4). It is not possible to make any conclusive statements about any horizontal component of movement. Toward the western limit of development on both 1 and 2 Level, the reef is

Plate 3. Alteration of a dark quartz vein to light quartz (11 level Mamba Shear Zone; peg 6573).

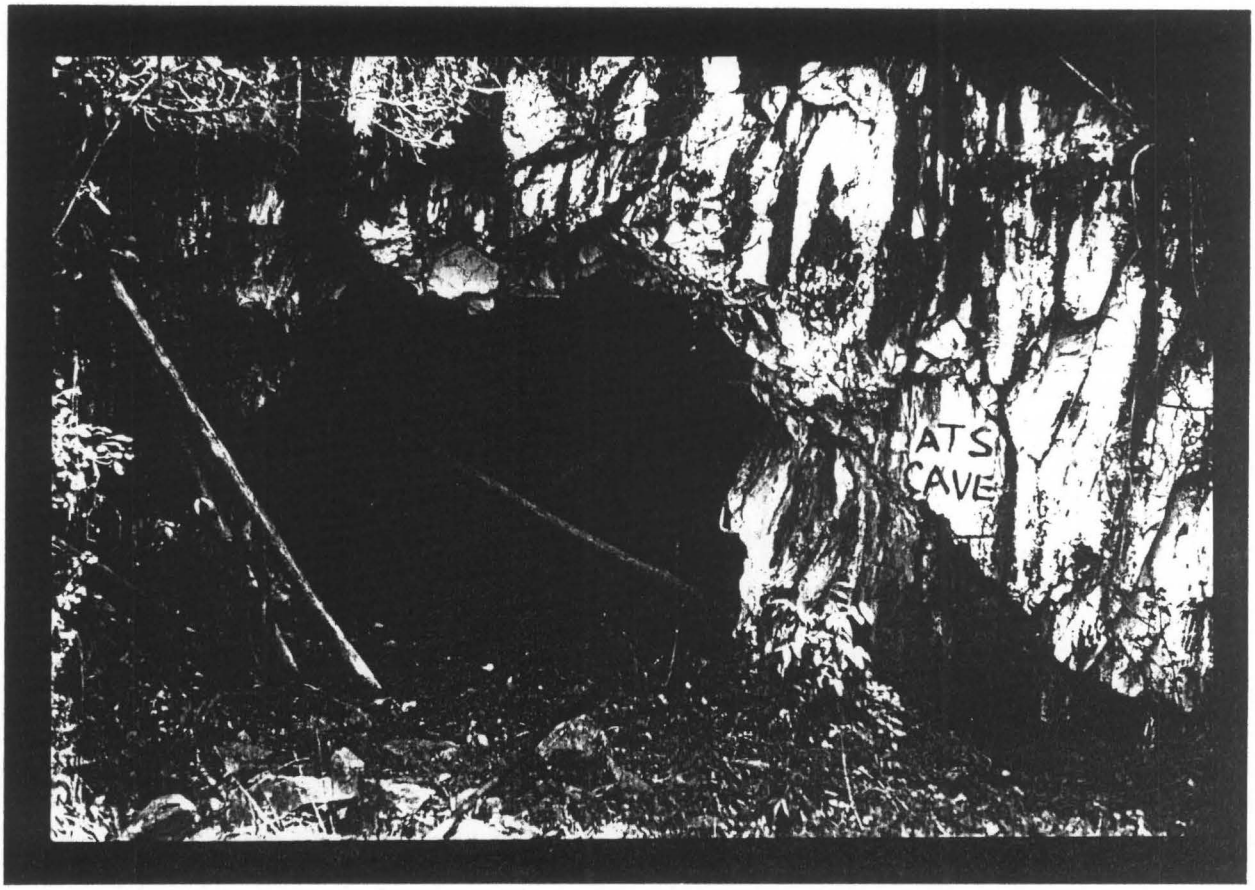

Plate 4. Shear zone drag on bedding, Cat's Cave Shear Zone (viewed looking west). The shear dips from the adit roof to the bottom right corner.

displaced by a north-west to south-east trending fault. The fault gouge is 20cm wide with a dextral displacement of 1.5m. No conclusive evidence could be found for vertical movement along the fault.

iv) **Discussion**

The shear zones at Mamba, Eureka, and Cat's Cave are all defined by the presence of sericite rich planar fabrics (foliation) around a central dark quartz vein. This central quartz vein is typically enclosed by the sericitic fabric but can locally cross cut or be cut by the shear fabric. This suggests the emplacement of the central vein into the ductile shear zone followed by localised reactivation. The central quartz vein occurs predominantly as discrete lenses, which are interpreted to represent boudins, and may well be associated with late stage deformation in the shear zone. Deformation in all three shear zone terminates with an age of calcite filled brecciation.

A total of nine quartz and quartz-carbonate vein ages were identified microscopically within the shear zones. These veins all show distinctive age relationships and compositions relative to each other, suggesting their formation as either distinct emplacement events or in response to distinct deformation events. Intense shearing and flattening has been responsible for the transposition and rotation of vein remnants into the parallelism with the shear zone fabric. This, combined with the boudinaging effect seen in the central quartz vein, suggests that the shear zones developed over an extended time period, and were frequently reactivated.

Movement within the north dipping shear zones has had the effect of creating substantial drag on bedding at the margins of the shear zones. This drag is best illustrated by the change in orientation of bedding on approaching the shear zone, until it is totally destroyed within the shear zone itself. In profile (Figure 7) this

drag clearly indicates a reverse sense of movement (i.e. north block up). This, combined with the orientation of mineral elongation lineations (Figure 10) defined by the long axis of tabular quartz indicates the displacement along the shear zones was dip-slip and reverse with translation directed towards the south-west. The thrust zones are developed in both quartzite and meta-arkose of the Clutha Formation and typically bifurcate up dip.

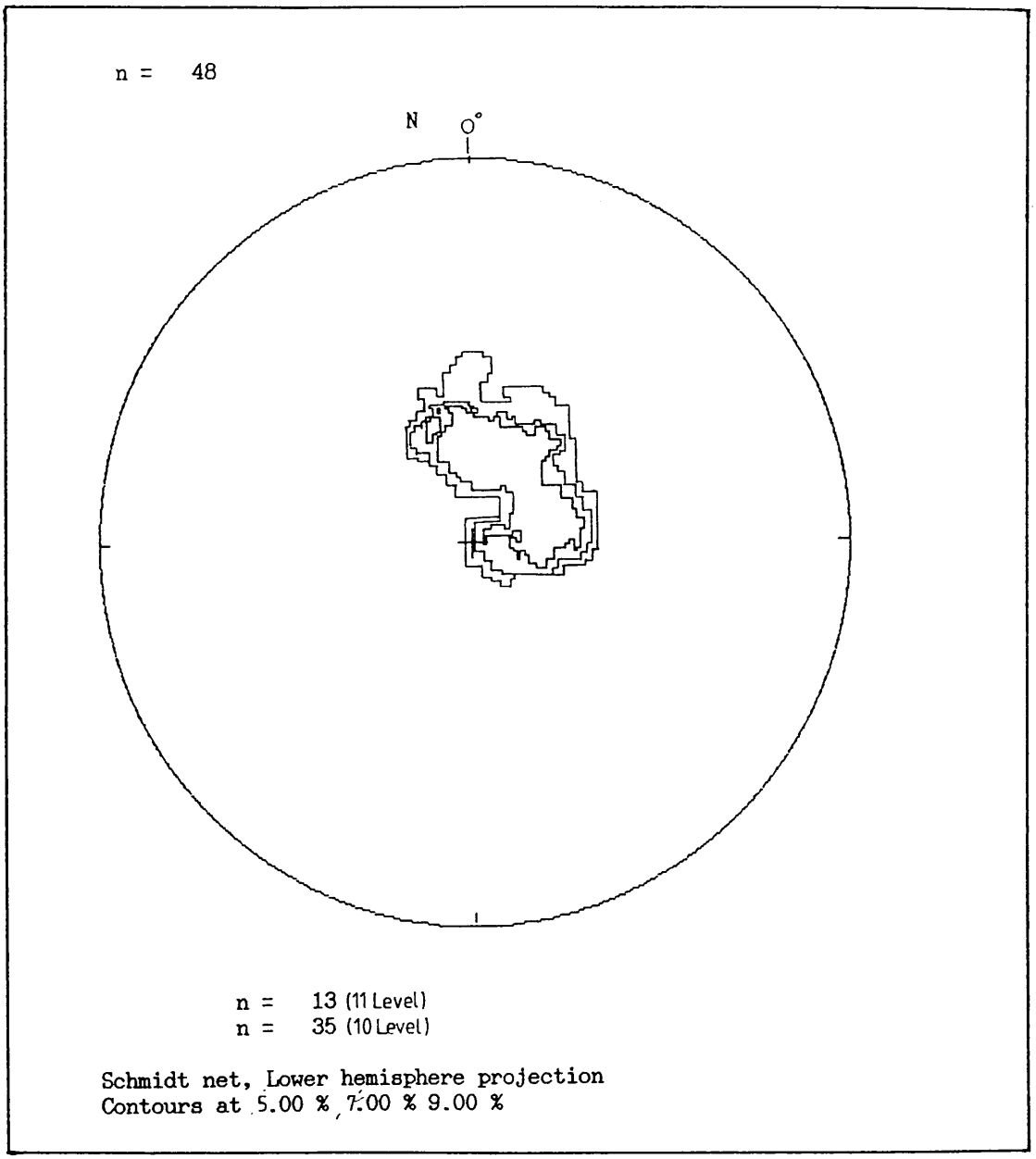

Figure 10. Stereographic projection showing the plunge of lineations within the Mamba Shear Zone (average plunge is 73°/021°).

These bifurcation sites show the greatest concentrations of sulphides and hence enriched gold values, and are best recognized by a marked deviation from the average dip of the shear zone. In cross section this bifurcation of the shear zone produces a characteristic imbricate pattern.

The termination of shear zones within the Margaret Section occurs in two ways, viz. by horsetailing or by localised brecciation. These terminations are anomalous in that they should form ideal sites for increased mineralisation (Phillips, 1972). However, they are without exception barren.

From the similarities demonstrated between the styles of mineralisation and the deformation history, it is suggested that the three shear zones were affected by similar mineralizing and shearing events. Deformation was dominantly within the brittle-ductile field and related to south-westerly directed thrusting. The three shear zones are interpreted as part of a northward dipping imbricate thrust set, within the footwall of the Sheba Fault Zone.

3.2 Structures associated with the Sheba Fault Zone

i) Introduction

The Barberton supracrustal remnant is characterized by the presence of several major sub-parallel, strike persistent shear zones, namely the Lily, Sheba, Barbrook, Saddleback, Inyoka and Komati faults (Anhaeusser, 1965; Ramsay, 1963; Roering, 1965; Robertson, 1989). Research in similar Archaean supracrustal remnants in Canada and Western Australia (Harris, 1987; Ho and Groves, 1987; Meuller and Harris, 1987; Sibson, 1987), as well as from other localities (Andrews, et al., 1986; Hamilton and Hodgeson, 1986; Sang and Ho, 1987; Sango, 1988), indicates such large scale shear zones play an important role in providing a structural en-

vironment suitable for economic gold mineralisation. Their role in the location of gold mineralisation is complex, but three of the more important aspects are:

(1) deformation along these structures produces induced permeability in the host rock and provides sites (cavities, gashes etc) for mineralisation.

(2) the shear zones provide channelways for concentrated fluid flow through any potential host rock.

(3) second order structures, such as conjugate fault sets, associated with the major shear zone provide potential sites for mineralisation.

The importance of these particular aspects becomes very obvious when one re-examines the criteria necessary for the formation of a hydrothermal orebody as outlined by Kerrich and Allison (1978). They are as follows: (1) a fluid medium to transport the solute, (2) access of hot fluids to large volumes of source rock, (3) a structure to focus the hydrothermal discharge and thus to precipitate ore constituents at a specific locus, together with a suitable chemical environment at the site of deposition, and (4) an energy source with sufficient time period to drive a long lived fluid motion.

The role of structurally induced permeability can be summarised as follows: a fluid moving through a rock will follow the path of least resistance. The presence of faults or shears will aid this movement greatly, particularly if such faults or shears provide uninterrupted access to shallow crustal levels where crystallization can occur. The larger the structure, the greater the probability that escaping hydrothermal fluids will find and use it.

Next, any movement along the major fault or shear will be accompanied by the development of secondary faults

and/or shears. The permeability induced by this faulting will satisfy the plumbing criterion (Sibson, 1987), while the development of secondary structures will satisfy the site requirements. The importance of these regional fault/shear zones in the Barberton supracrustal remnant is further emphasized by the close proximity of all the major historical and present day gold producers to these structures (Anhaeusser, 1986; Figure 11).

The Sheba Gold Mine claims are located on and around the regionally strike-persistent Sheba Fault, hence a discussion of the Sheba Fault in this area is important. Four localities were selected for investigation: (1) Eldorado Anticline, (2) Golden Quarry, (3) Royal Sheba, (Figure 2) and (4) 42 Level Fairview Mine (Figure 1). The reason these particular localities were selected is that the Royal Sheba and 42 Level Fairview outcrops lie respectively east and west of the D_3 axis of arcuation (Ramsay, 1963), while the Eldorado Anticline and Golden Quarry outcrops lie on the axis. Hence these outcrops represent sections of the Sheba Fault Zone across the arcuation zone.

ii) Previous Interpretations

Academic research in the northern and north-western portion of the Barberton supracrustal remnant has been lacking. Within the Sheba Mine area structurally biased research is limited to the work of Ramsay (1963), Roering (1965), Anhaeusser (1976), Robertson (1989), and the present study. All the above researchers identify at least three deformational events, and in some cases (Robertson, 1989), up to five events are described. In all previous studies the driving force behind the deformation has been assumed to be the emplacement of the surrounding granitoid masses. The deformation events are presented in Table 4, as modified from Robertson (1989). In all cases deformation events are numbered in compliance with their original description by Ramsay (1963).

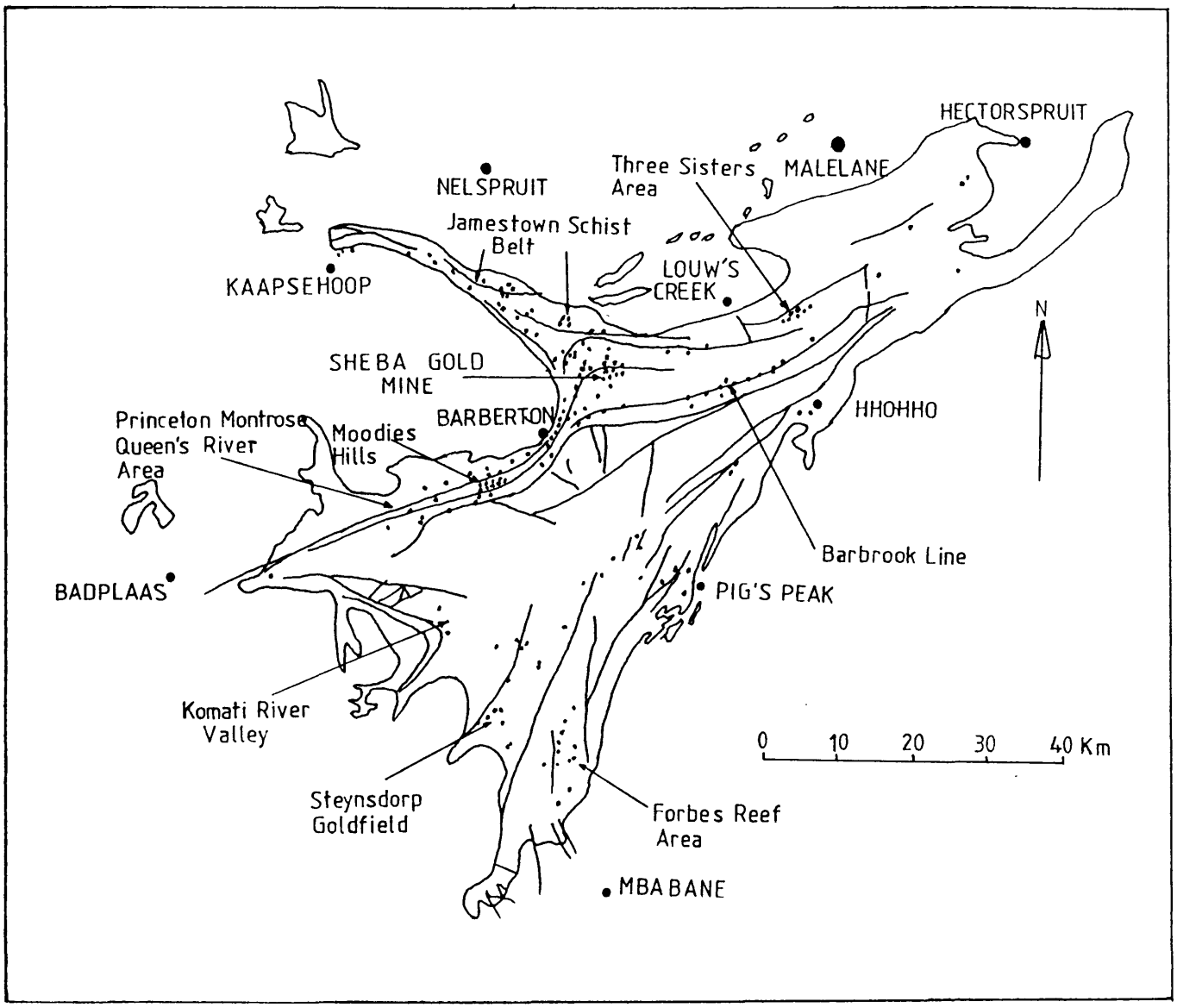

Figure 11. Regional structural trends and major gold occurrences (modified after Anhaeusser, 1976).

a) D_1 Structures

The earliest deformation event recognized by Ramsay (1963), was responsible for the development of a series of large folds (F_1), with an axial trace trending north-east to south-west. The largest of these

Table 4. The deformation history of the Barberton supracrustal remnant, Sheba Mine Area (modified after Robertson, 1989).

RAMSAY (1963)	*ROERING (1965)*	*ANHAEUSSER (1975)*	*ROBERTSON (1989)*
NORTHWESTERN FLANK	*NORTHWESTERN FLANK*	*SHEBA HILLS AREA*	*SHEBA GOLD MINE*
	Evidence for early (pre-D1) deformation		Pre-D1 Early sub-horizontal thrusting concentrated below chert units at the top of ultramafic sequences Thrusting probably due to initial emplacement of the Kaap Valley Tonalite pluton
	Main Phase structures:		
D1 Large scale isoclinal folds with NE-SW trend (F1) Major longitudinal faults	D1 Major ENE trending folds and regional strike slip faults Incipient arcuation of large folds	D1 Major NE-SW striking folds and faults Diapiric emplacement of the Kaap Valley Tonalite	D1 Steepening of stratigraphy and development of major NE-SW trending flods and faults during continued emplacement of the Kaap Valley Tonalite pluton Emplacement of the Nelspruit Batholith Regional dynamothermal metamorphism?
D2 Regional slaty cleavage and minor folds (F2)	D2 Slaty cleavage and minor folds	D2 Regional slaty cleavage	D2 Compression from the SE resulting in a regional cleavage being superimposed on D1 folds Continued compression caused thrusting of the folds to the NW and incipient arcuation of the Eureka and Ulundi synclines
	Post Main Phase structures:		
D3 Refolding/arcuation of F1 folds	D3 Conjugate folds and faults Arcuation of major folds Late Ulundi Trend of small scale folds having an ENE trend Development of flat lying folds	D3 Emplacement of Nelspruit granite Refolding of major folds about a NW-SE trending fold axis Thrusting of two major synclines to the NW	D3 Final emplacement of the Kaap Valley tonalite generating easterly directed stresses and reactivation of major faults as right lateral strike-slip faults Second and third order structures formed and acted as hosts to syntectonic mineralization
D4 Conjugate folds and faults			D4 Intrusion of the Stentor Pluton generating southward compression and possible late-stage reactivation and mineralization of fractures

early structures is the Eureka Syncline, which plunges towards the west, south-west, and south (due to later deformation events). The southern limb of this syncline is overturned. South of the Eureka Syncline is a second large syncline, the Ulundi Syncline. The two synclines are juxtaposed in a back-to-back arrangement along the line of the Sheba Fault. The Sheba Fault trend is thought to have developed during this early deformation event and to have been reactivated during later deformational events (Anhaeusser, 1965).

Immediately south of the Sheba Fault, within the Ulundi Syncline, is a zone of isoclinal anticlines known as the Sheba Anticlinorium (Ramsay, 1963). These anticlines expose fuchsitic-chloritic quartz-carbonate schists, talc-carbonate schists, and banded to massive cherts of the Zwartkoppie Formation (SACS, 1980). The northern limbs of these anticlines are typically absent, which Gribnitz (1964) ascribed to the development of a south dipping shear zone at the position of the overturned limbs. The anticlines plunge both east and west through large angles suggesting they may have a lingoid or sheath-like form.

b) D_2 Structures

The second deformation event is marked by the development of the regional finite strain fabric (cleavage) throughout the supracrustal remnant. These fabrics are both planar (slaty cleavage) and linear (grain elongation), (Ramsay, 1963). The greywacke units of the Fig Tree Group display the slaty cleavage particularly well, whereas it is often absent or at best poorly developed in the Moodies Group rocks. This is of course a direct result of their relative compositions, and in particular their clay mineral content, with the presence of abundant clay minerals in the Fig Tree argillites facilitating

cleavage development. The D_2 fabric in the Moodies Group rocks is typically defined by elongate conglomerate clasts (Ramsay, 1963). There is a notable absence of major folds related to this period of deformation although minor folding developed locally - the F_2 structures of Anhaeusser (1965). The widespread occurrence of planar fabric of F_2 orientation in the adjacent Nelspruit granite, has led to the suggestion that it was emplaced towards the end of the D_2 period of deformation (Robb, 1977a).

c) **D_3 Structures**

D_3 deformation is apparent from the broad arcuation of the Eureka and Ulundi synclines, as well as the arcuation of the Sheba Anticlinorium anticlines (Ramsay, 1963; Anhaeusser, 1965) along a north-west south-east trace. Further evidence for arcuation is seen in the radial pattern of slaty cleavage about the north-west south-east axis (Ramsay, 1963).

d) **D_4 Structures**

A fourth phase of deformation is recognized by the presence of low amplitude crenulations (crinkles) deforming the slatey cleavage. Ramsay (1963) suggested that these folds may be related to strong compression, developed on the inner arc of the buckled Moodies quartzites.

iii) **Present Study**

a) **Eldorado Anticline**

The Eldorado Anticline is the most northerly anticline of the Sheba Anticlinorium anticlines (Figure 2). At this locality the Sheba Fault Zone dips south, juxtaposing rocks of the Fig Tree and older Onverwacht groups south of the fault against

Moodies Group arkosites and quartzites to the north. Field mapping (Map 4) of the area has led to the recognition of an anticline of Onverwacht Group "greenschist" and cherts (which represent the Zwartkoppie Formation in this area, Anhaeusser, 1986; Ramsay, 1963), within the outcrop of Fig Tree greywackes and shales forming the hangingwall of the Sheba Fault (Map 4). Two chert horizons were identified and for simplicity called a northern and a southern chert. The northern chert terminates against the Sheba Fault, while the southern chert is dragged into parallelism with it (Map 4). The southern chert is characterised by numerous isoclinal parasitic folds which all plunge between 44° and 33° toward 096° (Map 4). In the eastern portion of the area mapped the northern chert dips steeply south while the southern chert dips at a shallower angle towards the south, thus defining an overturned anticline. The geometry of the Eldorado structure is supported by underground observations on other folds in the Sheba Anticlinorium (eg. Zwartkoppie anticline, Birthday 1 and 2 anticlines). These observations also indicate the anticlines of the Sheba Anticlinorium plunge both east and west implying a overall sheath-like geometry.

The "greenschists" occur in the area between the two cherts, and persist west of the position where the northern chert cuts out. The relationship here is thus "greenschist" directly against the Sheba Fault. The "greenschists" are poorly exposed, however where they do outcrop they contain a strong cleavage which dips at 38° toward 172°. Numerous irregular crosscutting quartz veins of short strike length also occur.

Both the Fig Tree greywackes and Moodies "arkosites" in this area are poorly exposed. Where exposed in a road cutting a weakly developed cleavage in the greywackes dips at 33° toward 181°,

but is absent in the arkosites.

The Sheba Fault in this area is represented by a zone of cataclasis, silicification and carbonatization of variable width (15cm up to 4 metres). Cataclasite fragments are dominantly of Moodies Group origin, and are often etched out by preferential weathering of the less silicified zones (Plate 5). The cataclasite zone dips south and strikes east-west. The southern contact of the cataclasite zone terminates sharply against sheared greywackes in the east and "greenschists" in the centre and west of the mapped area (Map 5), while the northern contact is gradational. This gradational contact is best defined by the decreasing abundance of white quartz veins, orientated parallel to the cataclasite zone (Plate 6). Silicification and carbonatization also decrease away from this zone. The sheared greywacke seen between the northern chert and the cataclasite zone, in the eastern portion of the mapped area, (Figure 7) is interpreted as a phyllonite (M.J.Tomkinson pers. comm., 1989), and may represent the shear zone related to the formation of the Zwartkoppie Anticlines. The similarity in plunge between the axis of the parasitic folds, the cleavage-bedding intersection lineations seen in the greywackes, and lineations seen in the chert layers, suggest a reorientation of all these features into parallelism with each other. No lineations are seen within the cataclasite zone, suggesting that it post-dates the "reorientation" event.

b) Golden Quarry

The site of the present day Golden Quarry (Figure 2) marks the first major gold find in the Sheba Hills area, by Edwin Bray in 1886. Production records show the Golden Quarry to have produced 29 232 kg of gold from a mined tonnage of 1 392 000 tonnes. The average grade for the deposit was 21.0 grams per tonne, and the average stope width 12 metres.

This was clearly one of the richest (in terms of grams per tonne) Archaean gold deposits ever discovered.

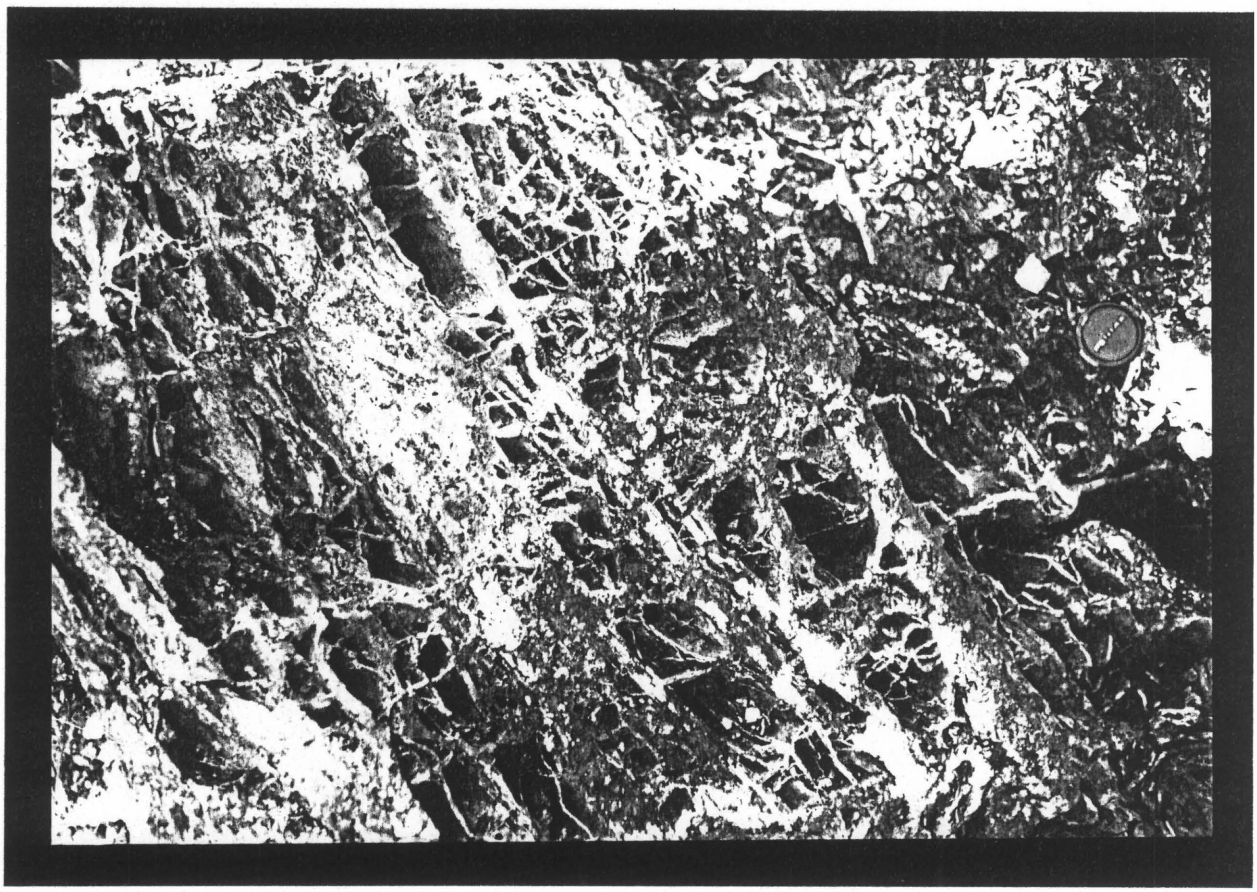

Plate 5. Weathered cataclasite, Eldorado Anticline (viewed looking west). The carbonate rich zones are etched out.

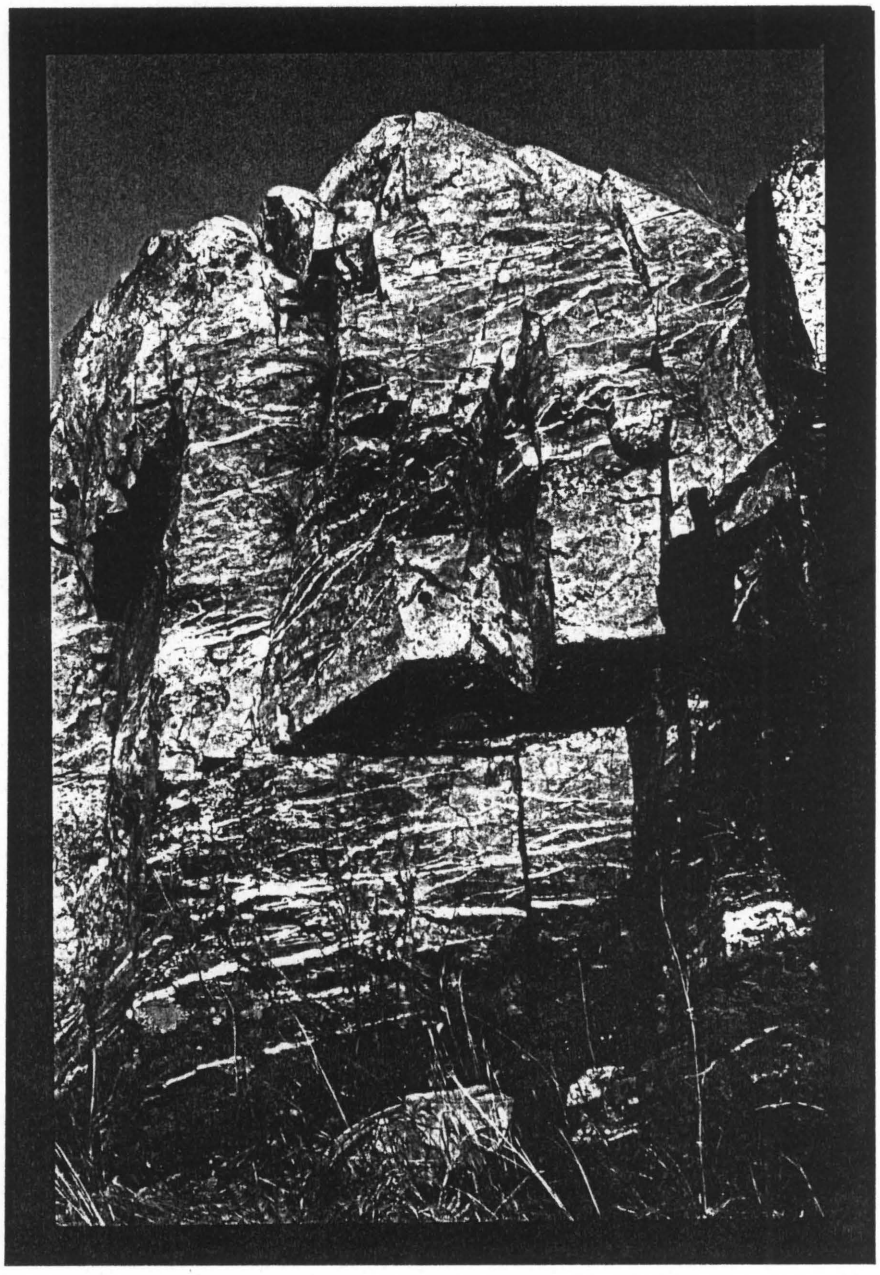

Plate 6. Orientated white quartz veins, Eldorado Anticline (viewed looking south). Vein material is dominantly quartz.

The Sheba Fault at this locality is well exposed in a road cutting immediately north of the Golden Quarry. The fault zone dips south and juxtaposes rocks of the Moodies and Fig Tree groups. The contact between these two groups is a fault gouge, locally termed "the clay seam" (Plate 8). To the north of the fault gouge the fault zone is defined by a stockwork of white quartz-carbonate veins (Plate 9), with the dominant vein orientation sub-parallel to the plane of the fault gouge (50 toward 185). The intensity of veining decreases northward from the fault gouge until only irregular- lar widely spaced, white quartz veins sub-parallel to the gouge orientation persist. A poorly developed cleavage can be recognized for approximately 20 metres to the north of the quartz veined zone.

The greywacke sequence south of the fault gouge has a strongly developed penetrative fabric. This fabric decreases in intensity away from the fault gouge, over a horizontal distance of approximately 120 metres.

Alteration identified at this locality is dominantly within the quartz-veined zone, with only minor carbonate alteration persisting north and south of this zone. Silicification is confined to the veined zone.

Within the actual pit at Golden Quarry minor folding is obvious. This outcrop is not accessible; however, it was observed that the fold axes plunge at a shallow angle to the east, possibly parallel to those on the Eldorado Anticline.

c) **Royal Sheba Outcrop**

The Royal Sheba orebody is the only orebody presently being mined at Sheba, within the Sheba Fault Zone (Figure 2). Mining operations commenced at Royal Sheba in 1896 and continued

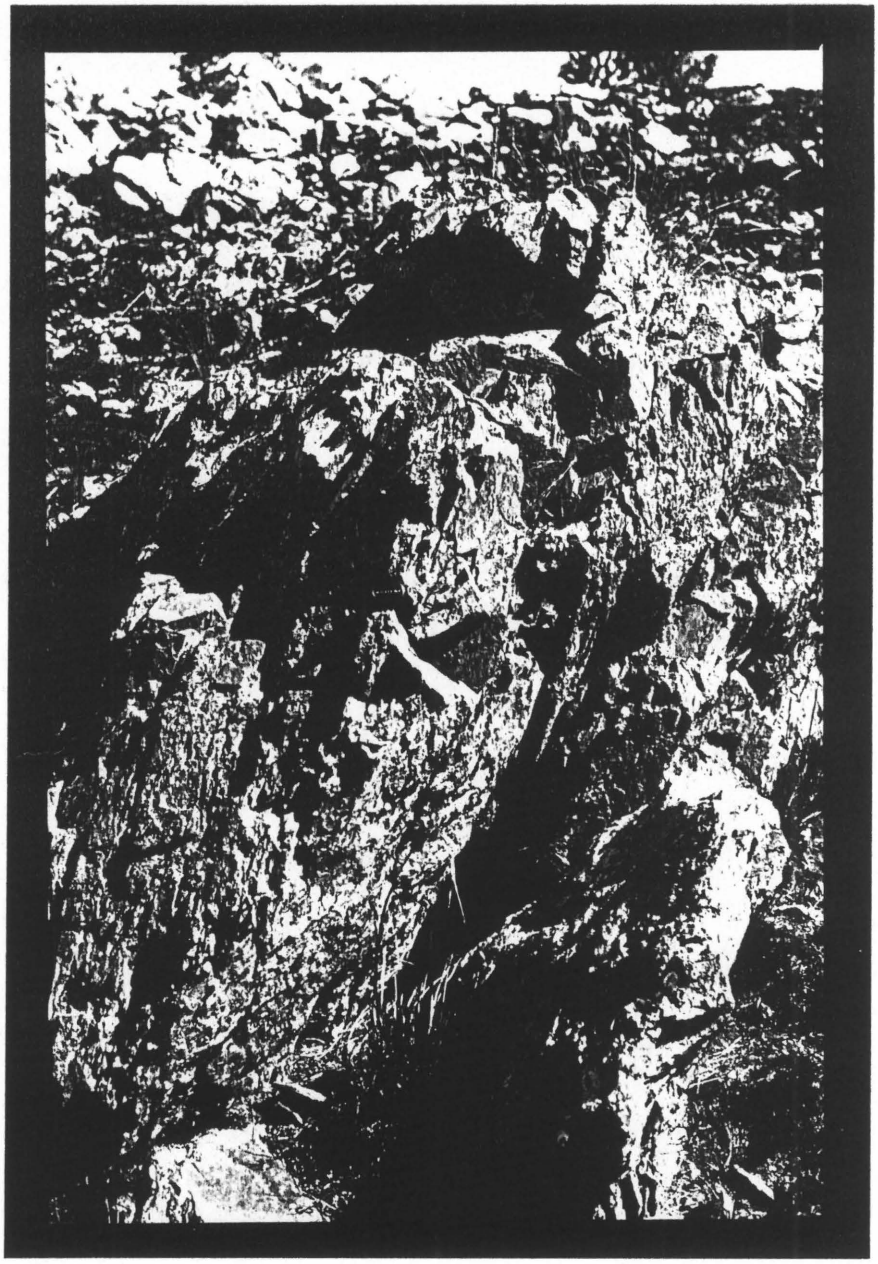

Plate 7. Phyllonite zone in greywackes (viewed looking west), eastern section Eldorado Anticline.

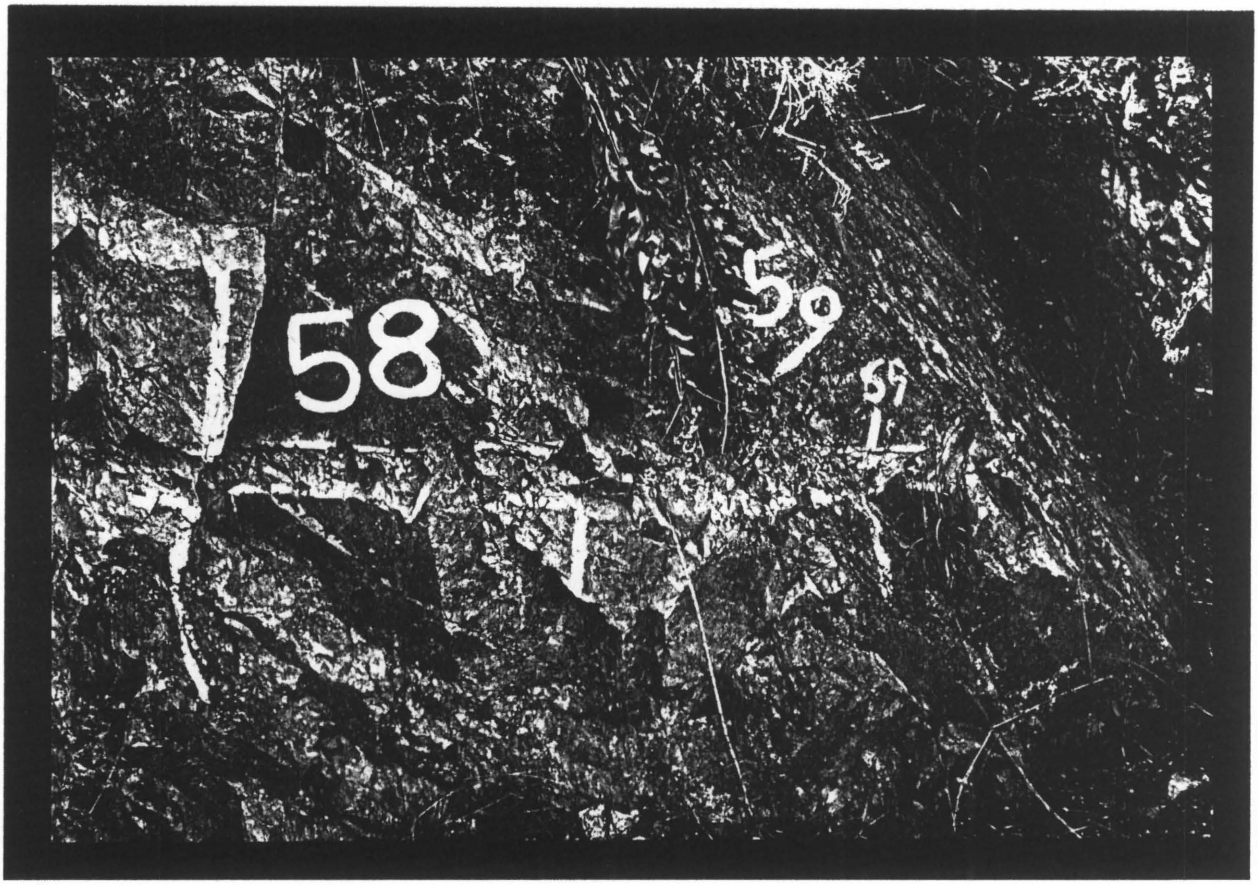

Plate 8. Fault gouge/"clay seam" Golden Quarry (viewed looking east). Moodies Group rocks on the left of photo and Fig Tree Group in the extreme right.

until 1942, when the mine flooded. Dewatering was completed in 1964 and mining operations restarted. Present mining activities are being conducted between 8 and 12 levels. To date the mine has produced approximately 1 254 kg of gold, from 327 612 tonnes of rock mined.

The exposure, both on surface and underground, at Royal Sheba provides an excellent cross section through the Sheba Fault zone, well east of the D_3 arcuation event mentioned by Ramsay (1963). The Sheba Fault in this area strikes almost due east and dips south, juxtaposing units of the older Fig Tree Group (the northern limb of the Ulundi Syncline) and the younger Moodies Group (southern limb of the Eureka Syncline). A schematic cross section across the orebody is provided in Figure 12. The Fig Tree Group rocks are dominated by rhythmic greywacke and shale cycles, which all fine toward the north. This suggests that, locally at least, the greywacke-shale cycles young north and not south toward the centre of the Ulundi Syncline, as would be expected.

Structurally below the greywacke-shale sequences is a well banded unit that is locally referred to as a banded chert-carbonate-shale or BCCS. This BCCS unit exhibits both conformable, gradational and sheared contacts with the overlying greywacke-shale cycles. The name banded chert-carbonate-shale, is by no means intended to have any genetic connotations, although primary chert units can be identified. The chert component of the BCCS is recognized by the presence of brecciated and/or sheared lenses of banded chert containing the mineral greenalite ($(Fe^{2+}\ Fe^{3+})_{5\text{-}6}Si_4O_{10}(OH)_8$) which is presumed to be of primary origin. The chert remnants are crosscut by an apparently random orientation of quartz veins, with minor associated pyrite. Syngenetic stratabound pyrite mineralisation is also present within the cherts. Al-

teration of the dark chert bands to a lighter coloured chert and vice versa is very common.

The dominantly banded nature of this unit is due to the sub-parallel to parallel orientation of chert and shale units. A closer investigation of the shale units reveals the existence of discrete shale horizons interlayered with thin (less than 2mm) felsic tuffaceous horizons. The shale horizons have a high siderite content (H.G.Philpot pers. comm., 1989). The tuffaceous horizons are highly carbonatized, with only minor recognisable remnants of feldspar. All the remnant minerals as well as neoformed minerals are orientated parallel to the dominant banding, suggesting a degree of flattening. The BCCS unit is tentatively correlated with the top of the Fig Tree Group.

Structurally below the BCCS unit is a series of arkosic quartzites locally referred to as arkosites. Mineralogically the arkosites comprise quartz, feldspar and white mica and are commonly characterised by conglomerate lenses. Both sheared and conformable contacts between the BCCS and the arkosites have been recognised. Shearing associated with the Sheba Fault has normally reorientated the white mica within the arkosite into parallelism with the banding in the BCCS, suggesting that individual bands of white mica have acted as discrete shear planes.

The arkosite has undergone extensive carbonate alteration and minor silicification. The main ore mineral at Royal Sheba (fine-grained euhedral pyrite) shows a direct grade correlation with the intensity of carbonate alteration. The alteration zone at Royal Sheba diminishes in an irregular pattern northward, but has a very sharp cut-off southward against the BCCS unit.

The Sheba Fault in the Royal Sheba Mine area comprises an intense ductile shear zone primarily within the BCCS unit. Shearing was preferentially located here due to the abundance of phyllosilicate minerals in this unit (facilitating easy movement) and due to the competency contrast between rock units. Evidence for ductile deformation is seen in the form of numerous shear bands (Plate 10), intrafolial folds (Plate 11), and phacoids. Ductile deformation in the form of a diffuse zone of discrete shears can also be recognized in both the greywacke-shale sequence and the arkosite sequence. Superimposed on the earlier ductile deformation is an age of thrust deformation. This is recognized by the presence of discrete shear planes which parallel and ramp through bedding and/or the earlier shear fabric. The reverse movement component is recognized from the rotation of bedding and pre-existing fabric (Figure 12), as well as from the presence of
slickenfibres which plunge south-east (Figure 13).

d) **42 Level Fairview Gold Mine**

The Sheba Fault is well exposed on 42 Level at the Fairview Gold Mine (Figure 2), where the fault juxtaposes rocks of the Moodies Group to the north and those of the Onverwacht and Fig Tree groups, to the south of the fault. The Moodies Group is represented by arkosic sandstones to orthoquartzites of the Clutha Formation, while to the south of the fault, "greenschist" of the Zwartkoppie Formation, Onverwacht Group, and greywackes of the Sheba Formation, Fig Tree Group occur. The Sheba Fault is a zone approximately 60 metres wide and is more correctly classified as a ductile shear zone. The shear zone is recognised by the development of an intense foliation at the contact between the Moodies Group quartzites and Zwartkoppie Formation greenschists. The zone of foliation is

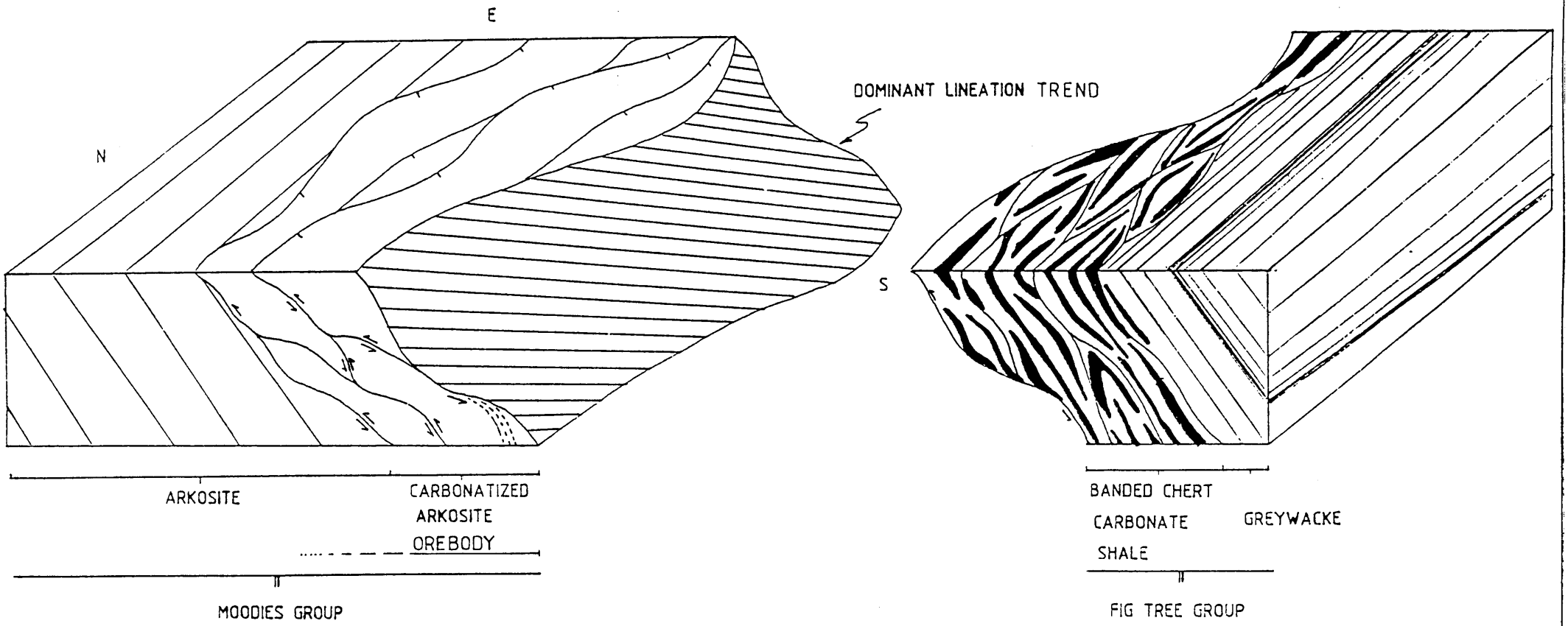

FIGURE 12. EXPLODED SCHEMATIC CROSS-SECTION THROUGH THE ROYAL SHEBA OREBODY, ILLUSTRATING THE TECTONIC RELATIONSHIPS

Plate 9. Orientated white quartz veins parallel to the fault gouge, Golden Quarry (viewed looking east).

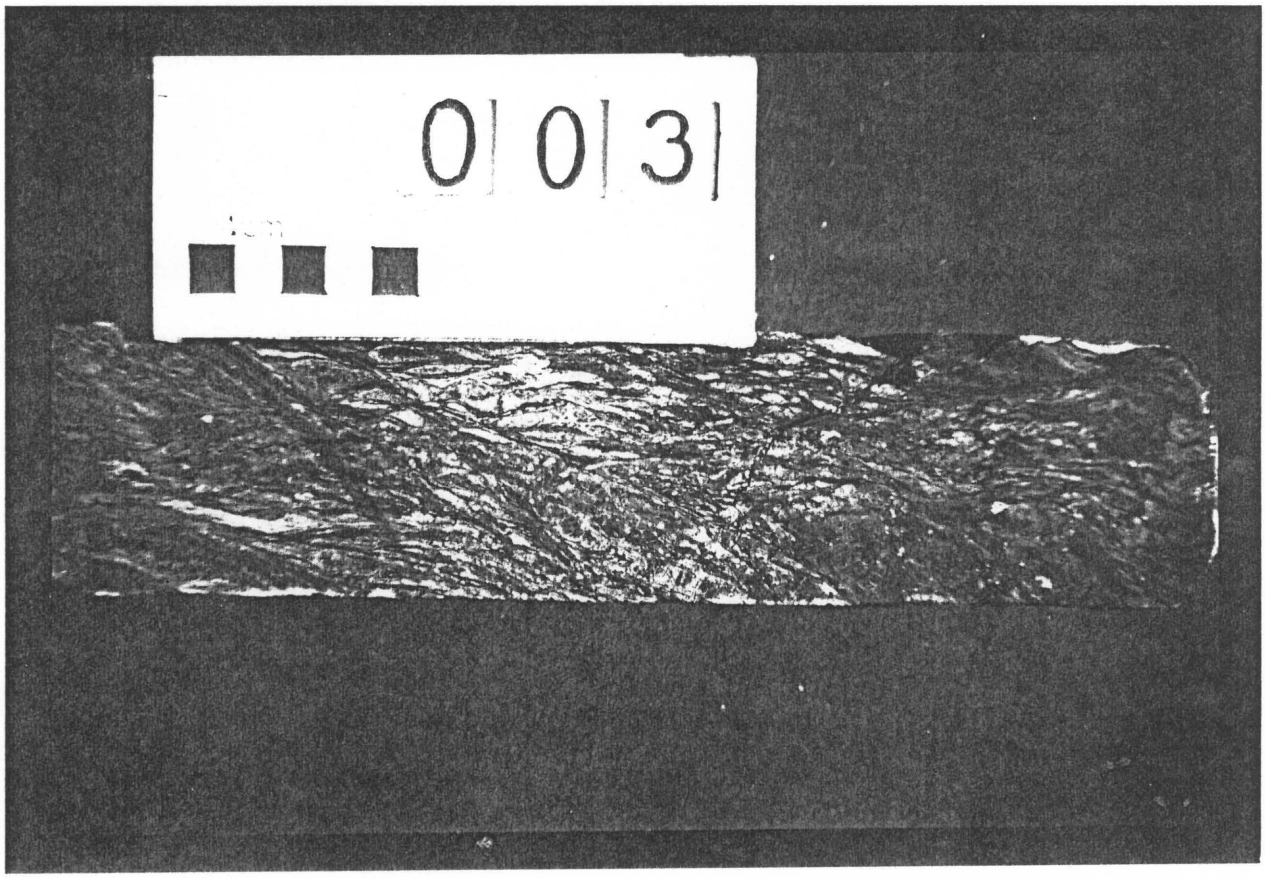

Plate 10. S-C fabrics and shear bands in drill core from Royal Sheba mine.

Plate 11. Intrafolial folds from the Royal Sheba outcrop. The fold nose plunges east.

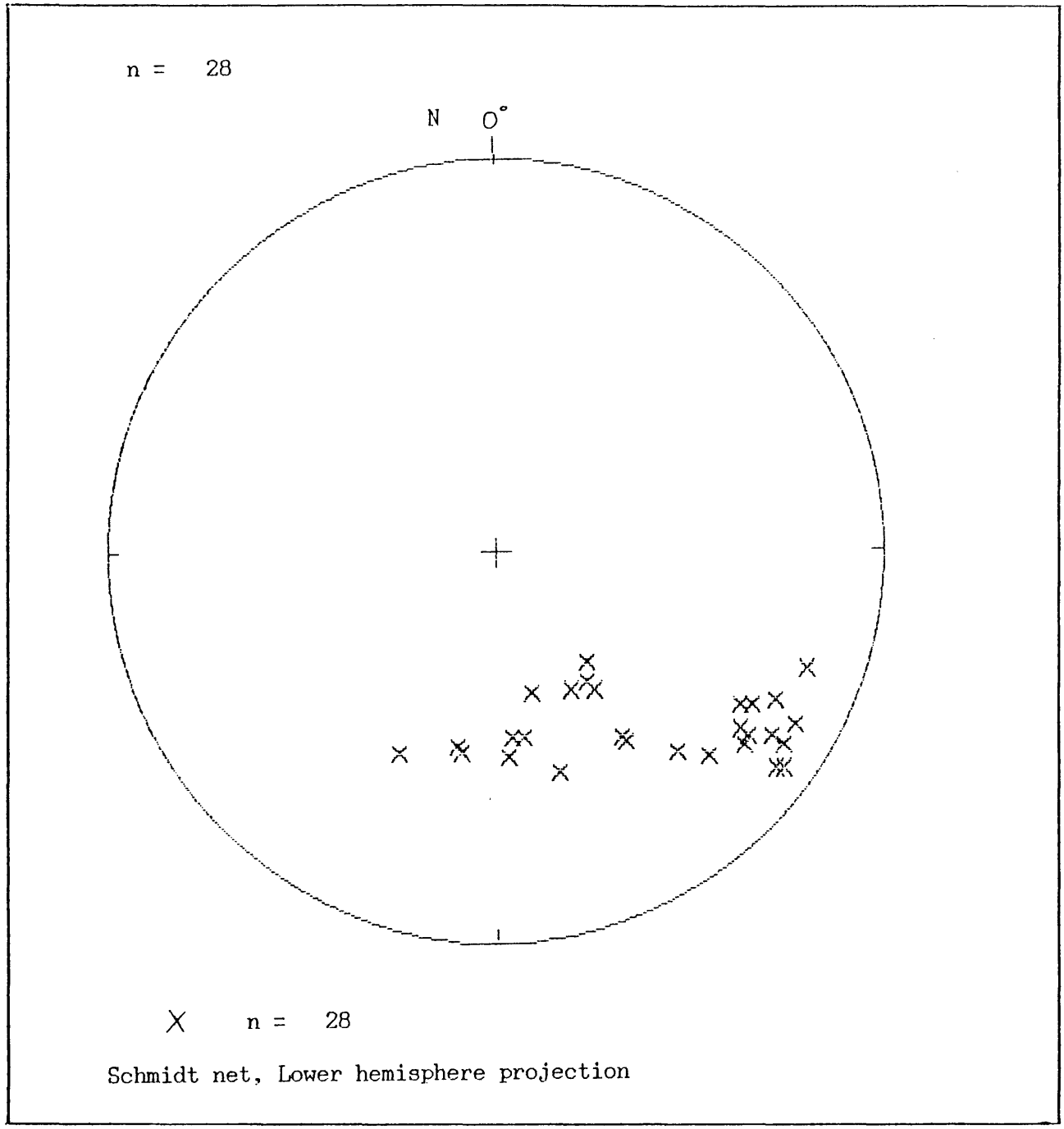

Figure 13. Stereographic projection of the plunge of mineral elongation lineations (quartz) at the Royal Sheba Mine (average plunge is 37°/141°).

asymmetrically distributed about the contact and biased in the direction of the greenschist. This is presumed to be due to the greater abundance of phyllosilicate minerals in the schists facilitating the development of a cleavage. The shear zone cleavage is orientated subparallel to the shear zone margins

implying high shear strain. Superimposed on the zone of foliation is a fault gouge that closely resembles the "clay seam" in the Edwin Bray Section of Sheba Mine. The fault gouge is developed sub-parallel to the shear zone cleavage and is interpreted as having formed during a later brittle deformation event.

Silicification, carbonatization, and sericitization are present within the shear zone. The carbonate alteration has an approximately 30 metre halo into the Moodies Group, while the silicification is more restricted. The alteration halo is less well defined within the "greenschist" package and not evident in the greywackes. A sheared, porphyritic dyke of apparent doleritic composition occurs within the Sheba shear zone (P.Pelly pers. comm., 1989). Zoned feldspar porphyrocrysts of up to 3cm in diameter can be seen in hand specimen, but in thin section are totally sericitized along with the groundmass (P.Pelly pers. comm., 1989). This porphyritic dyke is discontinuous along strike and dip.

e) **Discussion**

As an introduction to this discussion on the differences and similarities between the four outcrops of the Sheba Fault, it is important to recap on the major features observed at each locality (these observations are summarized in Table 5). The four localities under consideration are (1) Eldorado Anticline, (2) Golden Quarry, (3) Royal Sheba, and (4) 42 Level Fairview. It is also important to remember that outcrops 1 and 2 are located close to the axis of arcuation of the Eureka Syncline (D_3 event of Ramsay, 1963), while outcrops 3 and 4 lie east and west of this arcuation respectively.

Firstly the Golden Quarry outcrop. This outcrop juxtaposes rocks of the Moodies and Fig Tree

groups. Deformation across the Sheba Fault Zone in this area is characterized by the presence of a 20m thick stockwork (carbonate-rich, quartz-veined cataclasite) contained within the Moodies Group quartzites, which shows increased cataclasis toward the Fig Tree/Moodies Group contact. The contact itself is marked by the presence of a 20cm wide fault gouge (locally termed the "clay seam"). The Fig Tree greywacke pile immediately south of the fault gouge has a strongly developed cleavage. Carbonate and silicic alteration occur dominantly within the Moodies Group sediments. The interpretation of this outcrop is that in the vicinity of Golden Quarry the Sheba Fault is a brittle structure with a reverse sense of movement.

Table 5. Summary of the deformation events along the Sheba Fault Zone.

Golden Quarry	Eldorado Anticline	Fairview 42 Level	Royal Sheba
a) Stockwork veining b) Fault gouge c) Moodies against Fig Tree Group d) Silicification & carbonate alteration.	a) Shear zone at base of anticline b) Anticline & shear zone truncated by cataclazite zone c) Onverwacht & Fig Tree groups against Moodies group rocks d) Reorientatio of folds, cleavage, and lineations	a) Broad zone of ductile shearing b) Onverwacht group against Moodies group c) Possible late brittle event d) Silicification & carbonate alteration	a) Early ductile deformation in the Fig Tree group b) North directed thrusting event c) Fig Tree against Moodies group d) Silicification & carbonate alteration

Secondly, the Eldorado Anticline outcrop. Mapping has identified the presence of an anticlinal structure cored by rocks correlated with the Zwartkoppie Formation (Onverwacht Group), contained within a greywacke pile (Sheba Formation, Fig Tree Group). The northern limb of the Eldorado Anticline is truncated by a cataclasite zone of varying thickness

(30cm up to 5m). Parasitic fold axes on the southern limb of the anticline as well as the intersection lineation formed between cleavage and bedding in this area, are parallel to the mineral elongation lineations seen within the ductile shear zone at Royal Sheba, suggesting deformation along the shear zone after (or during) the development of the Eldorado Anticline. This deformation resulted in the reorientation of pre-existing structures. Although it is not possible to identify the origin of the stress field responsible for the deformation event, the fact that the anticline is truncated by the cataclasite zone places an age constraint on the two structures. Clear evidence for ductile deformation processes can be seen at the Eldorado Anticline outcrop in the form of shearing at the base of the anticlines with the resultant loss of the northern limb of the anticline and reorientation of all structures into parallelism. Of major importance is the fact that the cataclasite zone seen here is traditionally considered part of the Sheba Fault. Deformation at this locality is thus brittle, superimposed on an earlier ductile event, both with a reverse sense of movement.

Thirdly, the 42 Level Fairview suboutcrop. At this locality fuchsitic quartz-carbonate rocks of the Zwartkoppie Formation are thrust onto quartzites of the Clutha Formation. In this area the contact between the two units is seen as a broad zone of ductile deformation, biased toward the greenschists. At the contact between the two units there is a well developed fault gouge (again termed the "clay seam"). At this locality the Sheba Fault consists of an earlier zone of ductile shearing with a superimposed later event of brittle deformation.

Fourthly, the Royal Sheba Mine suboutcrop. At this locality the Fig Tree and Moodies groups are again juxtaposed due to thrusting. Deformation in this area is manifest as a broad zone of ductile shearing,

dominantly within a banded chert-carbonate unit correlated with the top of the Fig Tree Group, and to a minor extent with the Moodies Group quartzites themselves. Superimposed on this earlier ductile event is a second ductile deformation event in the form of northward directed thrusting.

In all previously published descriptions (eg. Anhaeusser, 1965; Ramsay, 1963; Robertson, 1989) the Sheba Fault is interpreted as having the same deformation style everywhere along its outcrop. The present study suggests this interpretation is too simple. In the central portion of its outcrop (eg. Eldorado Anticline and Golden Quarry) the deformation style is clearly brittle. In the eastern section (Royal Sheba) it is entirely ductile while to the west (42 level Fairview)both deformation styles can be recognised. From observation made on 42 level Fairview it is suggested that the cataclastic event seen at the Eldorado Anticline and Golden Quarry is superimposed on an earlier ductile event.

The similarities between the plunge of local cleavage-bedding intersection lineations, fold-axis plunges in the Eldorado Anticline area, and the lineations seen in the shear fabric at Royal Sheba, suggest that the reorientation may have been synchronous with the Royal Sheba event. From the exposures investigated it is clear that the presently exposed portion of the Sheba Fault has not undergone the same deformation history along its entire strike length, and for that reason should not be regarded as a single continuous fault zone. Of particular economic interest is the fact that a number of high grade gold deposits are located within the cataclasite zone, while only minor low grade deposits occur elsewhere in the ductile deformation portions of the Sheba Fault. From regional stratigraphic relationships and local kinematic indicators the dominant displacement component along the Sheba Fault is reverse to oblique

slip with the south block up.

CHAPTER 4

MINERALOGY AND ORE MICROSCOPY

4.1 Mineralogy of the Mamba Sheba Zone

The Mamba Shear Zone is hosted by the Clutha Formation of the Moodies Group. The entire Moodies Group has undergone low grade greenschist facies metamorphism, indicated by the presence of chlorite. Within the shear zones retrograde metamorphic processes were active, as seen from the superimposed mineral assemblages of the host rock. These differences in mineral assemblages are best described by comparing host rock mineralogy and shear zone mineralogy.

i) Host Rock Mineralogy

The host rock in this area has been described as a meta-arkose, or as it is locally known, an arkosite. Although the mineralogy of the Clutha Formation as a whole is very consistent, major mineralogical variations may occur on a local scale. To determine all minerals present, a number of samples were submitted for X-ray diffraction analysis (hereafter referred to as X.R.D.) and the following minerals were identified: albite, microcline, muscovite, chlorite, rutile, pyrite, quartz, carbonate minerals.

Both the albite and the microcline occur as euhedral to anhedral crystals with varying degrees of alteration to white mica. This reaction has been described by Meyer and Hemley (1967) and Barnes (1979) by the following equation:

$$3NaAlSi_3O_8 + K^+ + 2H^+ = KAl_3Si_3O_{10}(OH)_2 + 3Na^+ + 6SiO_2$$

(feldspar) (muscovite) (quartz)

The albite and microcline range in size from 3 micrometre up to 460 micrometre, and commonly display zoning and twins.

The muscovite identified on the X.R.D. trace can be separated into two generations by microscopic investigation. The first white mica closely resembles muscovite and forms by the breakdown of feldspar to muscovite (as described above, Plate 12) and/or chlorite to muscovite by the following reaction:

$2(\text{chlorite}) + 5Al^{3+} + 3Si(OH)_4 + 3K^+ + 2H^+ = 3(\text{muscovite}) + 10(Fe,Mg)^{2+} + 12H_2O$ (Meyer and Hemley, 1967; Barnes, 1979)

The alteration muscovite is less than 180 micrometres in length, and forms lath-like masses along feldspar margins. The second muscovite is distinguished from the first by the fact that it does not occur as a feldspar alteration product. These muscovite laths range in length from 40 to 430 micrometres (Plate 13), and are often rotated into parallelism with surrounding flattened quartz and feldspar crystals (Plate 14). This muscovite is considered to be of sedimentary origin.

Chlorite occurs in minor amounts throughout the host rock, is predominantly less than 25 micrometres in size and where observed is typically breaking down to white mica, in line with the reaction described above.

Rutile occurs throughout the host rock and is assumed to be of sedimentary origin. Two possible ages of rutile occur. The first is hosted entirely by the unsheared sedimentary units while the second is predominantly associated with zones of increased shearing. It is not possible to determine whether the shear-related rutile is of a totally different age and origin, or whether it is simply concentrated in these zones by processes such as remobilization or volume decreases (Beach, 1974; Barnes, 1979; Grathier, 1983). All rutile is less than 4 micrometres in size, and is predominantly rounded to oblate in shape.

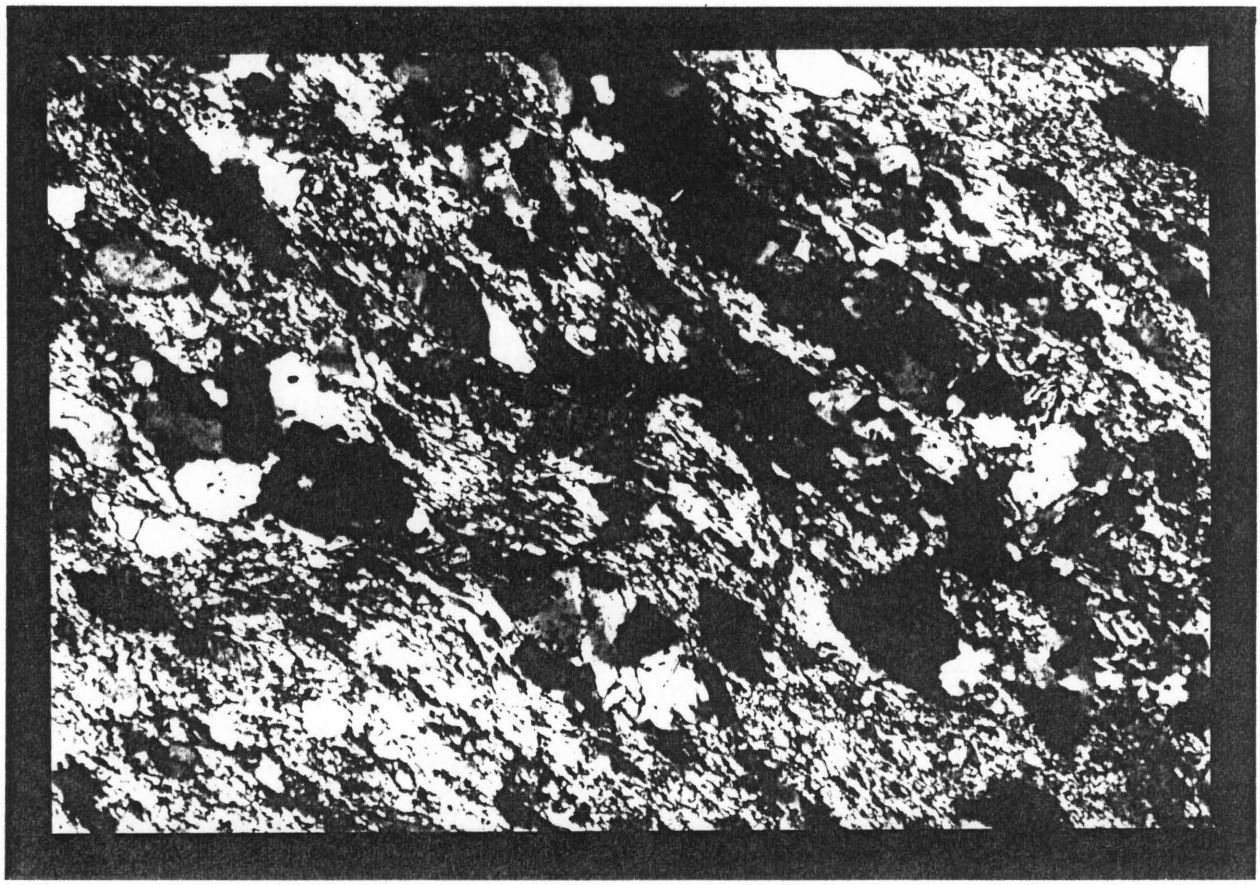

Plate 12. Breakdown of feldspar (F) to white mica (M), Mamba Shear Zone.

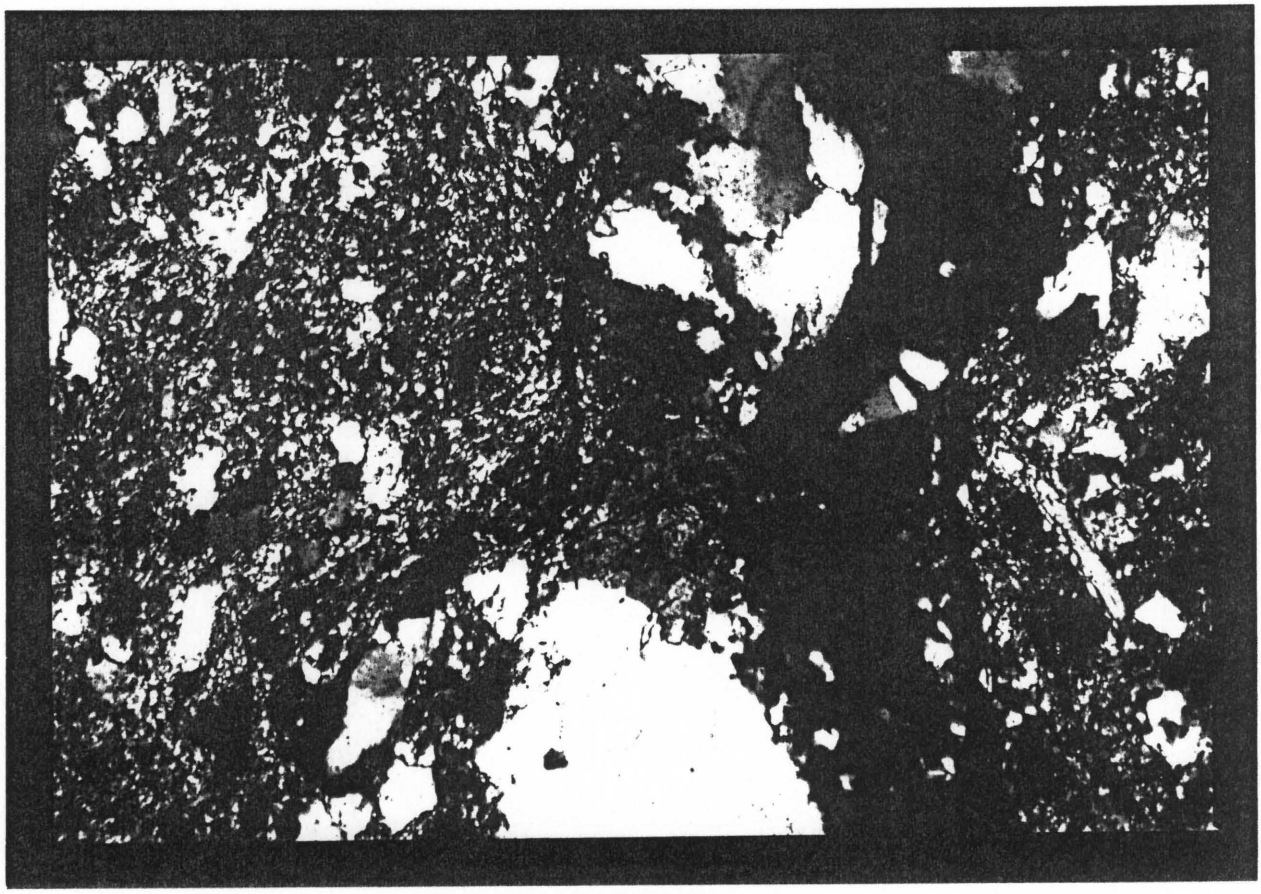

Plate 13. Residual mica (M) within the Mamba Shear Zone (C = carbonate, Q = quartz).

Pyrite is present throughout the host rock, where it occurs as euhedral and twinned crystals. The crystals range in size from 30 micrometres up to 280 micrometres in diameter. The pyrite over grows all minerals in contact with itself (Plate 15), and is therefore concluded to be very late in. Unlike the sulphide minerals within the shear zones this pyrite does not contain gold.

No primary carbonate minerals were identified in the host rock. However, numerous quartz-carbonate veins intrude the host. The carbonate associated with these veins was microscopically identified as dolomite and ankeritic. Several generations of quartz-carbonate veins exist and are discussed in Chapter 3 (Section c). The origin of the quartz-carbonate veins is unclear but it is suggested they may relate to one or more of the following processes:

1. product of a discrete quartz-carbonate event;
2. the result of pressure solution processes (Beach, 1974);
3. a reaction product from the hydrothermal alteration event/s (see alteration equations above).

Quartz occurs throughout the host rock and is by far the most dominant mineral. Locally the quartz content may be high enough to allow the rock to be classified as an orthoquartzite. The average quartz content of the rock is between 60% and 70%. Quartz grains are both rounded and angular, suggesting limited reworking at the time of deposition. The individual grains range in size up to 200 micrometres, with an average size of about 95 micrometres. Extensive undulose extinction within the grains indicats permanent strain of the host quartzites.

ii) Shear Zone Mineralogy

The mineralogy of the shear zones is essentially very similar to that of the host rock. However a number of notable exceptions occur. The most obvious of these is the presence of tourmaline. Additional minerals which

increase in abundance in the shear zone are quartz, white mica, rutile, carbonate minerals and sulphide minerals.

Quartz crystals within the shear zone all show extensive recrystallization along grain boundaries (Plate 16) and strain shadow development (Plate 16). This quartz can be broadly grouped into sedimentary quartz and vein quartz. The latter group includes at least six recognizable quartz and/or quartz-carbonate vein events. A description of these veins is given in Chapter 3 (Section c). Remnant quartz crystals are on average seldom greater than 30 micrometres in diameter, but much larger vein quartz remnants do occur. The subgrain development may be submicroscopic in size. Numerous sulphide minerals are associated with the quartz veins, the most important being pyrite.

White mica is present throughout the shear zone where it occurs as laths crosscutting or enclosing other minerals. The preferred orientation of these laths is responsible for the shear fabric seen in the rock (Plate 17). A second white mica orientation is sometimes developed at approximately 90 to the dominant orientation (Plate 18). White mica laths range in size from submicroscopic to 60 micrometres. The white mica shows many of the characteristics of fine grained muscovite and is concluded to be sericite (Deer et al., 1966).

Rutile occurs throughout the shear zone as rounded crystal remnants and no pristine crystals were observed. All remnants are less than 25 micrometres in diameter.

Three distinct forms of carbonate minerals are present in the shear zone. The first is a carbonate of fine crystal size that overgrows all other minerals (Plate 19) and is considered to be directly related to ore fluid alteration processes.

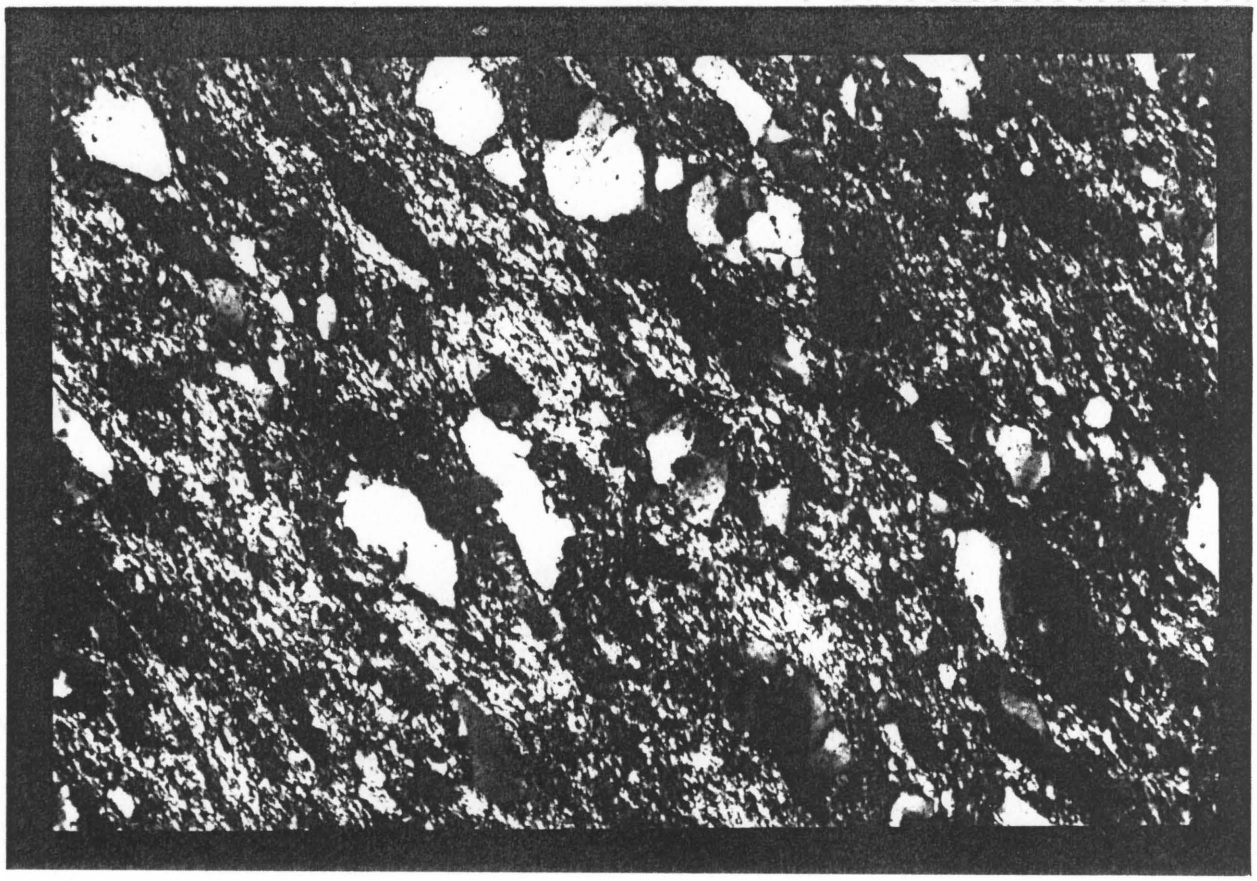

Plate 14. Residual micas rotated into the shear fabric (M = mica, F = feldspar).

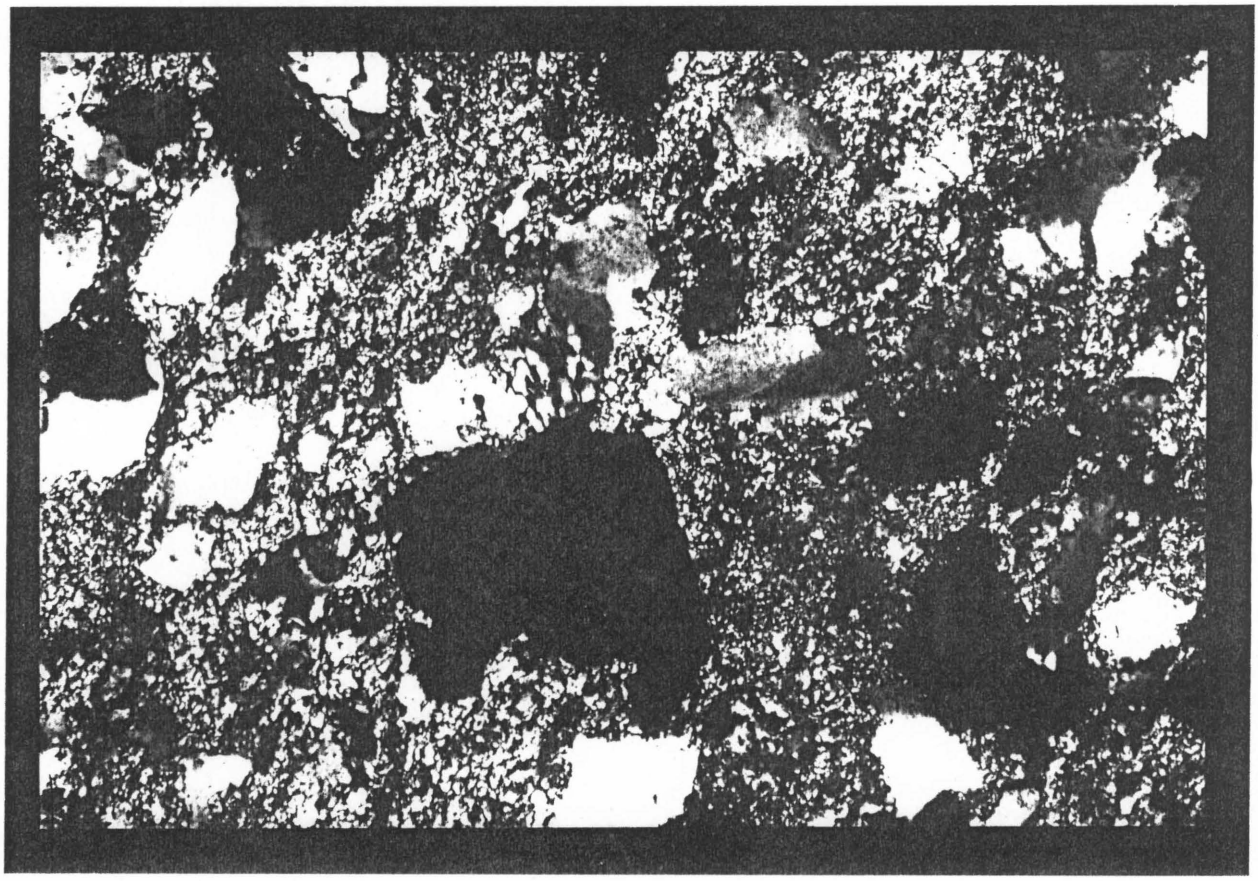

Plate 15. Late stage pyritic overgrowths (Py = pyrite).

Plate 16. Recrystalization of quartz along grain boundaries and undulose extinction in quartz, Mamba Shear Zone (Q=quartz).

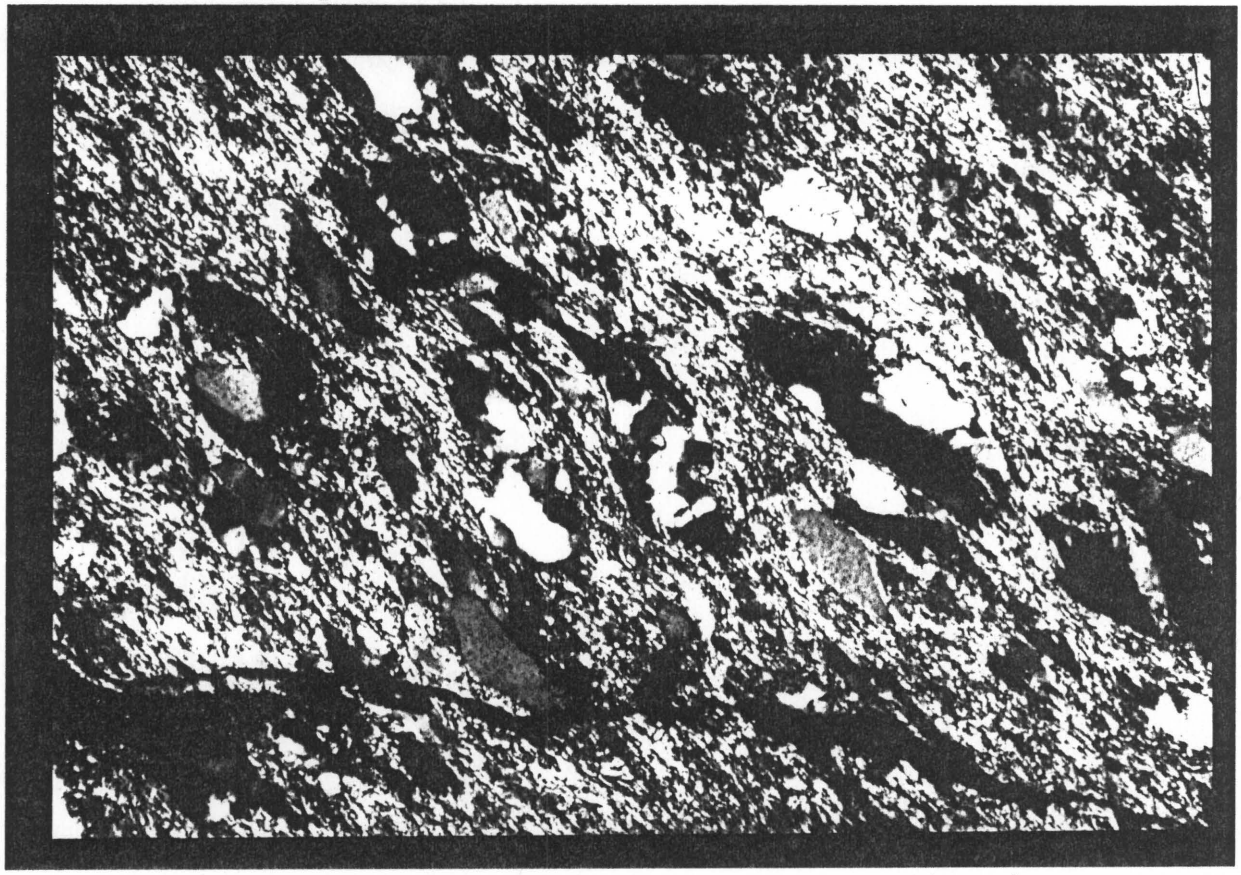

Plate 17. Shear fabric defined by orientated white mica flakes (M=mica, F=feldspar).

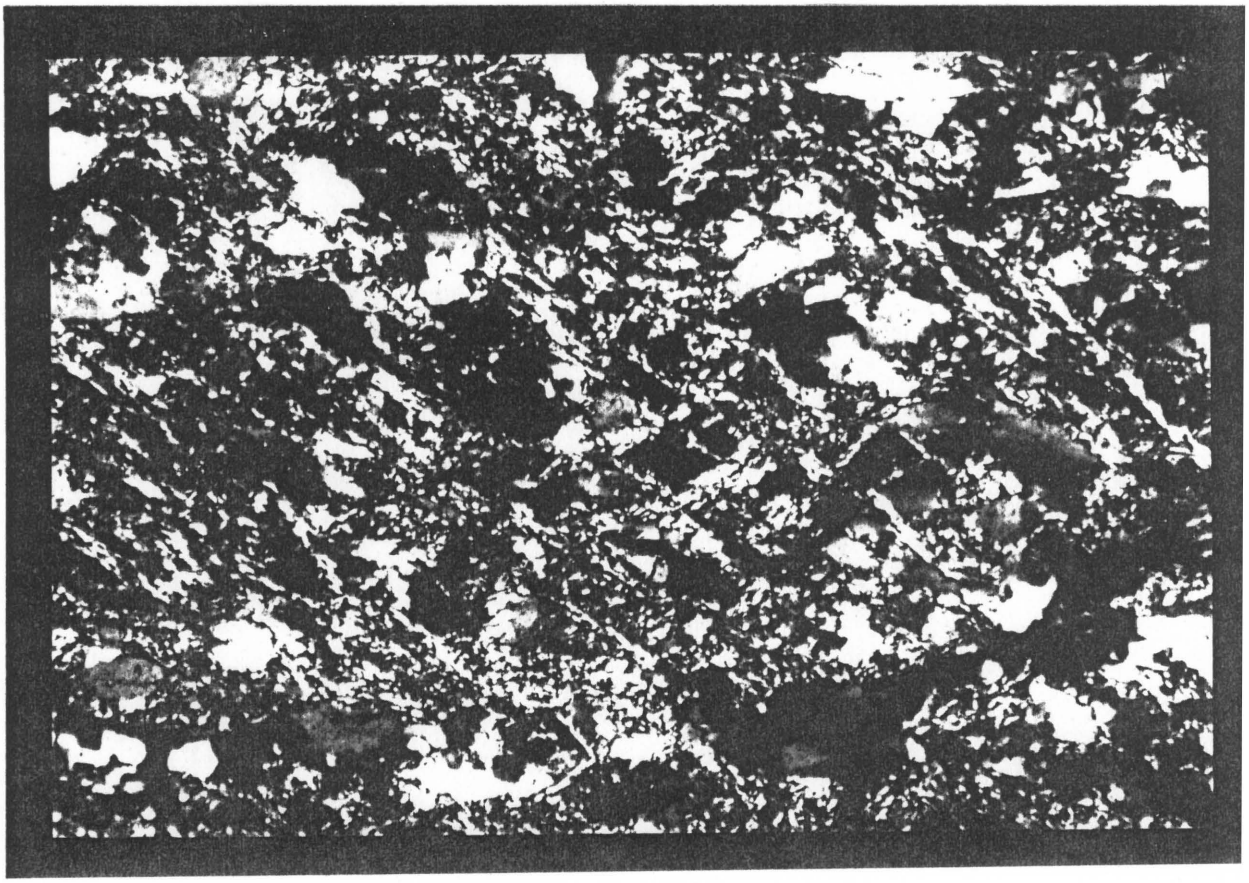

Plate 18. Second cleavage development (M = mica, S1 = primary, S2 = secondary cleavage).

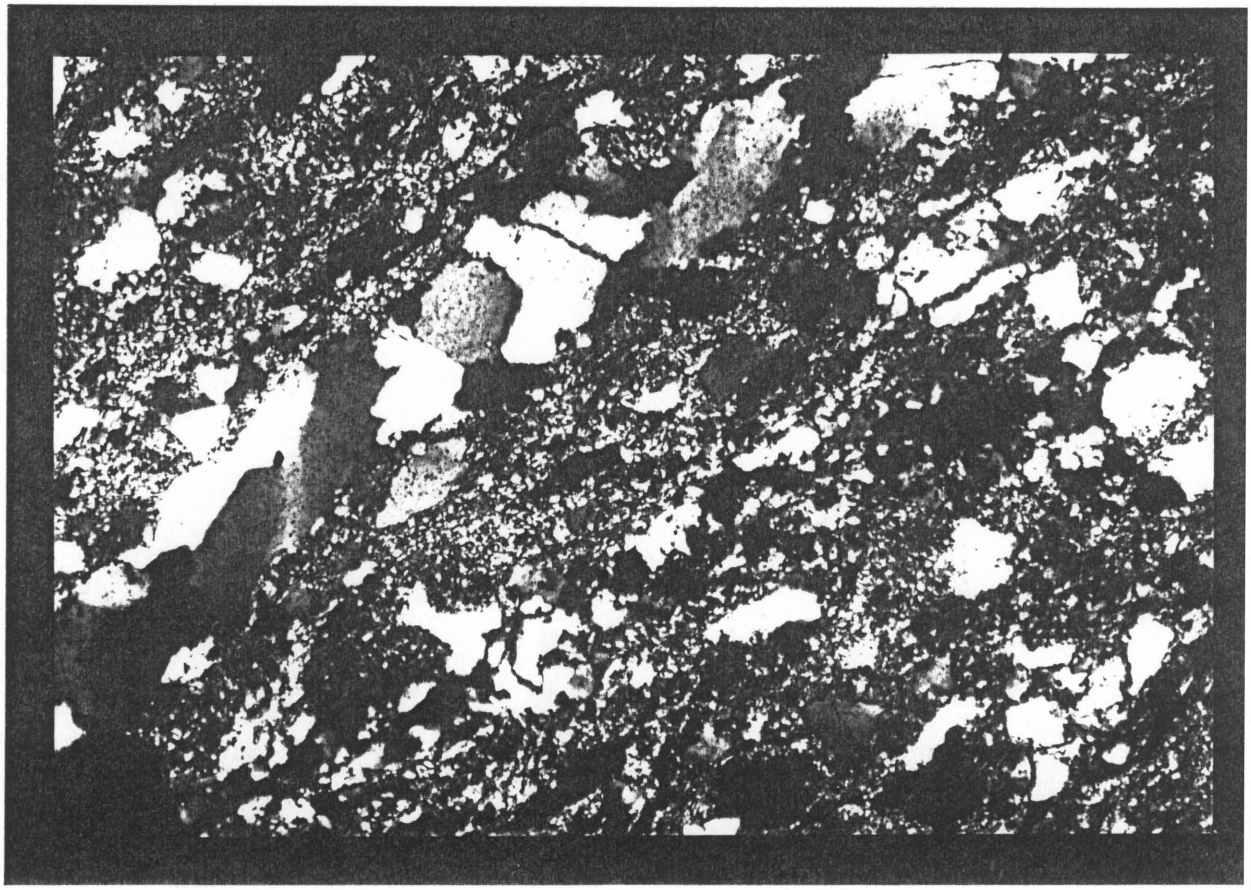

Plate 19. Fine grained groundmass carbonate alteration (Q = quartz, C = carbonate).

This form of carbonate mineral is less than 15 micrometres in diameter and is strongly associated with increased sulphide proportions (Plate 20), and increased gold values. The second carbonate mineral present occurs as large crystal-size overgrowths (up to 300 micrometres in diameter), and are extensively twinned (Plate 21). The youngest carbonate minerals present are those associated with the quartz-carbonate veins (Plate 22). The crystal size of these carbonates is largely dominated by the vein width itself. X.R.D. analyses of all three carbonates present showed the existence of dolomitic and ankeritic carbonate. It is, however, not possible to distinguish between the two microscopically.

The sulphide mineralogy is dominated by pyrite and arsenopyrite, while minor amounts of pentlandite, sphalerite, pyrrhotite, and Ni-Co sulphides occur. Pyrite occurs as both discrete crystals (Plate 23) or as pyrite-arsenopyrite assemblages (Plate 24). The former occurs as euhedral crystals dominantly less than 150 micrometres in diameter, while the latter occur as irregular masses up to 240 micrometres in diameter. The euhedral pyrite has fewer inclusions than the irregular masses.

The irregular masses of pyrite may enclose arsenopyrite crystals poikilitically to sub-poikilitically, while they enclose all occurrences of pyrrhotite, sphalerite and gold poikilitically (Plate 25). Both the pyrrhotite and sphalerite are less than 20 micrometres in diameter and have irregular crystal shapes.

Arsenopyrite occurs either in association with pyrite or in isolation. The former may be enclosed by the pyrite poikilitically or sub-poikilitically. Both forms of arsenopyrite are inclusion-poor and range in size from less than 10 micrometres up to 100 micrometres.

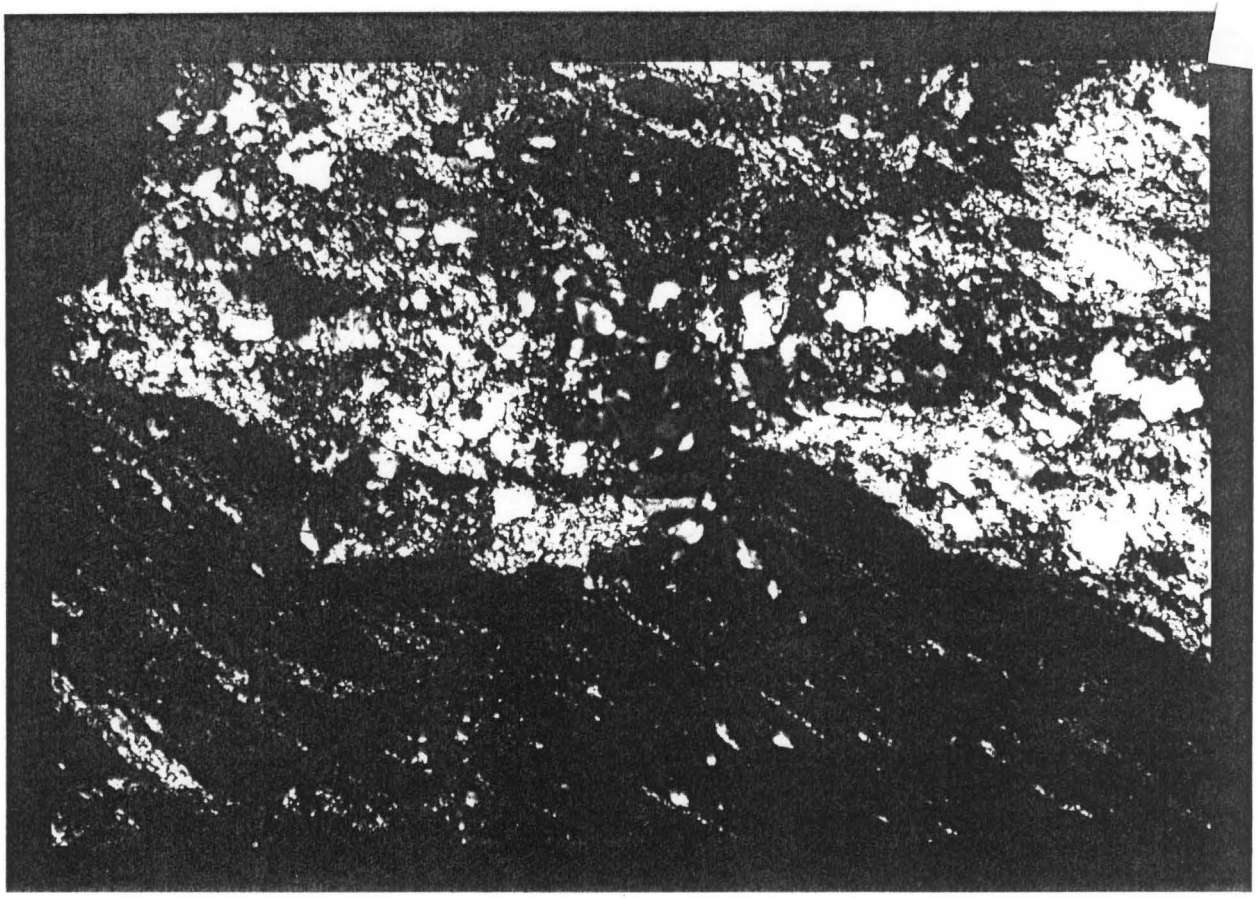

Plate 20. Fine grained groundmass carbonate-sulphide alteration (S=sulphide).

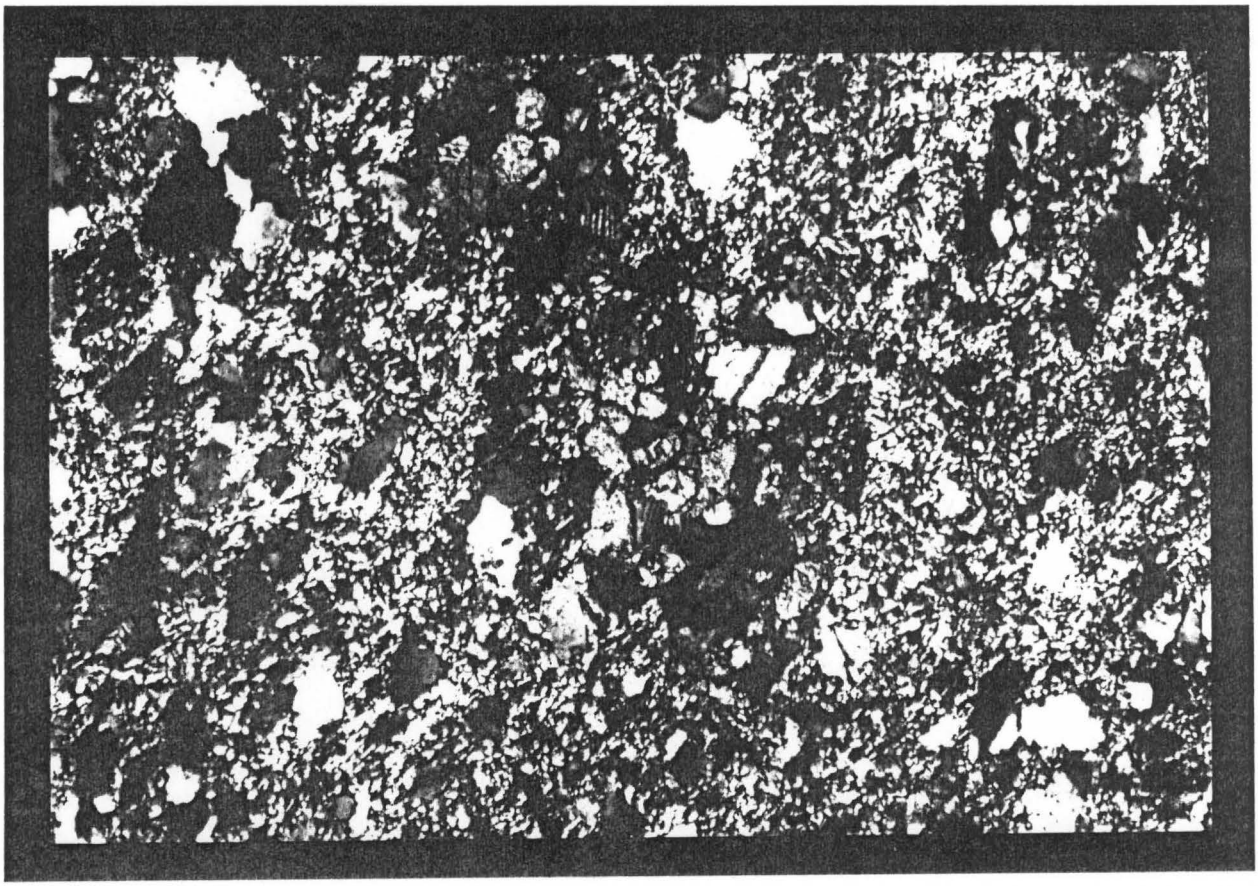

Plate 21. Large twinned carbonate alteration (C=carbonate).

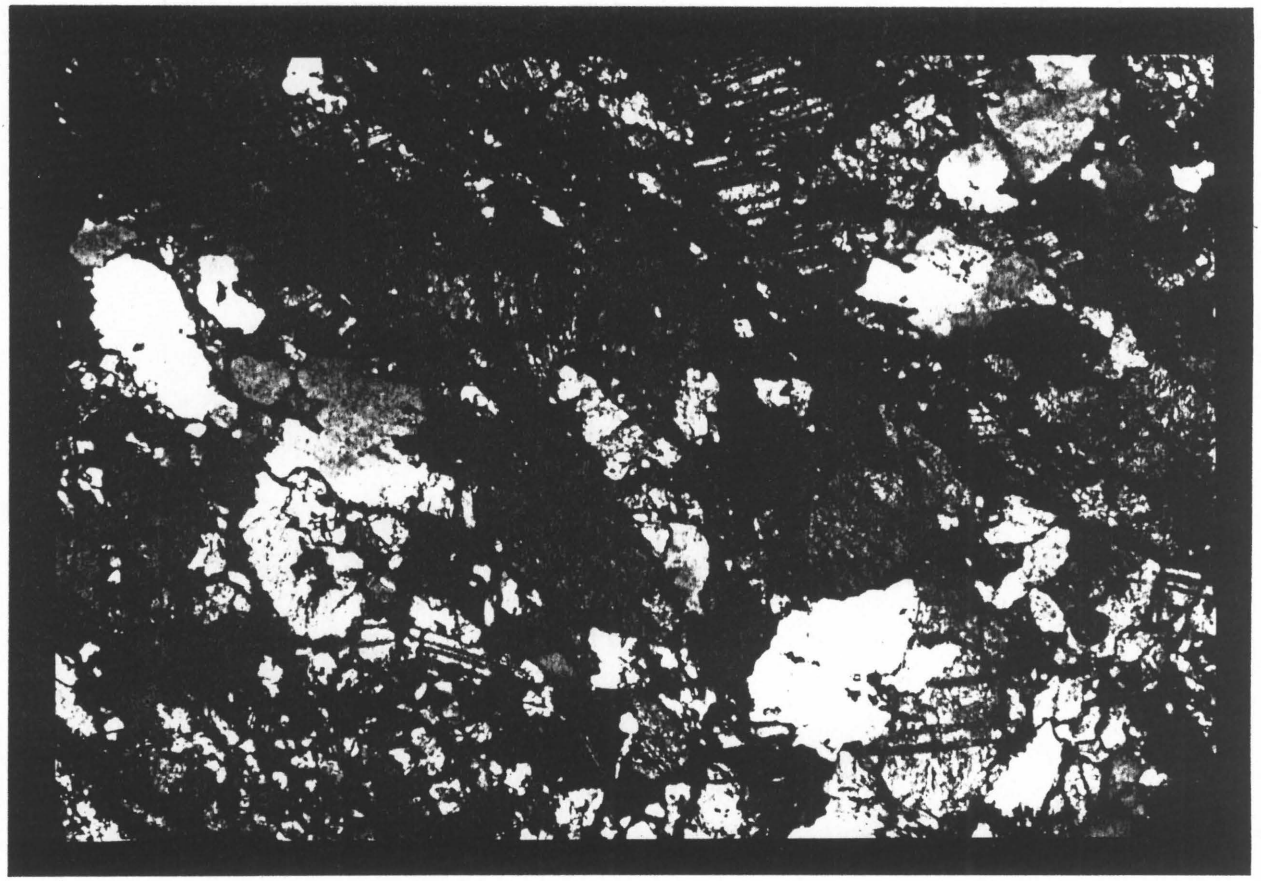

Plate 22. Twinned carbonate associated with veining (C=carbonate).

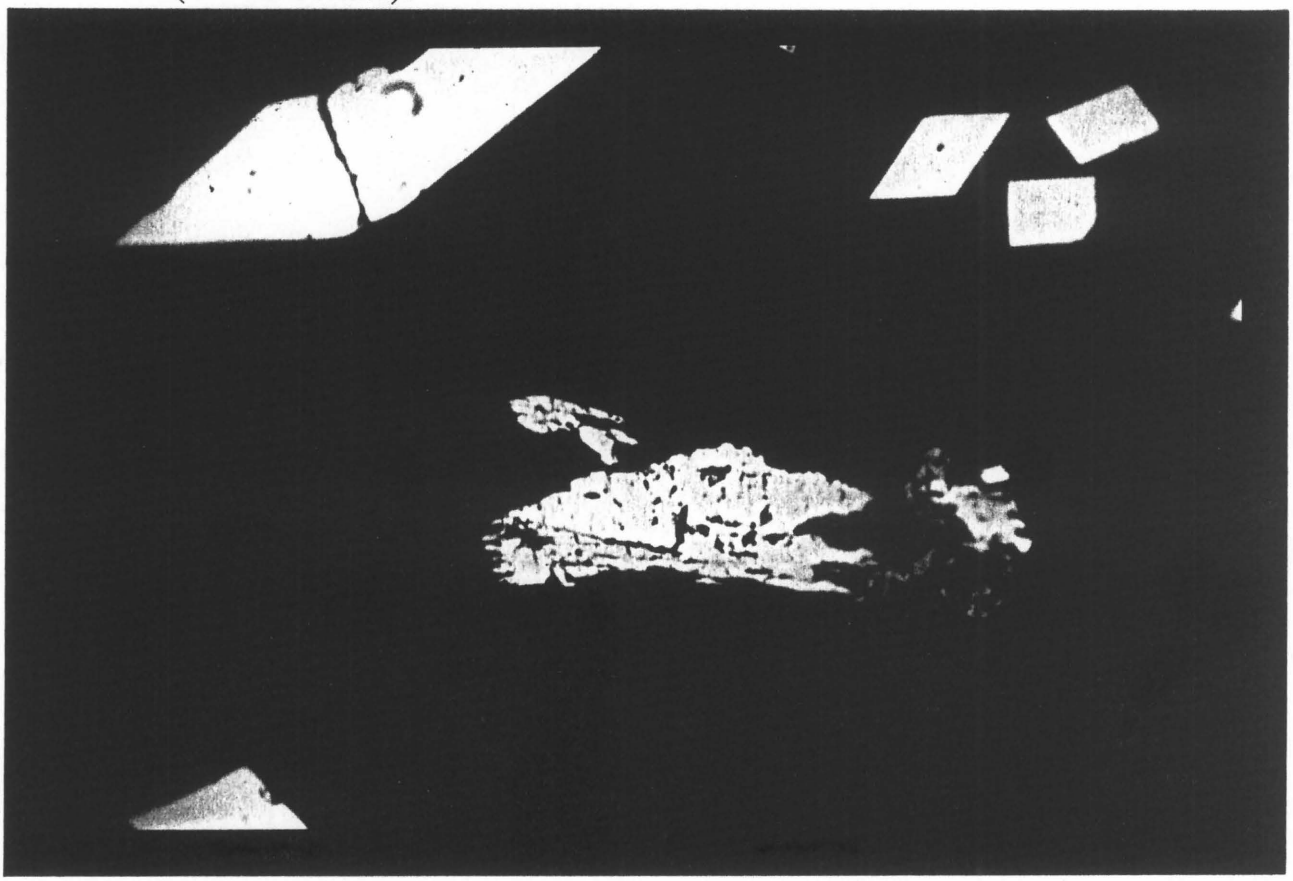

Plate 23. Discrete pyrite crystals (Py=pyrite, Apy=arsenopyrite).

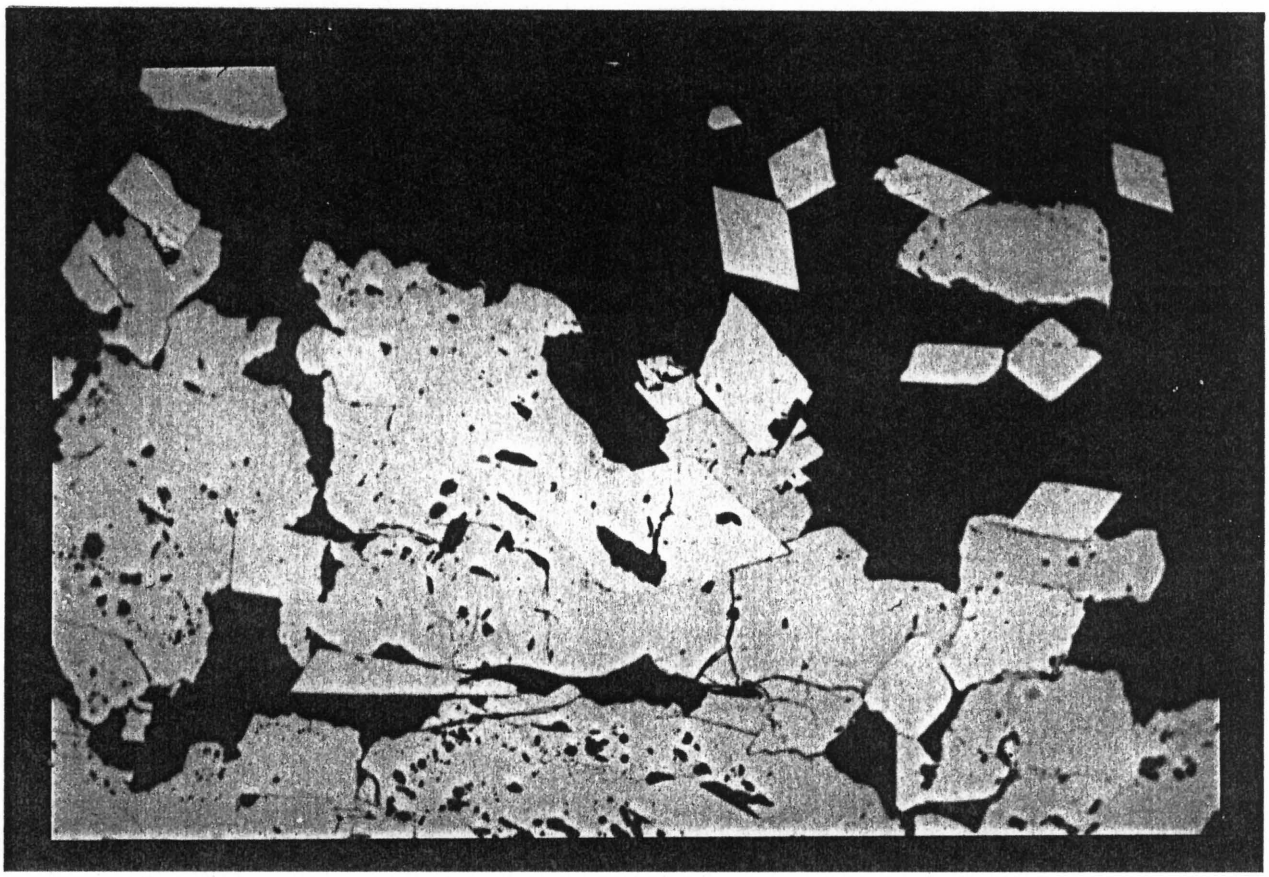

Plate 24. Pyrite-arsenopyrite associations (Py=pyrite, Apy=arsenopyrite).

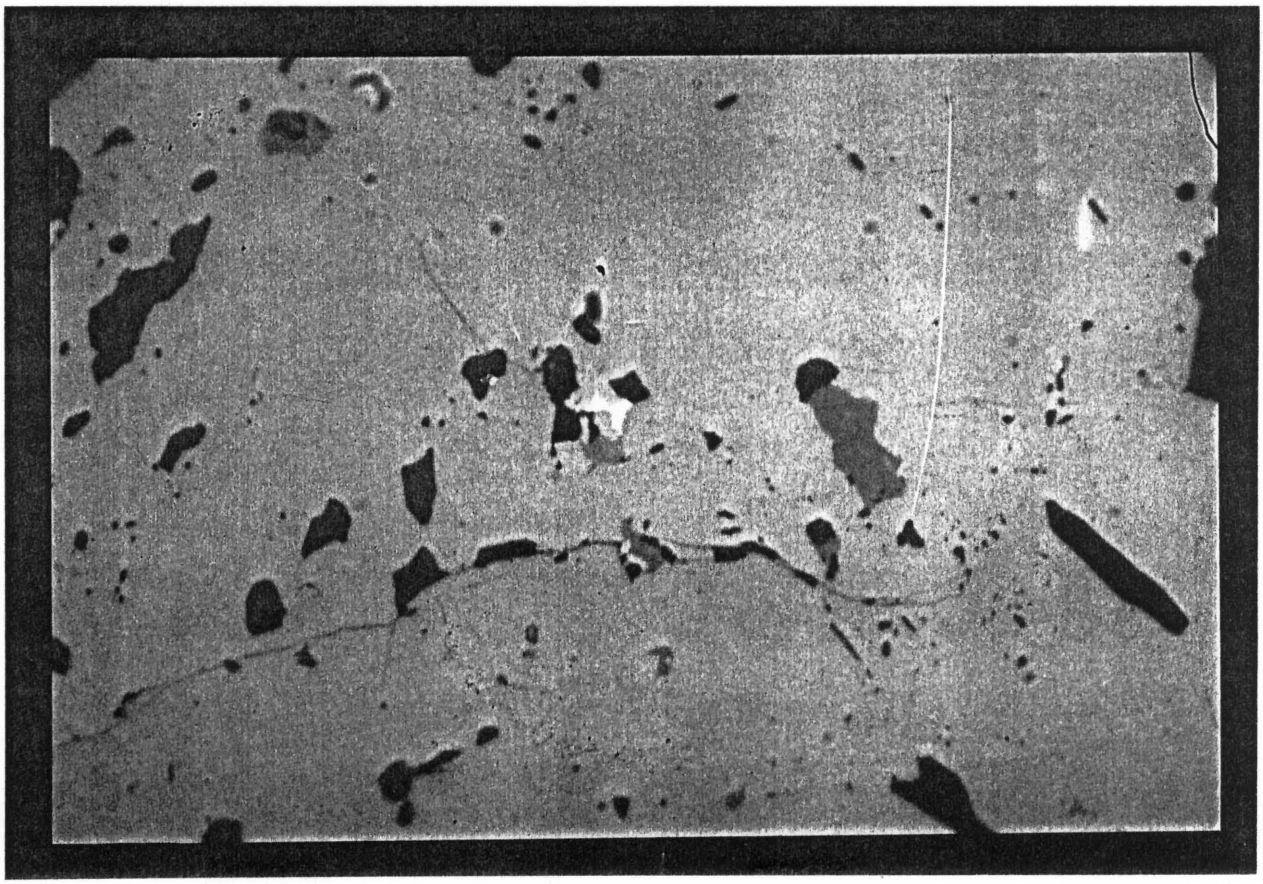

Plate 25. Pyrrhotite-sphalerite-gold in pyrite (Po=pyrrhotite, S=sphalerite, Au=gold).

The latter arsenopyrite occurs as discrete laths (up to 400 micrometres in length; Plate 26), as pseudorhombic crystals and twins (225 micrometres or less; Plate 26), or as rosettes of both lath shaped and euhedral arsenopyrite (Plate 27).

Pentlandite, sphalerite, and pyrrhotite are all poikilitically enclosed within the pyrite or arsenopyrite of the pyrite-arsenopyrite masses (Plate 25) and form less than 5% of the sulphides in the shear zone.

The occurrence of tourmaline in the Mamba Shear Zone is particularly interesting. The individual tourmaline crystals are generally exclusively associated with quartz and arsenopyrite. The tourmaline crystals show no preferred orientation, are well zoned (Plate 28) and are typically associated with elevated sulphide concentrations (Plate 29). Individual crystals range in size from less than 30 micrometres up to 1.6 mm in length. Only minor deformation of the crystals is seen, suggesting that they have been emplaced late in the development of the shear zone.

Gold in the Mamba Shear Zone is dominantly submicroscopic, and was only rarely identified in arsenopyrite laths or in the central portion of rutile-bearing quartz veins. In both cases the gold is less than 15 micrometres in size. A strong positive correlation exists between higher gold values and arsenopyrite concentration.

4.2 Mineralogy of the Eureka Shear Zone

Mineralisation within the Eureka Shear Zone is dominantly associated with arsenopyrite and to a lesser extent with pyrite. A single position was found where free gold occurred in association with the central quartz vein (Map 3).

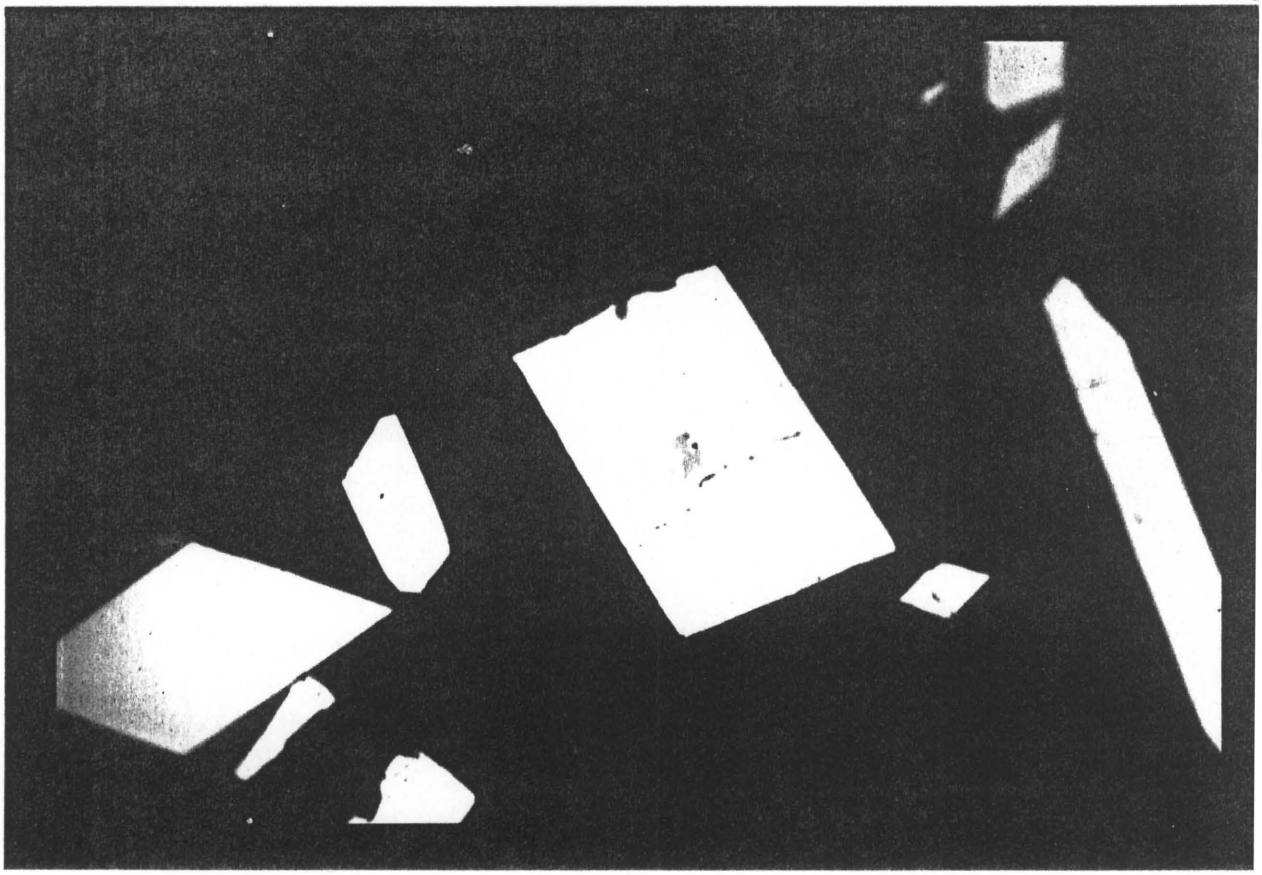

Plate 26. Psuedo-rhombic cross-section of arsenopyrite crystals (Apy=arsenopyrite, Po=pyrrhotite).

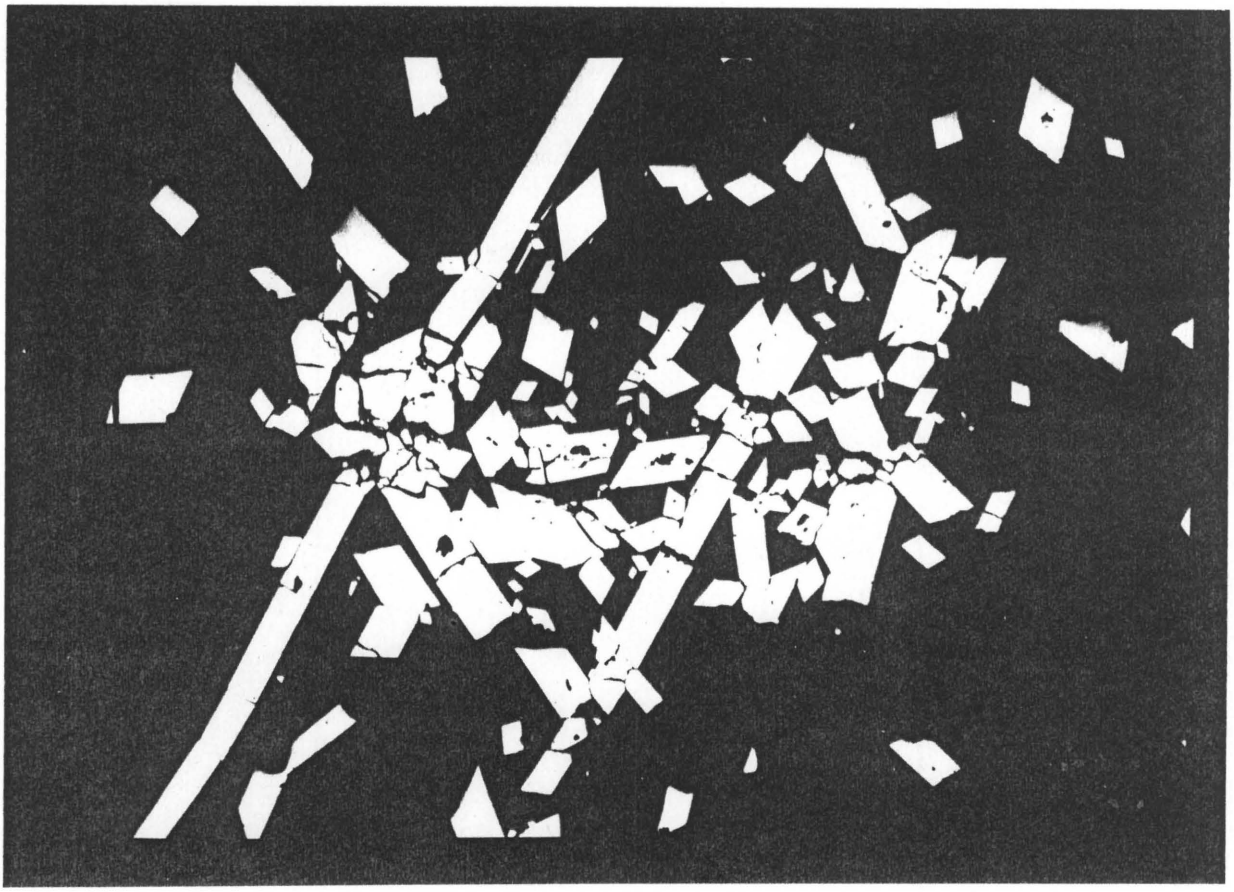

Plate 27. Arsenopyrite rosettes (Apy=arsenopyrite).

The arsenopyrite occurs as either vein of massive arsenopyrite or as disseminated acicular crystal growths within the shear zone. The greatest concentrations of arsenopyrite are often associated with quartz filled micro-fractures.

Pyrite mineralisation occurs dominantly as fine grained euhedral crystals, which are usually disseminated but may locally be massive. It is not possible to state conclusively how many mineralizing events have occurred within the Eureka Shear Zone; however, there was clearly mineralisation associated with the ductile deformation along the shear zone and with the central quartz vein.

Several forms of alteration are recognised within the shear zone, the most pervasive of which is carbonate alteration. In thin section at least two ages of carbonate alteration clearly overgrow all pre-existing fabric and veining. The older of the two carbonate alteration phases is a massive pervasive fine grained carbonate, while the younger is of a larger crystal size and often exhibits dolomitic/ankeritic twinning. This last phase clearly overgrows the massive carbonate phase. Silicification is limited to within the shear zone itself, while the carbonate alteration may extend up to 1.5m from the centre of the shear. Sericitic alteration of feldspar occurs within the shear zone. It is this sericite that is responsible for the main fabric development in the shear zone.

4.3 Mineralogy of the Cat's Cave Shear Zone

Mineralisation is in the form of fine grained to massive disseminated arsenopyrite with minor associated euhedral pyrite. Extensive oxidation of the ore minerals has occurred.

The alteration identified within and around the shear zone appears to be dominated by carbonate alteration and silicification, as seen from the pale green bleached zone which may extend up to 1m from the centre of the shear zone. It is not possible to ascribe the sericite to either the formation of sericite by alteration or to pre-existing sedimentary micas.

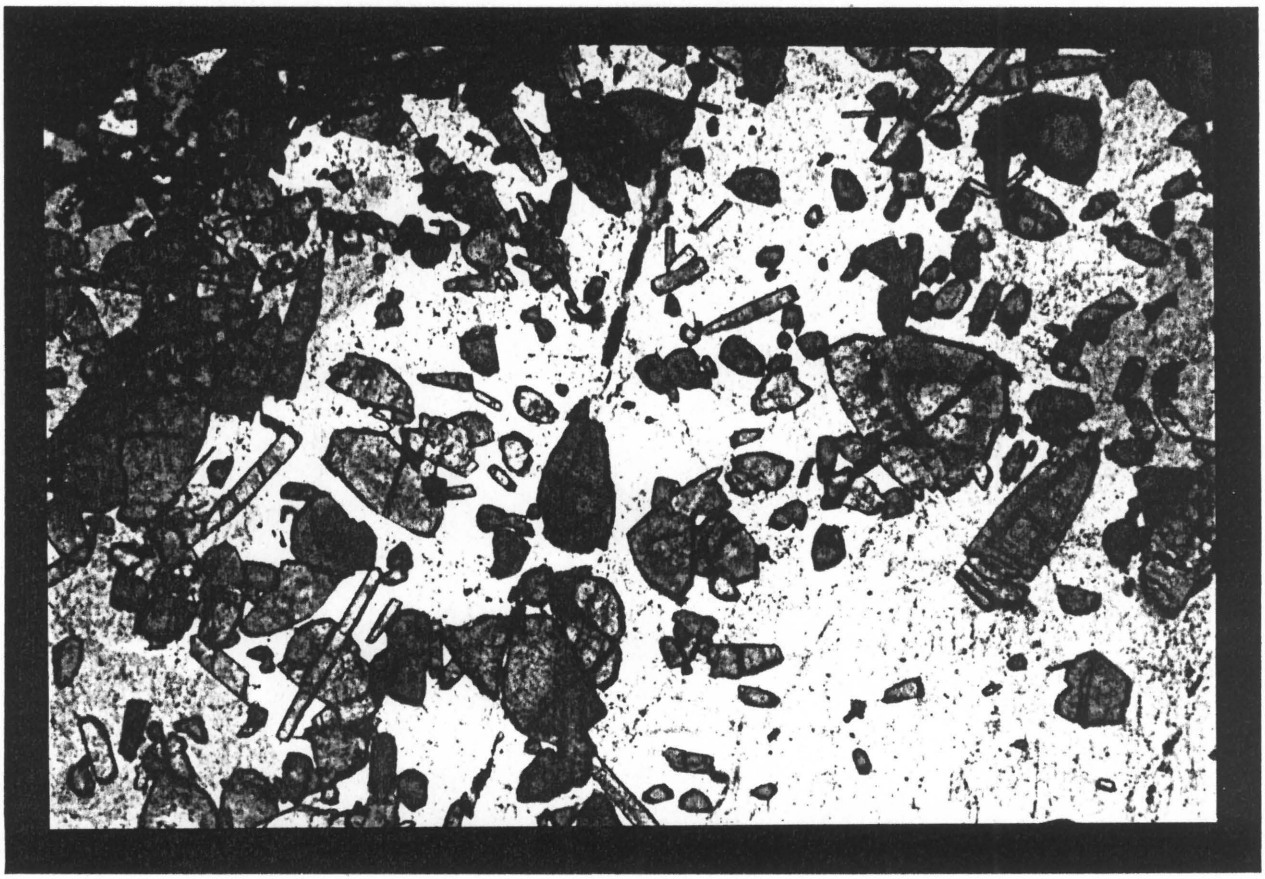

Plate 28. Randomly orientated, zoned tourmaline crystals (T=tourmaline, Q=quartz).

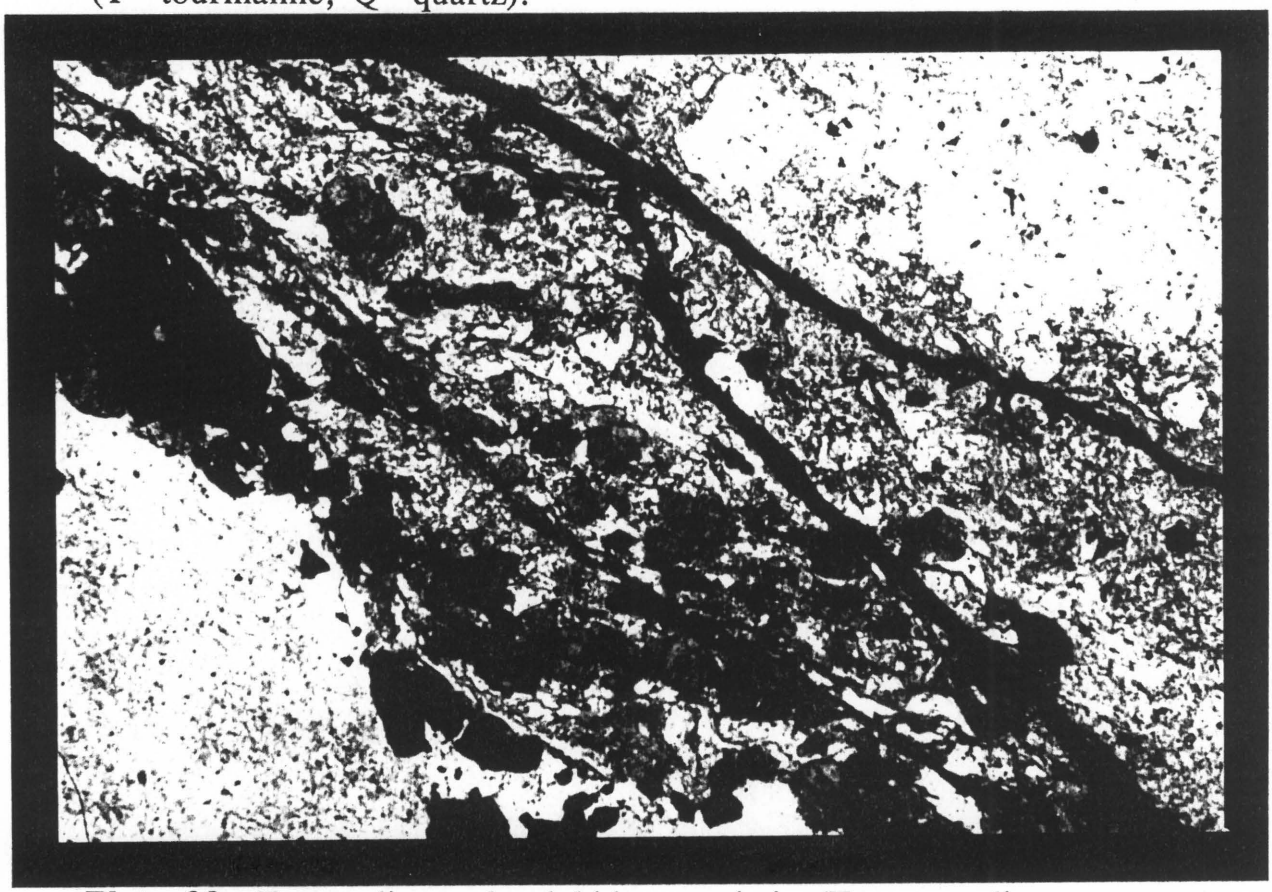

Plate 29. Tourmaline and sulphide associatio (T=tourmaline, S=sulphide).

4.4 Discussion

The host rock mineralogy in the Mamba and Eureka Shear Zones, is dominated by the presence of quartz, feldspar (dominantly plagioclase), and muscovite. Minor constituents such as chlorite, white mica, rutile and sulphide minerals may also occur. Rutile, quartz and feldspar remnants are all semi- to well-rounded, suggesting a degree of mechanical weathering presumably due to sedimentary reworking. This is in line with Eriksson's (1977, 1978, 1980) finding that the Moodies Group sediments, in the Eureka Syncline area, correspond to those formed by "active progradation of alluvial plain sediments building directly onto shelf accumulations or continental margins".

Chlorite is present in minor amounts, associated with both quartz and feldspar throughout the host rock, a situation which typifies lower greenschist facies metamorphism (Miyashiro, 1981; Turner and Verhoogen, 1960; Best, 1982). The host rock is also crosscut by a number of veins, dominantly of quartz-carbonate composition. These veins may be either sulphide-bearing or barren, and in both cases are not auriferous. The veins may have formed either as discrete intrusive events associated with, or independent from the neighbouring shear zone, as pressure solution features (Beach, 1974; Beach, 1979; Rutter, 1976), or as one of the alteration products from the sericitization process documented above.

The presence of tourmaline within the shear zones clearly points to a boron-rich fluid phase, the most obvious source of which is the surrounding adamellite terrane (e.g. the Nelspruit pluton, L.Robb pers. comm., 1989). Furthermore, the fact that the tourmaline is always associated with undeformed acicular arsenopyrite crystals and elevated gold values, suggests the movement of a late-stage auriferous granitic fluid along the shear zones. Mineralisation of this age is commonly found in zones of brecciated quartz. This brecciation is assumed to be due to fluid pressure exceeding the tensile strength of the host rock/shear zone, resulting in

hydraulic brecciation (Phillips, 1972; Kerrich and Allison, 1978; Sibson et al., 1988; Vearncombe, 1989). This brecciation then provides an increased porosity and an ideal site for mineralisation (Kerrich and Allison, 1978).

Several ages of sulphide precede the tourmaline-bearing age of mineralisation, as demonstrated by the numerous sulphide veins documented in Chapter 2. It is not possible to state that all these vein-associated sulphides are auriferous. However, elevated gold values were identified where the tourmaline-bearing vein phase was absent. The quartz veins present in the shear zone can be grouped into relative ages by various features such as composition and crosscutting relationships (Haynes, 1987). These ages are outlined in Table 3. Their major significance is that they serve to indicate that the shear zone did not form during a single deformation event, but rather as a progressive event and that mineralisation occurred over an extended time period.

Several ages of dominantly carbonate alteration have also been identified. In all cases the carbonate alteration overprints all pre-existing fabrics and minerals assemblages, suggesting it to be a late stage event. The carbonate alteration is generally evenly distributed about the shear zones, and decreases in intensity away from the shear zone. The last quartz-carbonate vein event was accompanied by dominantly dolomitic and/or ankeritic carbonate assemblages. Although only three phases of carbonate alteration were identified, it is tentatively suggested that each quartz and/or quartz-carbonate vein age may have had an associated carbonate alteration phase which was subsequently overprinted by the following alteration front.

In addition to the carbonate alteration, extensive sericitization also occurs within the shear zones, along cleavage, and gradationally into the host rock. Sericitization is strongest within the shear zones and decreases with increasing distance from the shear. From the above alteration equations, a potassic volatile phase is required for alteration to proceed. A potential source for such a fluid is the volatile phases

driven off during the emplacement of granites (L.Robb pers. comm., 1989). Emplacement of the various components of the granitic terrane, surrounding the Barberton supracrustal remnant, occurred over a prolonged period (Table 2), potentially generating several ages of volatiles, all of which were potentially mineralizing, and any number of which may have passed through the Margaret shear zones.

CHAPTER 5

GEOCHEMISTRY OF THE MAMBA SHEAR ZONE

5.1 Method

The aim of the geochemical investigation was to document the alteration halo associated with both a mineralized and an unmineralized quartz-filled shear zone. To achieve this a diamond drill borehole was drilled orthogonal to both the mineralized and unmineralized shear zones, with one of the boreholes being extended for 80 metres into the host rock to determine the background composition. Although the two shear zones are not along strike from each other, the host rocks are assumed to be chemically comparable. The core was then split and one half sampled. Individual samples were chosen on geological criteria and submitted to the University of Natal, Pietermaritzburg, for analysis. Detailed logging of the core was conducted prior to sampling, and is presented in Appendix 1.

Analyses were conducted using the Phillips PW 14-10 XRF spectrometer. The operating conditions, and the various X-ray tubes used for the analyses, are given in Appendix 2.

The chemical data were manipulated by means of the isocon method, as proposed by Grant (1986). The method involves plotting an analysed element from an unaltered sample, against the same element from an altered sample. This plotting process is then repeated for all the elements analysed. It is important to state that this method is only applicable if the assumption can be made that the starting compositions of both the altered and unaltered samples were initially the same. The isocon method requires altered sample compositions to be compared with a predicted composition as determined from an isocon determined for that sample. The isocon is constructed by drawing a line through the origin and the plot of an immobile element concentration on that plot. Aluminium is regarded as immobile in hydrothermal systems

(H.L.Barnes pers. comm, 1990) and was thus selected to locate the isocon. The relative concentrations of the immobile elements in each sample will vary, hence changing the slope of the isocon. The assumption that aluminium is immobile was substantiated to some degree by the fact that lanthanum and zirconium also plot close to the isocon.

Individual samples which plot above the isocon indicate enrichment of the element under consideration in the altered sample (y-axis is the altered sample, x-axis is the unaltered sample), while those that plot below the isocon show depletion for that element in the altered sample (Figure 14).

The concentration of a certain element, less the predicted original concentration at that point (as defined by the relative isocon), is referred to as the residual value for that sample. A plot of these residual values for a single element versus distance along a borehole thus reflects the relative enrichments or depletions of that element through the shear zone. Furthermore, the size of the residual value (either enriched or depleted) is a direct measure of the mobility of that element during hydrothermal activity along the shear zone, and may be directly compared to the mobility of the other elements within the same shear zone.

When comparing the residual data for the mineralized and un-mineralized shear it is important to remember that different background compositions were used to determine the residual values; hence a direct comparison of the mobility of elements between the two shear zones is not possible. Due to the fact that aluminium, lanthanum, and zirconium were used in defining the isocon, no residual values can be calculated for them.

The whole rock chemistry of the individual samples, as well as the relative enrichments and depletions per element (i.e. the residual values) are presented in Appendix 3. A number of important factors can influence the whole rock chemistry for each sample and will be discussed briefly below.

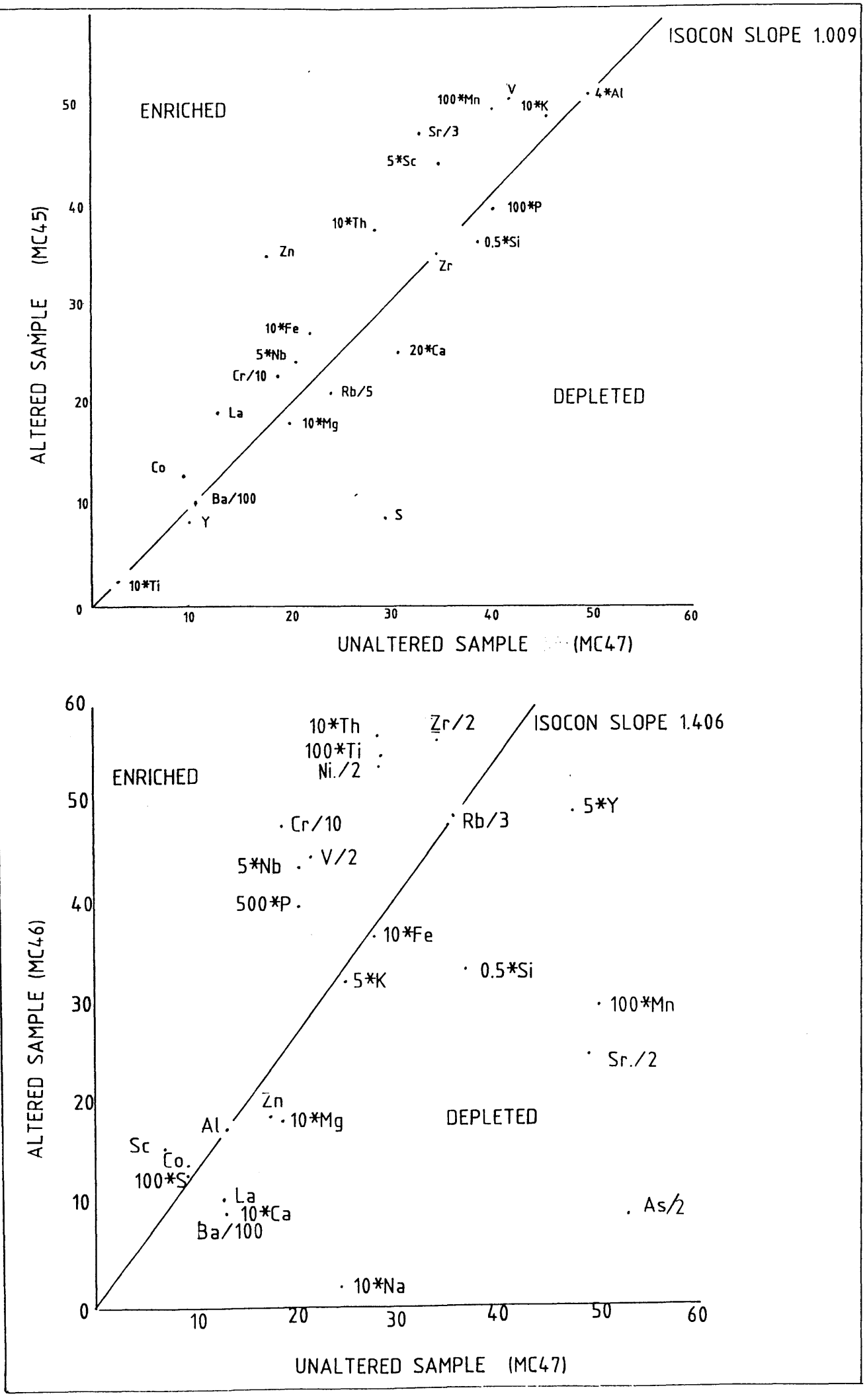

FIGURE 14. THE CONSTRUCTION OF AN ISOCON (after GRANT, 1986)

The first factor is the role of lithology. Although on first inspection and in the literature (SACS, 1980; Anhaeusser, 1986) the Clutha Formation of the Moodies Group, is considered to have a limited range of rock types, thin section evidence indicates a large range in composition on a local scale. Perhaps the most noticeable of these ranges is the varying abundance of plagioclase and the mechanical sorting of heavy minerals into distinct strata by sedimentary processes, both of which will have a marked effect on the whole rock geochemistry. It is important to note that in the analyses presented in Appendix 3 and in the geochemical trends below, no account is taken of possible lithological variations, and that only loss on ignition, and not individual CO_2 and H_2O^- values were determined. No opinion can therefor be expressed on the role of either of these compounds on the mineralisation process.

A second factor which requires mention is the role that basin dewatering and regional dynamothermal metamorphism had on the original whole rock composition (Barley, 1987). During the dewatering process of a sedimentary pile as thick as the Moodies Group (approximately 3025 metres; SACS, 1980) in combination with elevated geothermal gradients in the Archaean, there may have been minor modification of the original whole rock chemistry. In addition to this, the entire Barberton supracrustal remnant has been subjected to several local and regional dynamothermal metamorphic events (Ramsay, 1963; Anhaeusser, 1965; Roering, 1965; Anhaeusser, 1986). The sediments in the Moodies Group have been metamorphosed to lower greenschist facies (Viljoen and Viljoen, 1969a; Ramsay, 1963; Roering, 1965; Anhaeusser, 1965, 1986; Anhaeusser and Viljoen, 1965; Schouwstra, 1988; Robertson, 1989), which in turn may have resulted in modification of the original whole rock chemistry. If either one or both the above were effective then at no stage is the original chemistry of the Moodies Group arkoses apparent.

In addition to all the above, there is also the effect of late superimposed hydrothermal alteration associated with individual faults and shears. Although the hydrothermal alteration is superimposed on all the above conditions, the alteration trends may not be clearly visible for the following reasons: (1) structural evidence in-

dicates that the shear sets in the Moodies Group in the Sheba Mine vicinity were active over an extended time period, as seen from the numerous vein ages in the shear zones. It is feasible to assume that each vein event was accompanied by its own unique alteration halo over this extended period; (2) individual hydrothermal solutions may have had slightly differing compositions, resulting in different alteration fluid compositions, hence different alteration assemblages; (3) emplacement of the various veins and their associated alteration haloes need not have been in a symmetrical arrangement or in the centre of the shear zone, thus resulting in superimposition of alteration assemblages or even the alteration of pre-existing alteration assemblages.

To simplify these problems a discussion of the alteration patterns assumes: (1) rock types had the same initial chemistry, (2) the effects of dewatering have effected the host rocks uniformly, (3) metamorphic effects have been uniform throughout the area. The alteration halo is thus assumed to reflect the hydrothermal alteration only, and does not take account of individual alteration events.

5.2 Element Mobility during Hydrothermal Alteration

In all cases the discussion is restricted to that of the residual values as defined above. The element mobilities are grouped into intense, moderate, and low. The elements falling into the low mobility category effectively act as immobile elements. The low mobility calculated may be due to analytical problems associated with the detection limits for the respective elements at these low concentrations (eg. the detection of gold in low concentrations by fire assay). A further subdivision of individual elements can be made on the basis of their enrichment or depletion through the shear zone. The various element mobilities are summarized in Table 6.

SiO_2 is by far the most active element within both shear zones and shows a marked enrichment in both. MgO, K_2O, Na_2O, Fe_2O_3, CaO, and S comprise the moderate mobility group. Of interest is the fact that K_2O and CaO are enriched in both shear zones while the remaining elements show an antithetic relationship. TiO_2, MnO, and P_2O_5 form the low mobility group.

Table 6. Element Mobility During Hydrothermal Alteration, Mamba Shear Zone.

Relative	*Mineralized*		*Element*	*Unmineralized*		*Relative*
Concentration	*Shear*			*Shear*		*Concentration*
	Activity			*Activity*		
	Max.	**Min.**		**Max.**	**Min.**	
Enriched	-34	56	SiO2	-70	95	Enriched
Enriched	-0.9	1.1	MgO	-3.4	0.4	Depleted
Enriched	-1.0	1.1	K2O	-4.6	1.9	Enriched
Depleted	-3.9	1.1	Na2O	-1.8	1.2	Enriched
Enriched	-0.8	2.2	Fe2O3	-5.1	1.4	Depleted
Enriched	-0.6	1.9	CaO	-1.4	4.6	Enriched
Enriched	-0.2	1.6	S	-0.2	0.33	Irregular
Constant			TiO2			Constant
Constant			MnO			Constant
Constant			P2O5			Constant
Depleted	-160	65	Ba	-80	190	Enriched
Depleted	-140	240	U	-600	750	Enriched
Enriched	-30	250	Cr	-200	60	Depleted
Enriched	-50	1400	As	-70	430	Enriched
Enriched	-21	29	Rb	-110	10	Depleted
Enriched	-16	18	V	-64	11	Depleted
Enriched	-22	36	Ni	-150	10	Depleted
Depleted	-12	20	Cu	-20	18	Irregular
Enriched	-37	63	Zn	-65	15	Irregular
Enriched	-10	130	Pb	-3	35	Enriched
Irregular	-0.8	1.1	Th	-0.4	1.6	Irregular
Enriched	-0.7	2.7	Nb	-1.7	1.3	Depleted
Irregular	-3	4	Y	-3.9	1.6	Irregular
Enriched	-4.3	4.7	Ga	-16	2	Enriched
Enriched	-3.4	4.1	Sc	-12	3	Depleted
Irregular	-5.7	4.3	Co	-17	1	Depleted
Enriched	-0.2	2.1	**Au**	0.0	0.66	Enriched

The trace elements can be grouped in exactly the same manner with Ba, U, Cr, and As comprising the high mobility group. Of interest is the strongly developed antithetic relationship between these elements in the two shear zones, the exception being As which is enriched in both. Rb, V, Ni, Cu, Zn, and Pb make up the moderate mobility group. The antithetic relationship persists in this group, with Pb being the exception in that it is enriched in both shears. Th, Nb, Y, Ga, Sc, Co, and Au comprise the low mobility group. Where predictions are possible the antithetic relationship between the two shears persists as seen from Nb and Sc which are both enriched in the mineralized shear and depleted in the unmineralized shear zone.

5.3 Mineral Assemblage Predictions

Firstly, residual major element trends were investigated across the shear zone with the aim of identifying coupled elements and hence predicting mineral assemblages present. Secondly, residual trace element trends were investigated and used to further isolate the minerals present across the shear zone. This exercise was repeated for both the mineralized and unmineralized shear zones. A central dark quartz vein (CDQV) is used as a reference point and is indicated on all major and trace element plots.

a) Mineralized Shear Zone: Major Element Trends

In an attempt to identify elements with similar residuals (coupled elements), attention was given to firstly grouping elements with similar ionic radius and ionic charge (Figure 15), and secondly by testing the potential correlation between the residuals of the elements by means of a correlation matrix (Table 7).

i) Residuals of CaO, Fe_2O_3 and MgO

A strong correlation exists between Fe_2O_3 and MgO (no attempt was made to distinguish between ferrous and ferric iron) and to a lesser extent between calcium, magnesium and iron. Iron and magnesium showed a sympathetic relationship up to 20m from the CDQV, indicating activity up to this point. Calcium shows particularly good correlation peaks with MgO and Fe_2O_3 in and around the CDQV, but is less reliable beyond 20m (Figure 16). Several individual CaO peaks were apparent, within the 20m zone, which were characterized by the lack of associated Fe_2O_3 and MgO peaks (Figure 17). No other major elements peak in the same area, thus suggesting that the peaks represent calcite veins or calcite-rich zones. The CaO, Fe_2O_3 and MgO peaks are not accompanied by SiO_2 peaks, and are thus attributed to dolomite and/or ankerite formation.

An important inference from this is the fact that the dolomite/ankerite presence is most noticeable in the immediate vicinity of the CDQV.

ii) Residuals of K_2O, Fe_2O_3 and MgO

As has already been discussed there is a strong correlation between Fe_2O_3 and MgO throughout the shear zone. However, at a distance of 10m and less there is a marked antithetic relationship between K_2O on the one hand and Fe_2O_3 and MgO on the other (Figure 18). The regional metamorphic grade is lower greenschist (Anhaeusser, 1986; Schouwstra, 1988, Robertson, 1989) which is characterized by the presence of chlorite, of which Fe_2O_3 and MgO are important constituents (Deer et al., 1966). The antithetic relationship between K_2O and Fe_2O_3 and MgO at less than 10m suggests the breakdown of chlorite, accompanied by the growth of a K-rich mineral.

iii) Residuals of K_2O and Na_2O

In the search for elements with a strong positive correlation it became evident that certain elements are equally characteristic by their negative correlation or antithetic relationship (Table 7). The most obvious example of this is K_2O and Na_2O. Three distinct zones are seen along the mineralized borehole trace, viz. (1) less than 10m, (2) 10 to 18m, and (3) greater than 18m (Figure 19). In the less than 10m zone K_2O and Na_2O show a strongly developed antithetic relationship (Figure 20), from 10 to 18m they are sympathetic, and from 18 to 43m they are unrelated. The primary source of Na in the metaarkoses can be ascribed to plagioclase, and that of K_2O to sericite and/or muscovite. It is therefore tentatively suggested that the area greater than 18m is affected primarily by sedimentary distribution of muscovite and plagioclase, while the 10 to 18m zone

is marked by minor sericitization of plagioclase with little primary muscovite. The zone adjacent to the CDQV is characterized by intense sericitization at the expense of plagioclase, hence the marked antithetic relationship. This relationship implies K metasomatism for a distance of at least 8m from the CDQV.

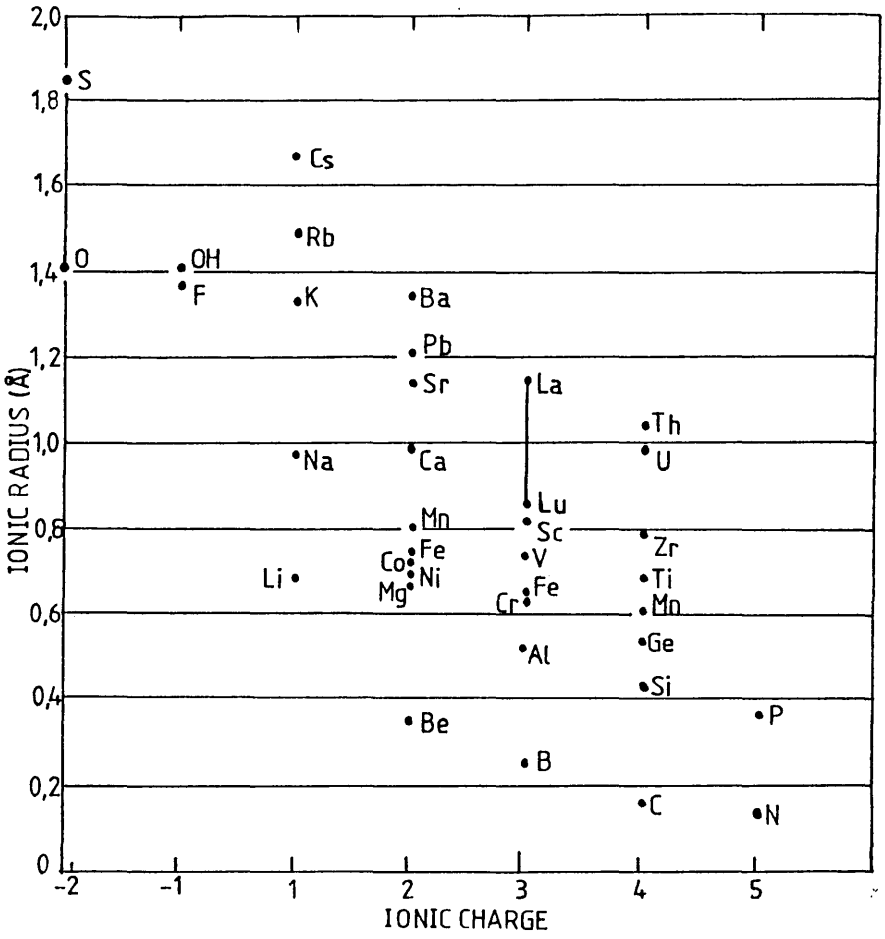

Figure 15. Relationship Between Ionic Charge and Ionic Radius for the More Common Elements

iv) Residuals of Fe_2O_3, S and As

Sulphur shows a particularly interesting peak arrangement across the mineralized borehole section. The most obvious effect is the presence of a broad peak in the immediate vicinity of the CDQV (Figure 21). This peak extends for up to 3m either side of

Table 7. Correlation Matrix For The Major Elements Across A Mineralized Shear Zone.

	SiO2	TiO2	Fe2O3	MnO	MgO	CaO	K2O	Na2O	P2O5	S	Au
SiO2	1.0000	-0.2355	0.5005	0.5200	0.4191	0.5741	0.4975	0.0826	0.3659	0.2241	0.7272
	0.0000	0.1071	0.0003	0.0002	0.0030	0.0000	0.0030	0.5767	0.0105	0.1257	0.0000
TiO2	-0.2355	1.0000	0.5528	-0.0587	0.3574	-0.0210	0.1140	-0.3688	0.3771	0.3365	0.0358
	0.1071	0.0000	0.0000	0.6920	0.0126	0.8872	0.4405	0.0099	0.0082	0.0193	0.8089
Fe2O3	0.5005	0.5528	1.0000	0.4310	0.7695	0.4519	0.3402	-0.2100	0.5259	0.4464	0.5353
	0.0003	0.0000	0.0000	0.0022	0.0000	0.0013	0.0180	0.1519	0.0001	0.0015	0.0001
MnO	0.5200	-0.0587	0.4310	1.0000	0.4891	0.6840	0.1997	-0.0591	0.3055	0.2285	0.4528
	0.0002	0.6920	0.0022	0.0000	0.0004	0.0000	0.1736	0.6897	0.0347	0.1182	0.0012
MgO	0.4191	0.3574	0.7695	0.4891	1.0000	0.5924	0.4050	-0.1492	0.2618	0.1668	0.2952
	0.0030	0.0126	0.0000	0.0004	0.0000	0.0000	0.0043	0.3115	0.0723	0.2572	0.0417
CaO	0.5741	-0.0210	0.4519	0.6840	0.5924	1.0000	0.1518	-0.3134	0.4921	0.4894	0.5839
	0.0000	0.8872	0.0013	0.0000	0.0000	0.0000	0.3031	0.0301	0.0004	0.0004	0.0000
K2O	0.4975	0.1140	0.3402	0.1997	0.4050	0.1518	1.0000	0.0837	-0.1559	-0.0888	0.0657
	0.0003	0.4405	0.0180	0.1736	0.0043	0.3031	0.0000	0.5718	0.2901	0.5483	0.6573
Na2O	0.0826	-0.3688	-0.2100	-0.0591	-0.1492	-0.3134	0.0837	1.0000	-0.4365	-0.8051	-0.2625
	0.5767	0.0099	0.1519	0.6897	0.3115	0.0301	0.5718	0.0000	0.0019	0.0000	0.0715
P2O5	0.3659	0.3771	0.5259	0.3055	0.2618	0.4921	-0.1559	-0.4365	1.0000	0.6536	0.7356
	0.0105	0.0082	0.0001	0.0347	0.0723	0.0004	0.2901	0.0019	0.0000	0.0000	0.0000
S	0.2241	0.3365	0.4464	0.2285	0.1668	0.4894	-0.0888	-0.8051	0.6536	1.0000	0.5739
	0.1257	0.0193	0.0015	0.1182	0.2572	0.0004	0.5483	0.0000	0.0000	0.0000	0.0000
Au	0.7272	0.0358	0.5353	0.4528	0.2952	0.5839	0.0657	-0.2625	0.7356	0.5739	1.0000
	0.0000	0.8089	0.0001	0.0012	0.0417	0.0000	0.6573	0.0715	0.0000	0.0000	0.0000

Coefficient

Significance Level

Figure 16. Plot of residual CaO, Fe2O3

& MgO vs Distance

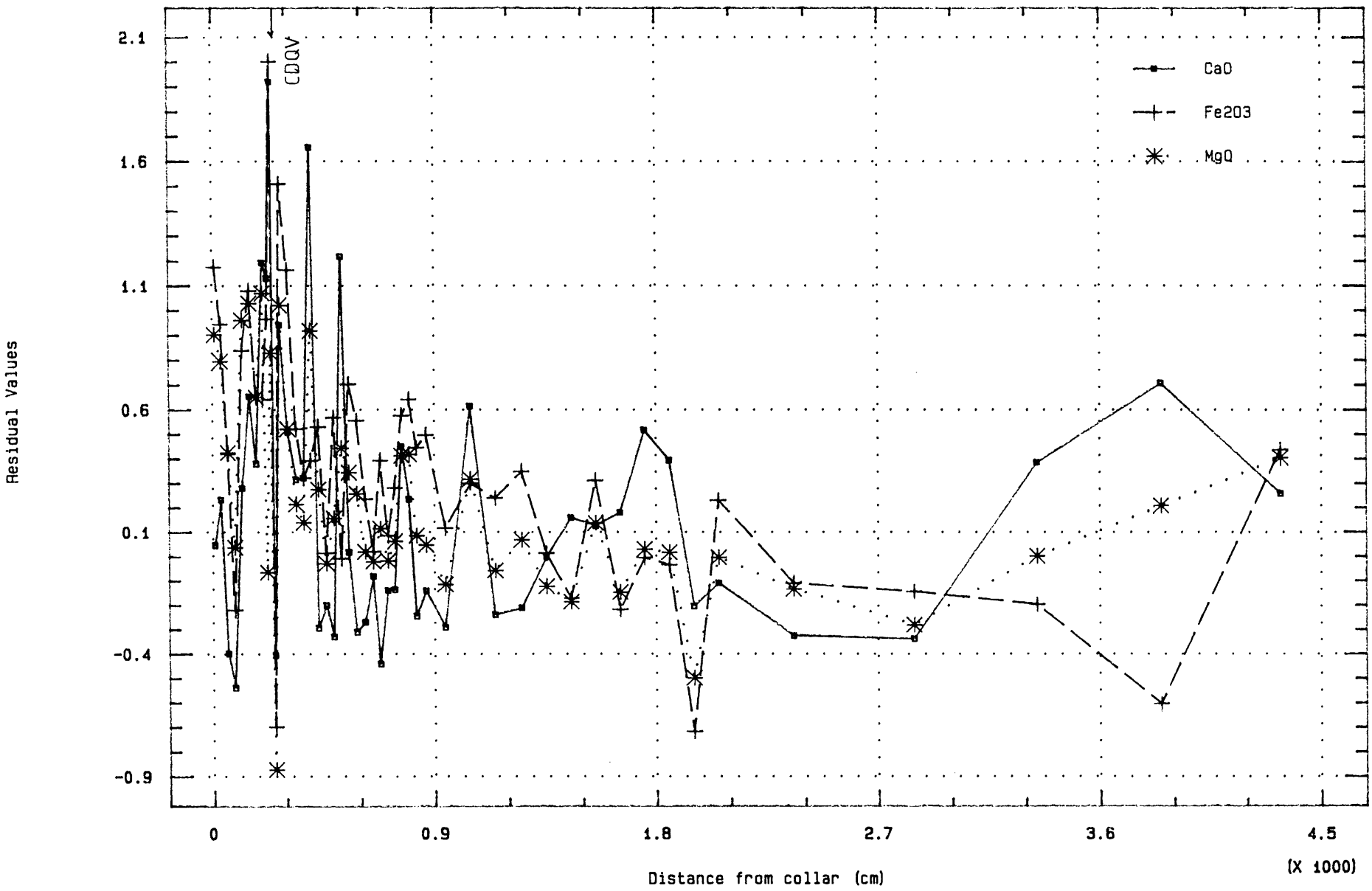

Figure 17. Plot of residual CaO, Fe2O3

& MgO vs Distance

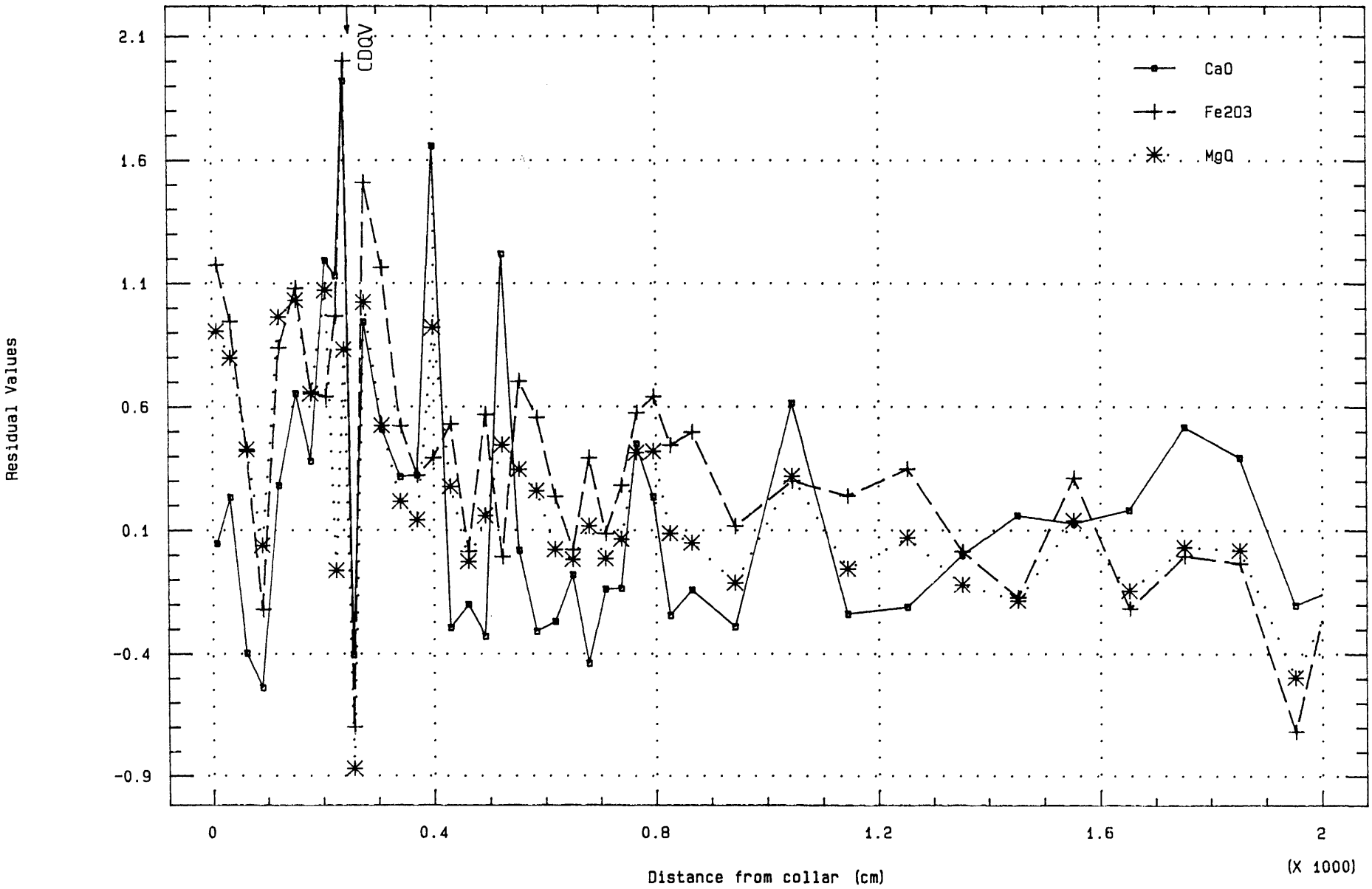

the CDQV in a roughly symmetrical shape, implying that this sulphidisation event may have accompanied the CDQV event, or that the CDQV is superimposed centrally on a pre-existing sulphur-enrichment zone. When the Fe_2O_3 and As peaks are superimposed on the broad S peak an immediate correlation can be made between Fe_2O_3 and S (Figure 21). Of further interest is the fact that Fe_2O_3 and S peaks occur both on the margins of the CDQV as well as within it (Figure 22), suggesting either a single origin for the Fe and S fluid or two similar source fluids. The superimposition of the As peaks with the Fe_2O_3 and S peaks show strong correlation, with one notable exception, viz. immediately south of the CDQV (Figure 22). At this point there is no accompanying Fe_2O_3 peak, suggesting an As-S-rich phase only. The correlation between Fe_2O_3-As-S peaks indicates either (1) arsenopyrite development or (2) simultaneous arsenopyrite and pyrite development.

b) Mineralized Shear Zone: Trace Element Trends

Identification of coupled trace elements was attempted in the same manner as for major elements, viz. by residual element plots and by means of a correlation matrix (Table 8).

i) Residuals of Ni and Cu

Ni shows an erratic distribution throughout the borehole; however, at less than 10m there is a marked increase in concentration. The Ni trace closely approximates that of S, as seen from the broad S peak correlation in the CDQV area as well as the individual peak within the CDQV itself. A comparison of the Ni, S and Fe_2O_3 peak shows a weak correlation (Figure 23), while no correlation exists between the As and Ni peaks. This suggests the presence of pyrite around the CDQV, with the dominant development occurring to the north of it.

Figure 18. Plot of residual K20, Fe203

& MgO vs Distance

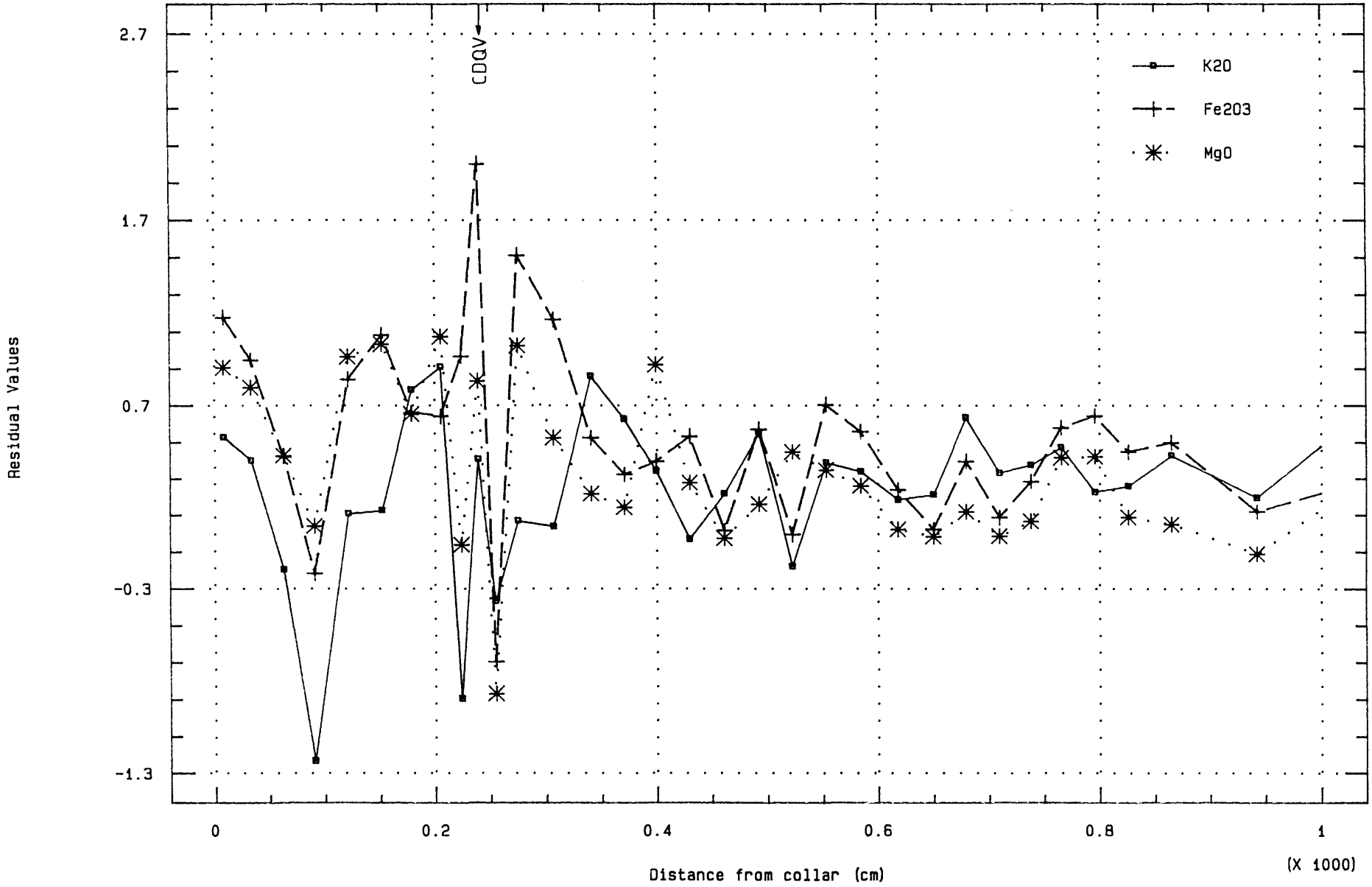

Figure 19. Plot of residual K20 & Na20

vs Distance

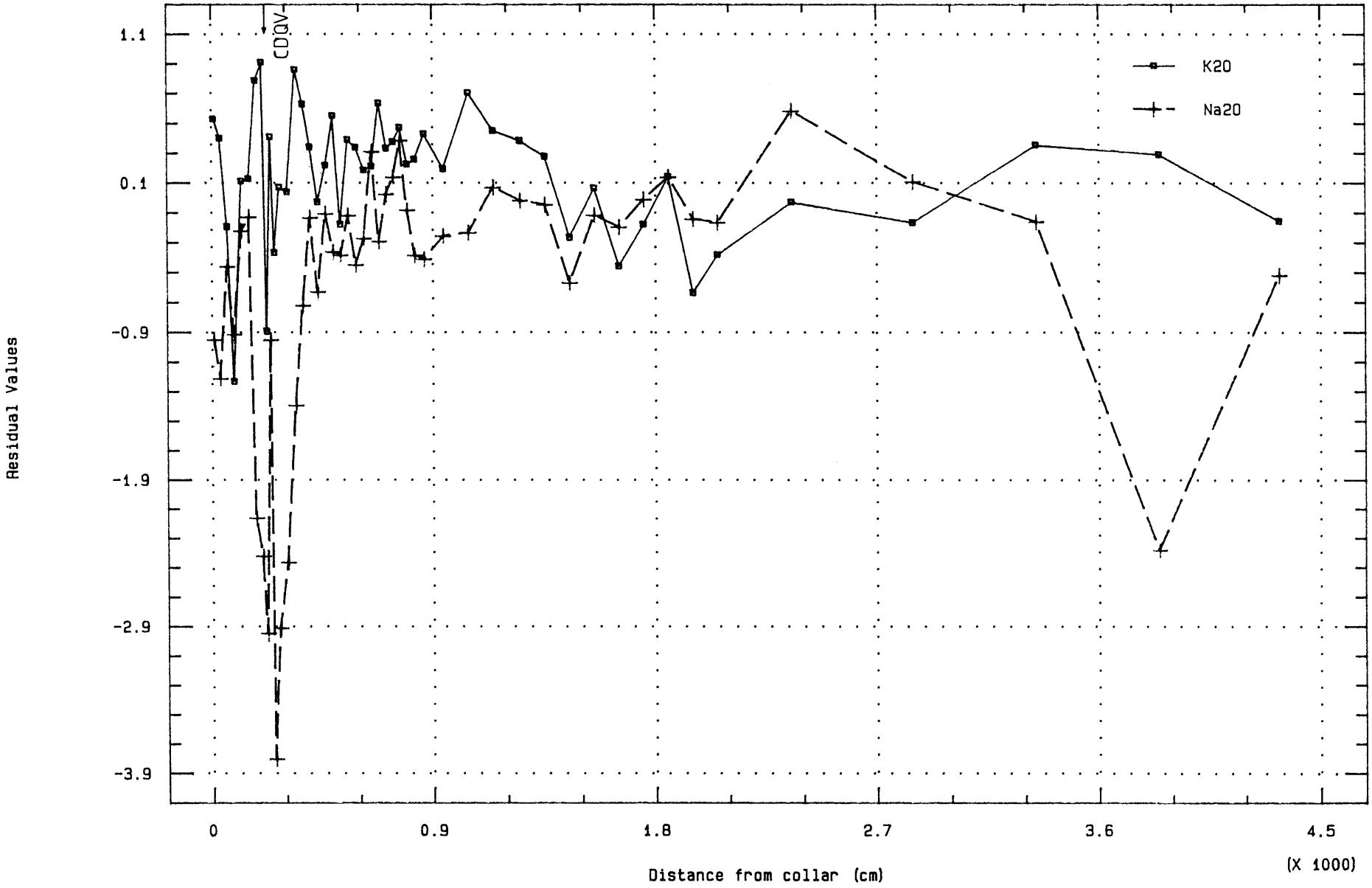

Figure 20. Plot of residual K20 & Na20

vs Distance

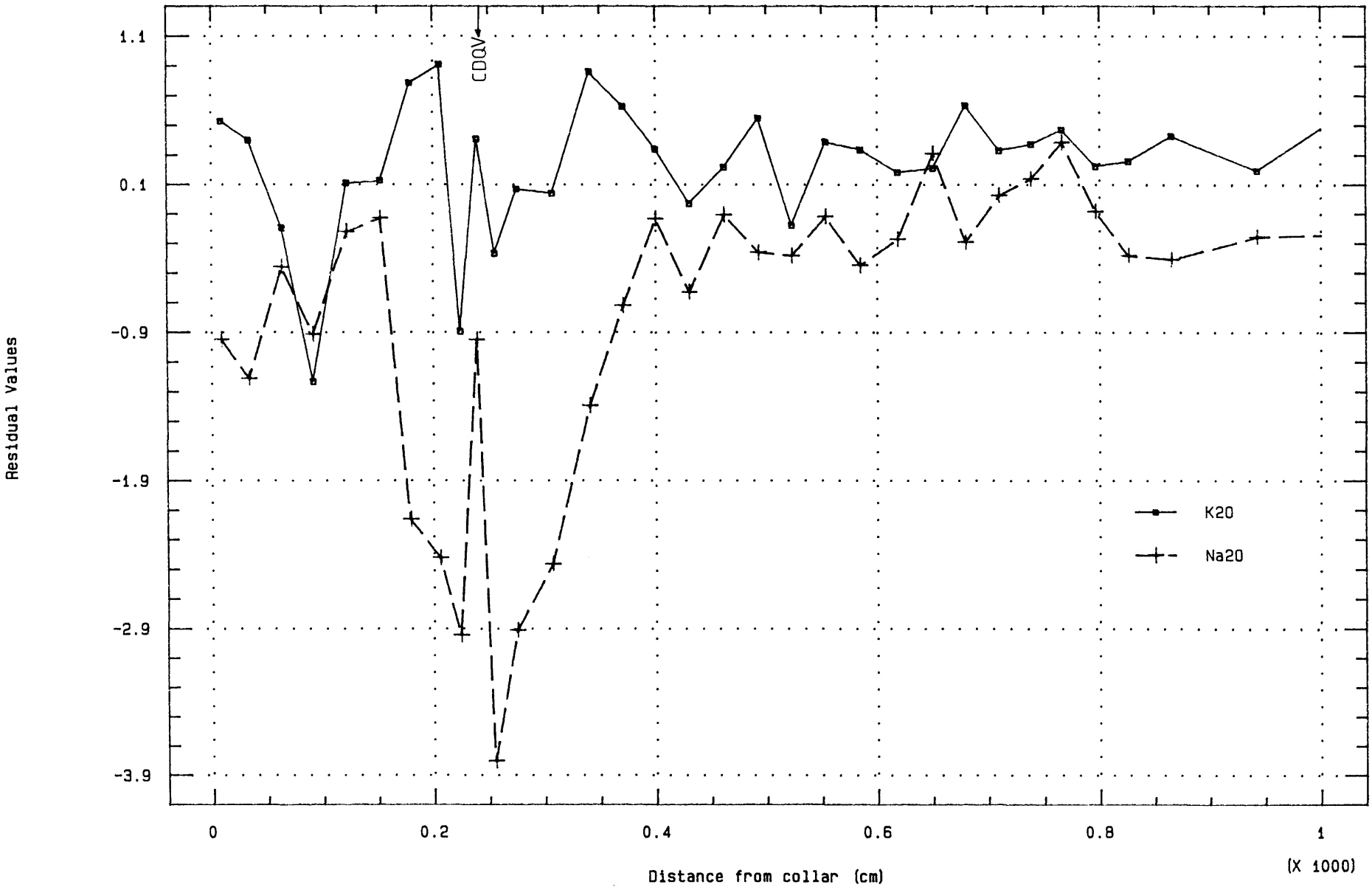

Figure 21. Plot of residual Fe203, S & As vs Distance

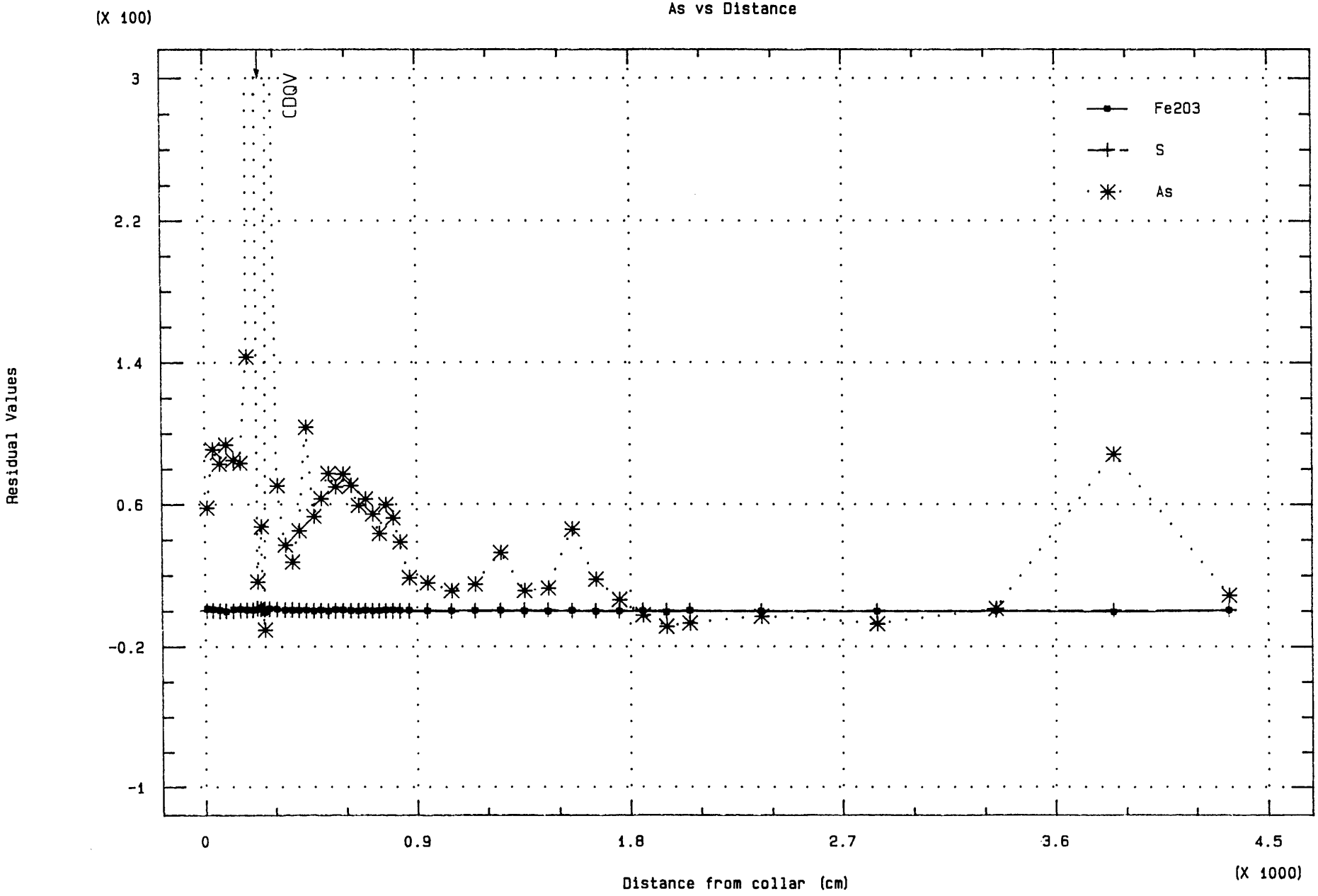

ii) **Residual Co**

Cobalt displays a similar relationship to that seen for Ni, in that there is increased concentration at a distance of less than 10m, with irregular background values. At less than 10m Co shows a broadly sympathetic relationship with Fe_2O_3, As and S. Co also peaks with the anomalous S and As peak south of the CDQV (Figure 24). The close correlation between the Fe_2O_3, S, As and Co peaks suggest the existence of arsenopyrite. The high As peak south of the CDQV is anomalous in its lack of Fe_2O_3, which may indicate a separate As-bearing fluid to that associated with the Co and Fe-rich arsenopyrite. The arsenopyrite is developed dominantly between 2-5m, with only minor development less than 2m. This may be interpreted to mean that neither the Fe-depleted hydrothermal fluid, nor the Co and Fe-enriched arsenic hydrothermal fluid, was centred on the CDQV.

iii) **Residuals of Co, MgO, Ba, Pb and Zn**

Co and MgO behave in a broadly sympathetic manner at a distance of less than 28m (Figure 25), while at greater than 28m their behaviour is irregular. At less than 10m there is increased activity as well as an excellent correlation between Co and MgO in the immediate vicinity of the CDQV (Figure 26). This supports the existence of dolomite/ ankerite in this area. Ba may also be present in the dolomite/ankerite structure (Deer et al., 1966; Phillips and Griffen, 1981) hence the correlation between residual Co, MgO and Ba was investigated. In all instances, with the exception of a single co-ordinated peak in the CDQV itself, no correlation existed (Figure 26). The Zn, MgO and Co also show elevated activity at less than 10m with a strong correlation between the elements (Figure 26). This, together with the Co, MgO and Ba relationships,

Figure 22. Plot of residual Fe203, S & As vs Distance

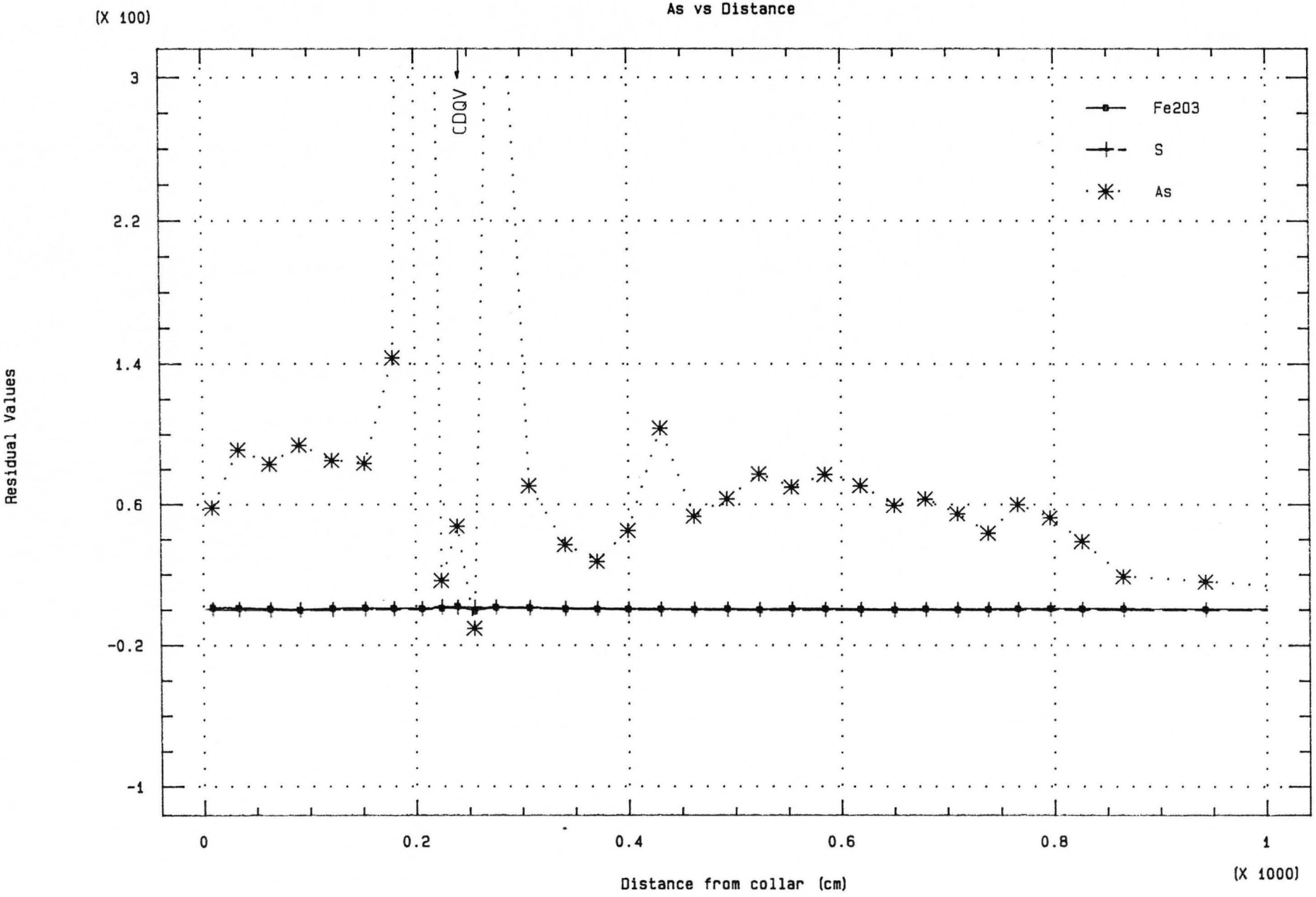

Table 8. Correlation Matrix For The Trace Elements Across A Mineralized Shear Zone.

	Rb	Ba	Nb	Y	Ga	Sc	Cr	V	Co	Ni	Cu	Zn	Pb	As	Au
Rb	1.0000	0.0524	0.0347	0.2958	0.4254	0.5283	0.1502	0.6629	0.2180	0.3804	0.0411	0.2797	-0.0303	0.4092	0.0475
	0.0000	0.7237	0.8148	0.0412	0.0026	0.0000	0.3081	0.0000	0.1366	0 0077	0.7815	0.0542	0.8382	0.0039	0.7483
Ba	0.0524	1.0000	-0.1355	0.6128	0.0189	-0.0686	-0.2711	-0.1580	0.2288	0.0937	0.0569	0.3370	0.1836	-0.0822	0.2544
	0.7237	0.0000	0.3587	0.0000	0.8987	0.6430	0.0624	0.2835	0.1177	0.5265	0.7010	0.0192	0.2117	0.5788	0.0811
Nb	0.0347	-0.1355	1.0000	-0.1534	0.0385	0.1304	0.2628	0.1178	0.1367	0.4945	0.1057	0.0993	0.2140	-0.0548	0.1049
	0.8148	0.3587	0.0000	0.2978	0.7949	0.3772	0.0711	0.4252	0.3540	0.0004	0.4747	0.5019	0.1442	0.7115	0.4779
Y	0.2958	0.6128	-0.1534	1.0000	0.2449	0.2797	-0.0278	0.1446	0.2106	0.1446	0.1005	0.1160	0.1269	0.0973	0.2544
	0.0412	0.0000	0.2978	0.0000	0.0934	0.0542	0.8515	0.3267	0.1508	0.3267	0.4956	0.4322	0.3902	0.5104	0.0810
Ga	0.4254	0.0189	0.0385	0.2449	1.0000	0.3129	0.0484	0.4609	-0.1132	-0.0733	-0.1617	0.1716	-0.3869	0.2812	-0.3175
	0.0026	0.8987	0.7949	0.0934	0.0000	0.0304	0.7439	0.0010	0.4435	0.6205	0.2724	0.2435	0.0066	0.0529	0.0279
Sc	0.5283	-0.0686	0.1304	0.2797	0.3129	1.0000	0.4335	0.8779	0.3839	0.4514	-0.1511	0.2301	-0.0339	0.1450	0.0254
	0.0001	0.6430	0.3772	0.0542	0.0304	0.0000	0.0021	0.0000	0.0071	0.0013	0.3052	0.1156	0.8192	0.3256	0.8638
Cr	0.1502	-0.2711	0.2628	-0.0278	0.0484	0.4335	1.0000	0.4177	0.2515	0.2667	-0.2282	-0.1402	0.0186	0.2402	0.0687
	0.3081	0.0624	0.0711	0.8515	0.7438	0.0021	0.0000	0.0031	0.0846	0.0669	0.1187	0.3420	0.9001	1.0000	0.6429
V	0.6629	-0.1580	0.1178	0.1446	0.4609	0.8779	0.4177	1.0000	0.3233	0.4421	-0.1514	0.2297	-0.1851	0.3412	-0.0927
	0.0000	0.2835	0.4252	0.3267	0.0010	0.0000	0.0031	0.0000	0.0250	0.0017	0.3043	0.1162	0.2078	0.0176	0.5310
Co	0.2180	0.2288	0.1367	0.2106	-0.1132	0.3839	0.2515	0.3233	1.0000	0.6463	0.1312	0.2600	0.3153	0.2381	0.3613
	0.1366	0.1177	0.3540	0.1508	0.4435	0.0071	0.0846	0.0250	0.0000	0.0000	0.3740	0.0743	0.0290	0.1031	0.0116
Ni	0.3804	0.0937	0.4945	0.1446	-0.0733	0.4514	0.2667	0.4421	0.6463	1.0000	0.2876	0.3885	0.4171	0.0615	0.3429
	0.0077	0.5265	0.0004	0.3267	0.6205	0.0013	0.0669	0.0017	0.0000	0.0000	0.0474	0.0064	0.0032	0.6780	0.0170
Cu	0.0411	0.0569	0.1057	0.1005	-0.1617	-0.1511	-0.2282	-0.1514	0.1312	0.2876	1.0000	0.0707	0.6584	-0.0193	0.6139
	0.7815	0.7010	0.4747	0.4956	0.2724	0.3052	0.1187	0.3034	0.3740	0.0474	0.0000	0.6330	0.0000	0.8966	0.0000
Zn	0.2797	0.3370	0.0993	0.1160	0.1716	0.2301	-0.1402	0.2297	0.2600	0.3885	0.0707	1.0000	0.2728	-0.1778	0.0167
	0.0542	0.0192	0.5019	0.4322	0.2435	0.1156	0.3420	0.1162	0.0743	0.0064	0.6330	0.0000	0.0606	0.2268	0.9102
Pb	-0.0303	0.1836	0.2140	0.1269	-0.3869	-0.0339	0.0186	-0.1851	0.3153	0.4171	0.6584	0.2728	1.0000	-0.0733	0.8588
	0.8382	0.2117	0.1442	0.3902	0.0066	0.8192	0.9001	0.2078	0.0290	0.0032	0.0000	0.0606	0.0000	0.6203	0.0000
As	0.4092	-0.0822	-0.0548	0.0973	0.2812	0.1450	0.2402	0.3412	0.2381	0.0615	-0.0193	-0.1778	-0.0733	1.0000	0.1790
	0.0039	0.5788	0.7115	0.5104	0.0529	0.3256	1.0000	0.0176	0.1031	0.6780	0.8966	0.2268	0.6203	0.0000	0.2234
Au	0.0475	0.2544	0.1049	0.2544	-0.3175	0.0254	0.0687	-0.0927	0.3613	0.3429	0.6139	0.0167	0.8588	0.1790	1.0000
	0.7483	0.0811	0.4779	0.081	0.0279	0.8638	0.6429	0.531	0.0116	0.0170	0.0000	0.9102	0.0000	0.2234	0.0000

Coefficient

Significance Level

Figure 23. Plot of residual Ni, S & Fe203 vs Distance

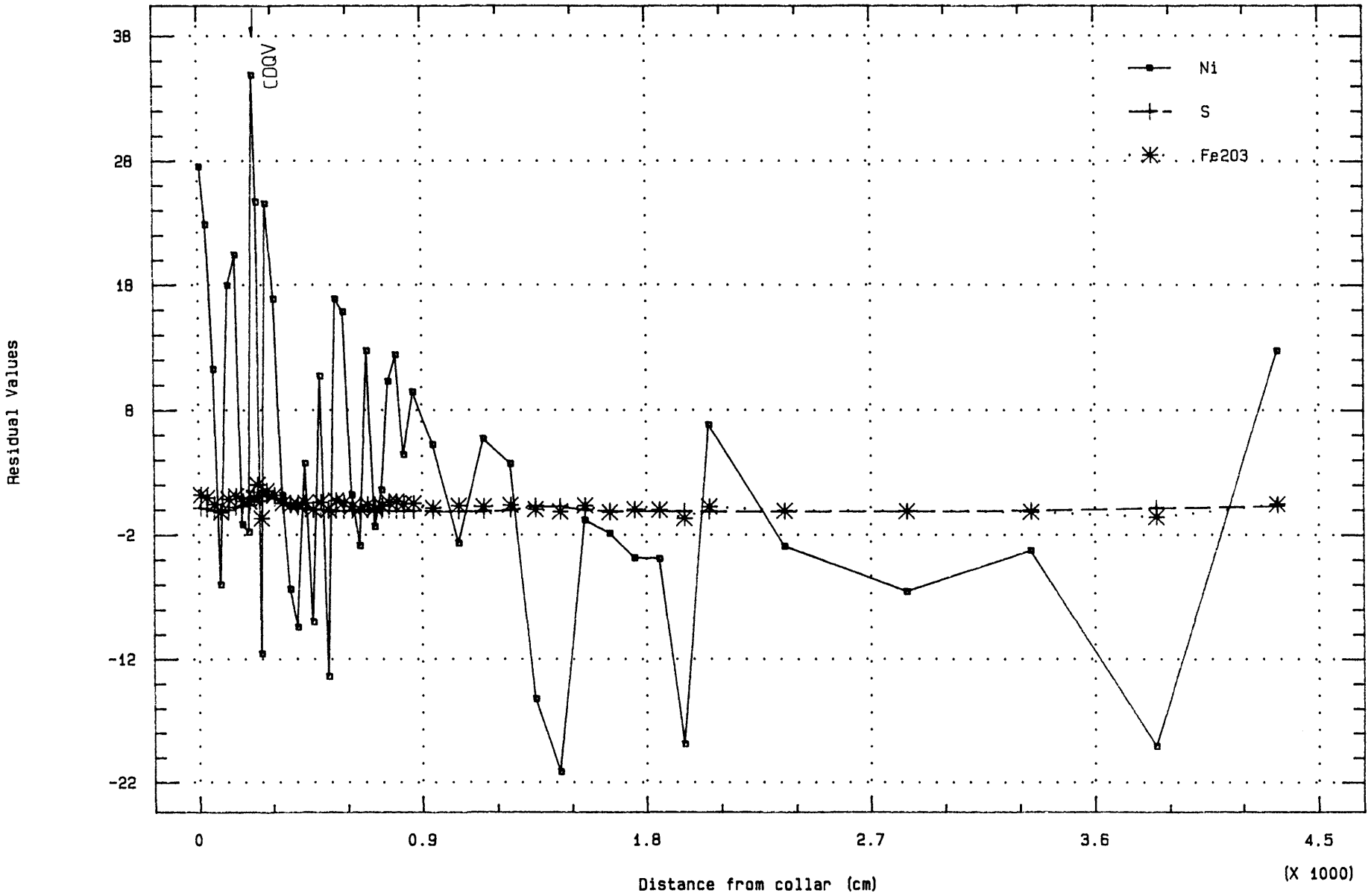

Figure 24. Plot of residual Co, Fe203,

As & S vs Distance

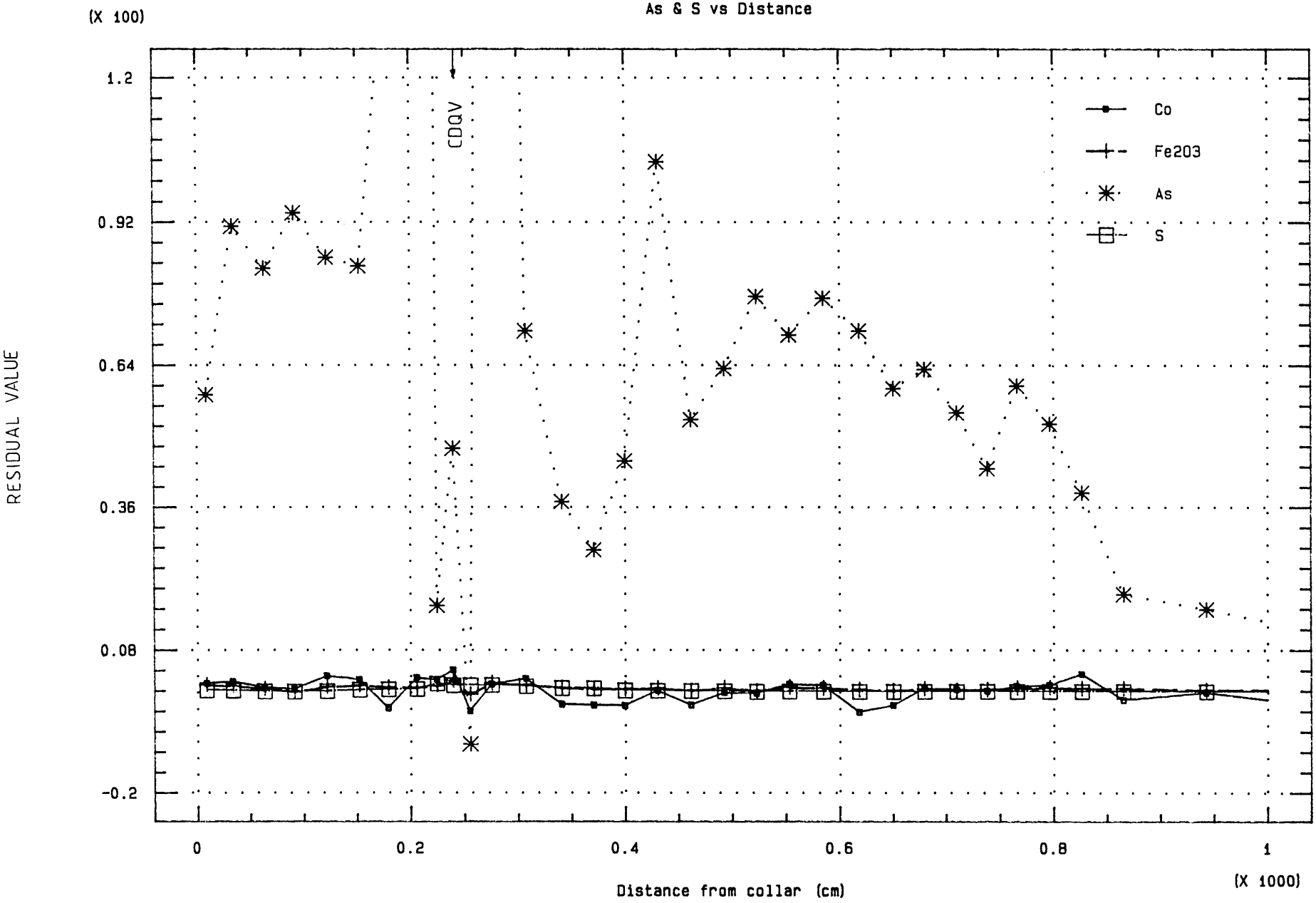

suggests the existence of Zn- and Co-bearing dolomite/ankerite. Three Zn-rich peaks occur at 5.4, 6.8 and 7.8m, which were not correlated with either Co, Zn, or MgO (Figure 26), and are tentatively ascribed to sphalerite formation.

iv) **Residuals of Rb and Ba**

Both Rb and Ba can substitute freely for K in most silicate structures (Deer et al., 1966; Phillips and Griffen, 1981), and as has been suggested in Section 3.2.1.3 a K-rich mineral phase is developed at the expense of Na. Both Ba and Rb showed increased activity in the area less than 10m, and showed varying correlation with K peaks (Figure 27). The Rb-K_2O trace shows a strong correlation closer to 10m from the CDQV, except in the area immediately north of the CDQV where large K_2O peaks have only minor associated Rb peaks (Figure 28). The K_2O-Ba trace show excellent correlation at less than 8m from the CDQV, but is irregular between 8-16m (Figures 27 and 28). The antithetic relationship between Na_2O and K_2O-Rb-Ba suggest sericitization to be at the expense of sodic plagioclase.

c) **Unmineralized Shear Zone: Major Element Trends**

The geochemistry of the unmineralized shear zone is dominated by the presence of a major quartz vein. The number of analyses from this shear is smaller than for the mineralized shear zone and the shear zone shows less mineralogical variation. The elements were handled in the same manner as for those from the mineralized shear zone, viz. (1) by visual inspection and (2) by analysis of a correlation matrix of the residuals (Table 9). In this case the identification of coupled elements is not as easily recognised.

Figure 25. Plot of Co, MgO, Ba, Pb & Zn

vs Distance

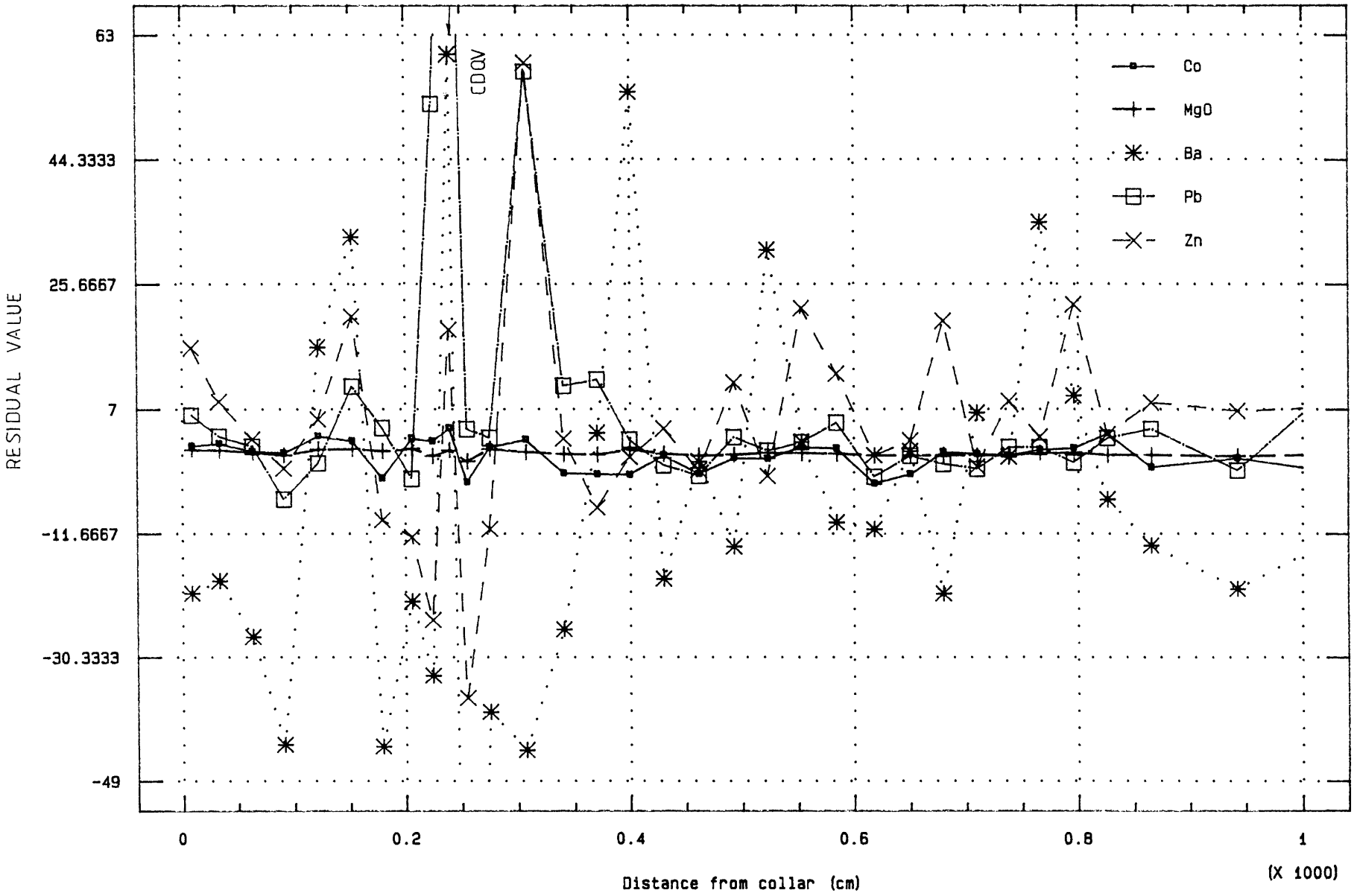

Figure 26. Plot of residual Co, MgO, Ba,

Pb & Zn vs Distance

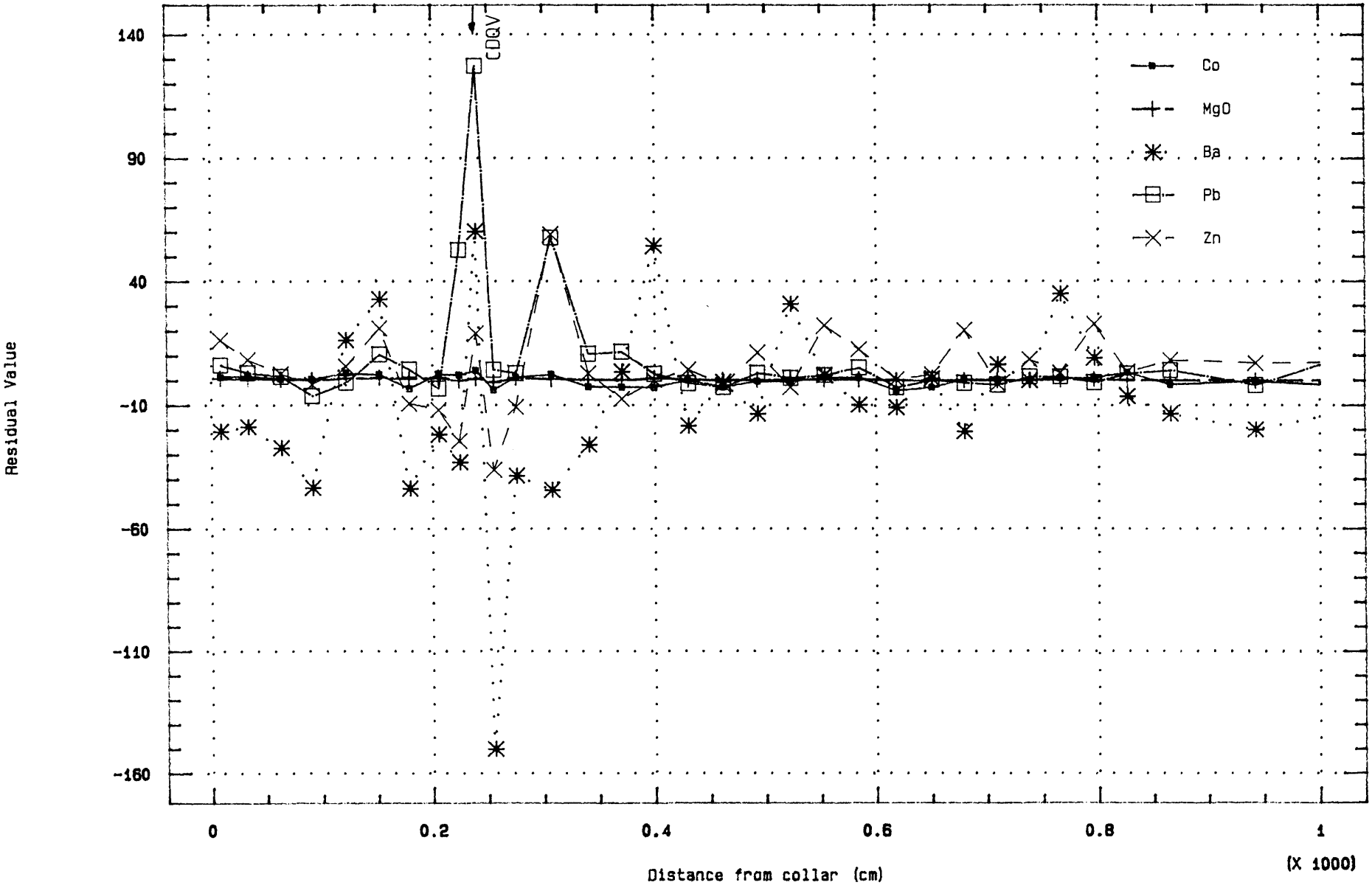

Figure 27. Plot of residual Rb, Ba & K2O

vs Distance

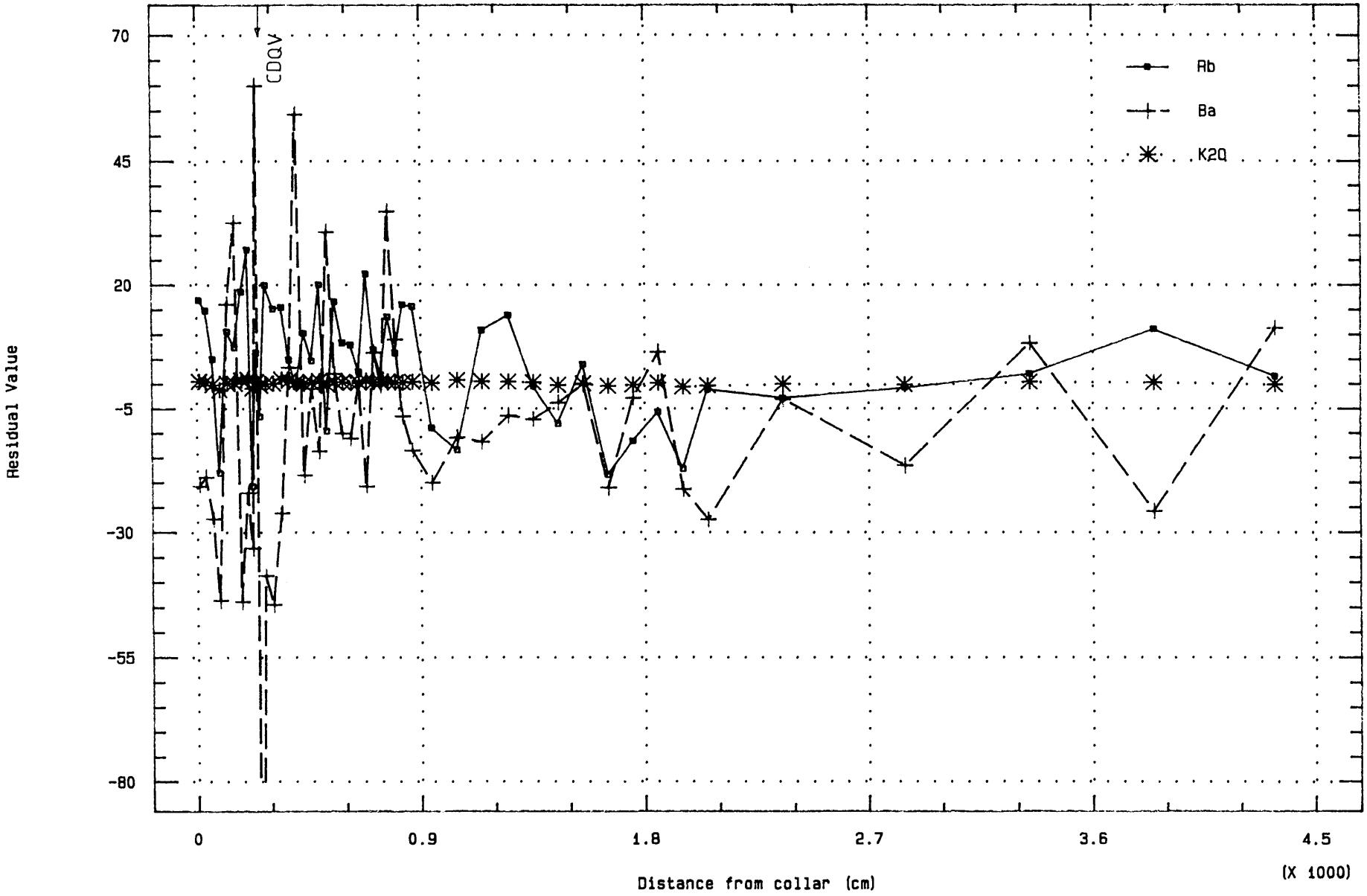

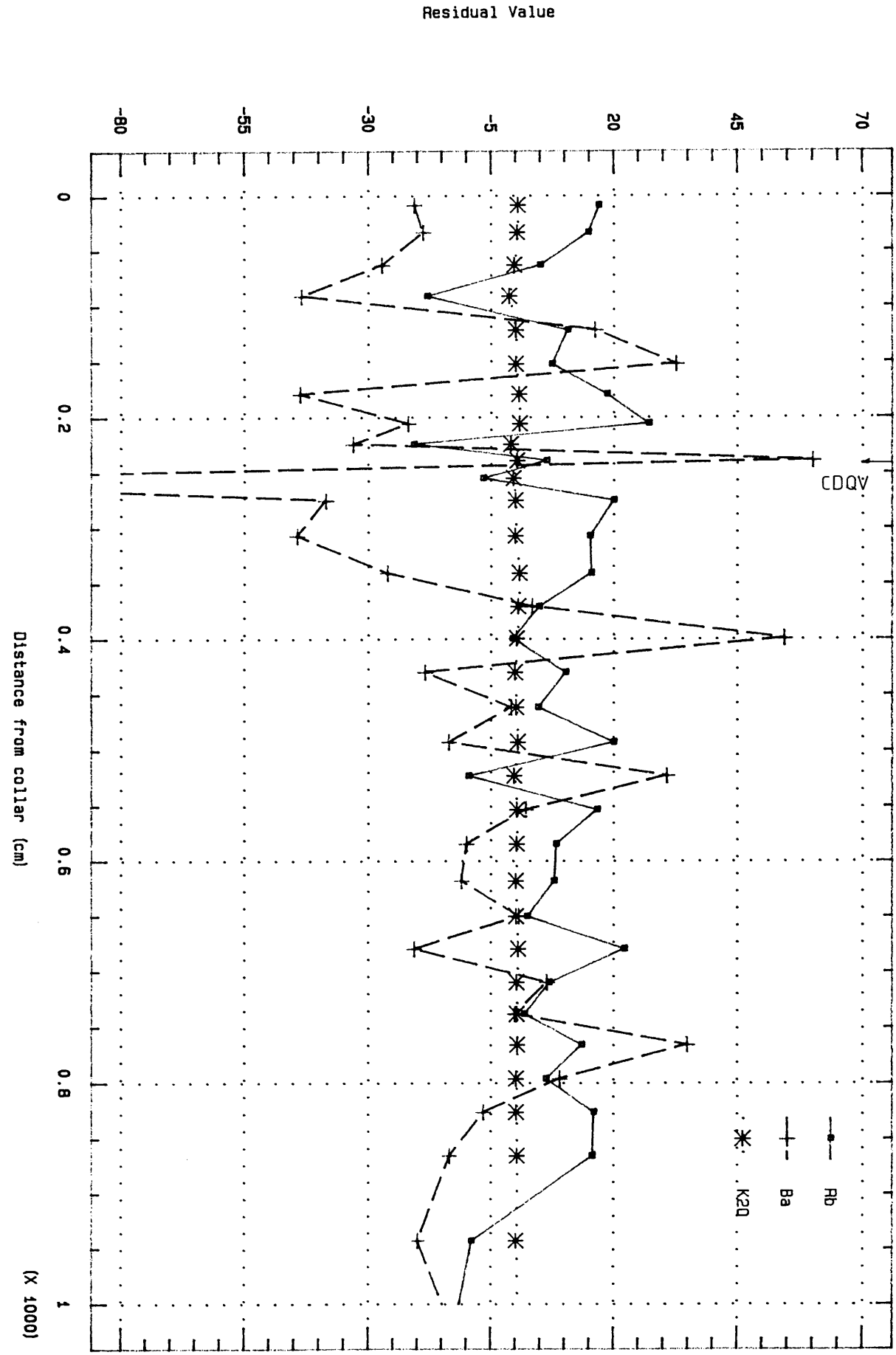

Figure 28. Plot of residual Rb, Ba & K2O vs Distance

Figure 29. Plot of residual SiO2

vs Distance

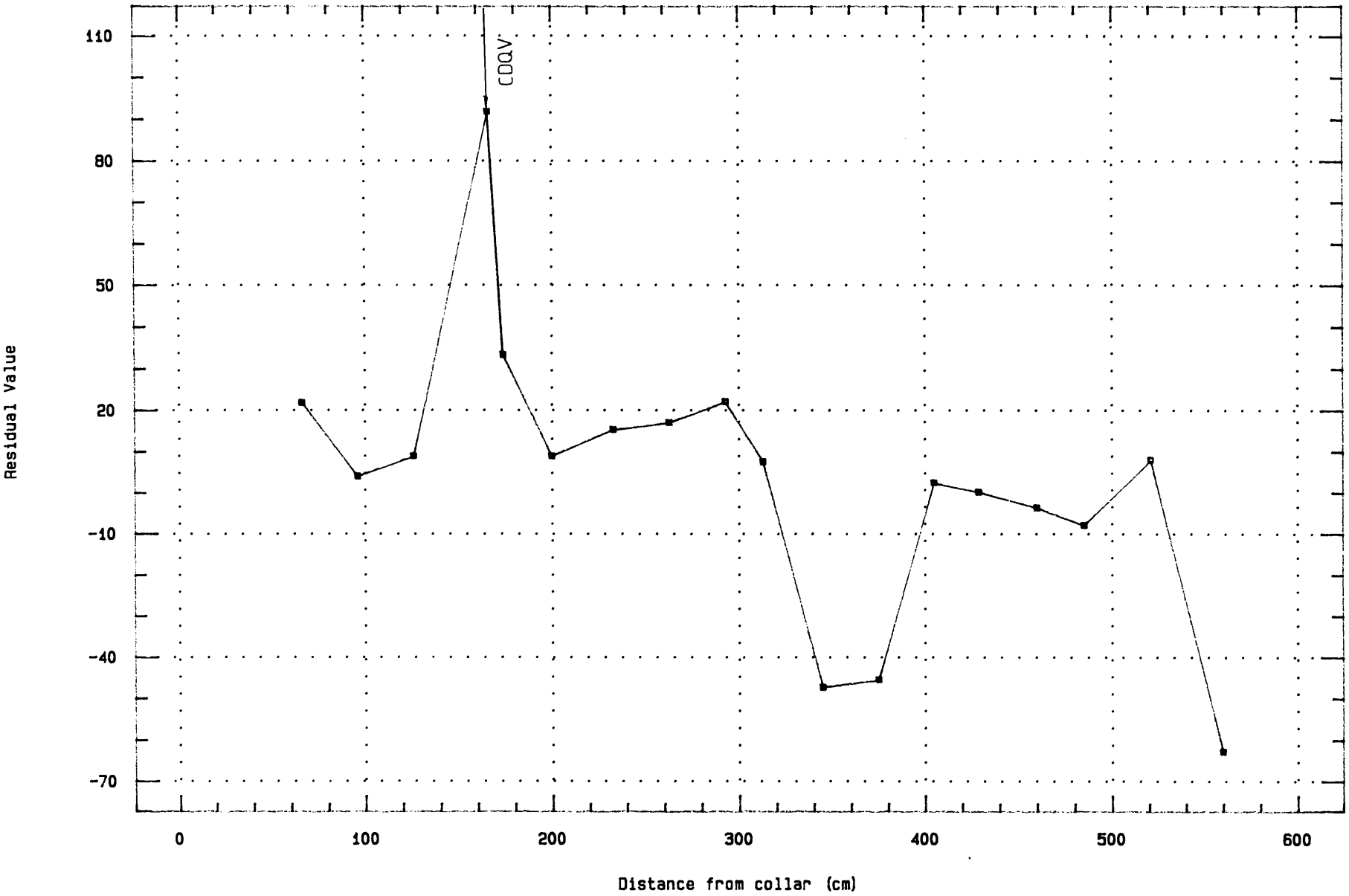

i) Residuals of SiO_2

The SiO_2 trace across the shear zone is dominated by a single major peak, corresponding to the quartz vein itself (Figure 29). The lack of associated SiO_2 peaks may indicate a single stage emplacement of the vein.

Table 9. Correlation Matrix for the Residuals of the Major Elements Across an Unmineralized Shear Zone.

	SiO2	TiO2	MnO	MgO	CaO	K2O	Na2O	P2O5
SiO2	1.0000	0.7170	0.7254	0.7249	0.6111	0.7641	0.5743	0.5210
	0.0000	0.0060	0.0004	0.0004	0.0054	0.0001	0.0101	0.0222
TiO2	0.7170	1.0000	0.6881	0.8801	0.4029	0.8082	0.6606	0.4133
	0.0006	0.0000	0.0011	0.0000	0.0872	0.0000	0.0021	0.0786
MnO	0.7254	0.6881	1.0000	0.8500	0.8148	0.7136	0.5711	0.6390
	0.0004	0.0011	0.0000	0.0000	0.0000	0.0006	0.0107	0.0032
MgO	0.7249	0.8801	0.8500	1.0000	0.5703	0.7357	0.5569	0.4781
	0.0004	0.0000	0.0000	0.0000	0.0108	0.0003	0.0114	0.0384
CaO	0.6111	0.4029	0.8148	0.5703	1.0000	0.6064	0.3770	0.9139
	0.0054	0.0872	0.0000	0.0108	0.0000	0.0059	0.1116	0.0000
K2O	0.7641	0.8082	0.7136	0.7357	0.6064	1.0000	0.7368	0.5033
	0.0001	0.0000	0.0006	0.0003	0.0059	0.0000	0.0003	0.0280
Na2O	0.5743	0.6606	0.5711	0.5569	0.3770	0.7368	1.0000	0.3548
	0.0101	0.0021	0.0107	0.0114	0.1116	0.0003	0.0000	0.1361
P2O5	0.5210	0.4133	0.6390	0.4781	0.9129	0.5033	0.3548	1.0000
	0.0222	0.0786	0.0032	0.0384	0.0000	0.0280	0.1361	0.0000

Coefficient
Significance level

ii) Residual of K_2O and Na_2O

The K_2O trace shows a regular background with minor fluctuations (Figure 30). These fluctuations may be attributable to the presence of sedimentary muscovite. There is a minor increase in K_2O on the margins of the quartz vein, particularly towards the south of the vein. This K_2O increase has an antithetic Na_2O trough in the same position.

Figure 30. Plot of residual K20 & Na20

vs Distance

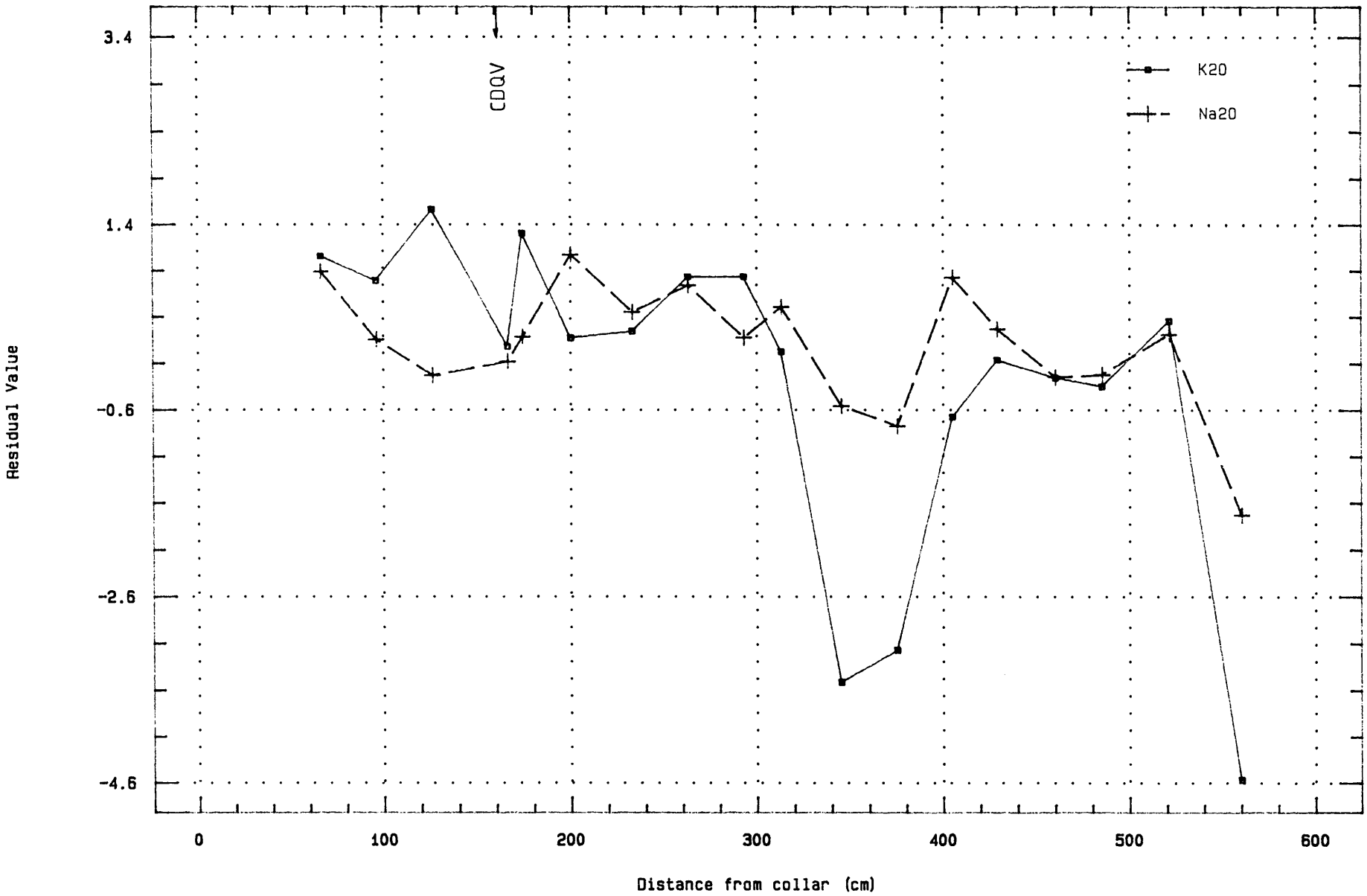

Figure 31. Plot of residual CaO, Fe203

& MgO vd Distance

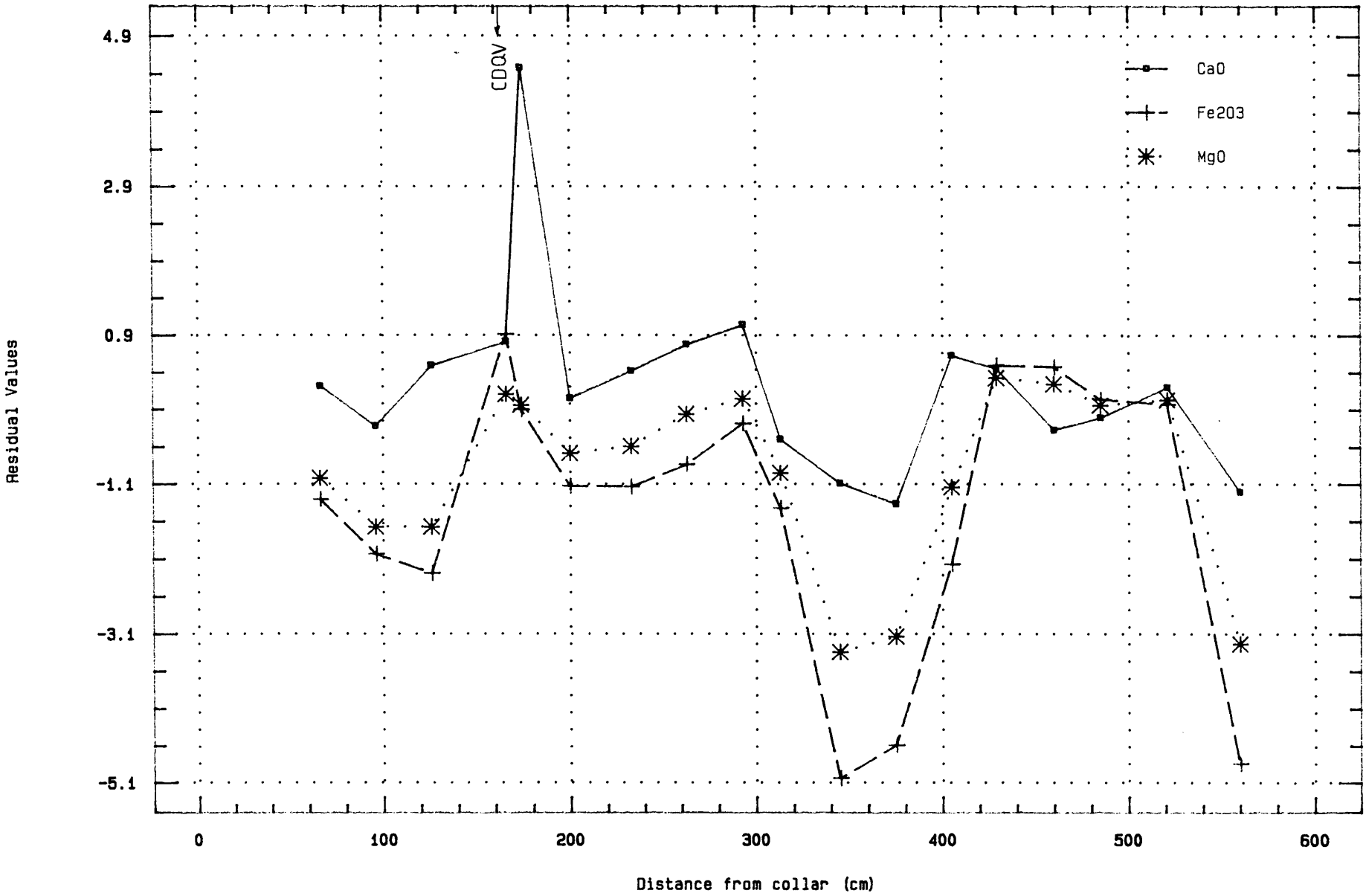

The Na_2O trough is most strongly developed to the south of the quartz vein, but is limited to close to the vein itself. The K_2O increase at the expense of Na_2O is attributed to sericite development at the expense of plagioclase. The limited extent of this sericitization suggests limited wallrock alteration. The Na_2O background trace is highly erratic and may indicate irregular concentrations of sodic plagioclase.

iii) **Residuals of CaO, Fe_2O_3 and MgO**

Fe_2O_3, MgO and CaO all show increased concentrations within the quartz vein itself (Figure 31), suggesting the presence of dolomite/ankerite. Fe_2O_3 displays a regular background trace while MgO is far more erratic. Both Fe_2O_3 and MgO show a sudden step-wise increase at 4 metres, which may be due to a lithological control. The CaO trace is highly erratic and is not easily linked to the Fe_2O_3 and MgO traces (Figure 31), except in the quartz vein. This may indicate that the quartz vein contains dolomite/ankerite. Fe_2O_3 and MgO show a slight trough close to the quartz vein, which is associated with a K_2O peak (Figure 31). From this relationship it is suggested that the Fe_2O_3 and MgO in the background are associated with chlorite and that minor sericitization of the chlorite may have occurred near the quartz vein.

d) **Unmineralized Shear Zone: Trace Element Geochemistry**

The trace element geochemistry across the unmineralized shear zone is highly erratic. One noticeable exception to this generalization is that all elements show an elevated concentration in the quartz vein. This close association between elements and the quartz vein is highlighted by a consideration of the correlation between SiO_2 and the remaining elements in the correlation matrix (Table 10). The only elements indicating a negative correlation with

SiO_2 are Na_2O and Co.

5.4 Discussion

The residual element traces across both a mineralized and unmineralized shear zone from the Mamba Shear zone are particularly informative, with regard to (1) the extent of the alteration halo around the two shear zones (i.e. the extent of wallrock-fluid interaction), (2) the nature of the hydrothermal fluid in the shear zones, (3) the potential alteration assemblages formed from the wallrock-fluid interaction, and (4) highlighting the differences between the two shear zones and possibly indicating the reason for gold mineralisation occurring in the one in preference to the other.

1) The extent of the hydrothermal alteration requires mention. The different elements, either within the hydrothermal fluid or those in minerals exposed to the hydrothermal fluid, will all have different mobilities during each phase of alteration. This mobility is determined by factors such as temperature, pressure, pH, and oxidation potential (Forster et al., 1979). In addition to these factors it must be remembered that more than one fluid phase may have passed through the shear zone and the host rocks, and that each fluid pulse probably had its own characteristic composition, element mobility etc. To complicate matters further, the spacing at which samples were taken affects the accurate location of the hydrothermal alteration front. Thus it is extremely difficult to pin-point the exact limit of each element's path away from the shear zone. However, for the mineralized shear zone, elements such as K_2O, S, As, Ni, Co, Zn, Ba and Rb show extensive activity in the immediate area of the central dark quartz vein and as far as 10m away from it. CaO, Fe_2O_3 and MgO also showed considerable activity within this range and up to 20m away. Their reliability as hydrothermal fluid indicators is doubtful though, as the Moodies Group sediments often contain carbonate-rich horizons (H.G.Philpot pers. comm., 1989). From these observations it is tentatively suggested that the

Table 10. Correlation Matrix For The Residuals Of The Trace Elements Across An Unmineralized Shear Zone.

	SiO2	Nb	Y	Ga	Sc	Cr	V	Co	Ni	Cu	Zn	Pb	As	Au
SiO2	1.0000	0.2720	0.1750	0.4784	0.4449	0.3508	0.5102	0.4191	0.4995	0.5579	0.4843	0.5728	0.7517	0.6712
	0.0000	0.2750	0.4873	0.0446	0.0643	0.1535	0.0305	0.0834	0.0348	0.0161	0.0417	0.0130	0.0003	0.0023
Nb	0.2720	1.0000	0.5408	0.4995	0.7300	0.7757	0.6725	0.5636	0.6919	0.5562	0.6100	-0.0084	0.2929	0.0575
	0.2750	0.0000	0.0205	0.0348	0.0006	0.0002	0.0020	0.0149	0.0015	0.0165	0.0072	0.9736	0.2382	0.8207
Y	0.1750	0.5408	1.0000	0.0957	0.3306	0.4705	0.2439	0.3488	0.2674	0.1985	0.2668	0.1567	0.3634	0.1948
	0.4873	0.0205	0.0000	0.7058	0.1803	0.0488	0.3294	0.1561	0.2835	0.4297	0.2845	0.5346	0.1383	0.4386
Ga	0.4784	0.4995	0.0957	1.0000	0.9019	0.6923	0.9170	0.7548	0.8888	0.6929	0.7999	-0.0500	0.2882	0.2807
	0.0446	0.0348	0.7058	0.0000	0.0000	0.0015	0.0000	0.0003	0.0000	0.0014	0.0001	0.8437	0.2461	0.2591
Sc	0.4449	0.7300	0.3306	0.9019	1.0000	0.9108	0.9754	0.8707	0.9759	0.7635	0.9043	0.0347	0.4158	0.2336
	0.0643	0.0006	0.1803	0.0000	0.0000	0.0000	0.0000	0.0000	0.0000	0.0002	0.0000	0.8912	0.0861	0.3509
Cr	0.3508	0.7757	0.4705	0.6923	0.9108	1.0000	0.8884	0.9007	0.9189	0.7099	0.8435	0.0228	0.4210	0.1208
	0.1535	0.0002	0.0488	0.0015	0.0000	0.0000	0.0000	0.0000	0.0000	0.0010	0.0000	0.9284	0.0819	0.6330
V	0.5102	0.6725	0.2439	0.9170	0.9754	0.8884	1.0000	0.8685	0.9773	0.7992	0.9179	0.0866	0.4088	0.2460
	0.0305	0.0020	0.3294	0.0000	0.0000	0.0000	0.0000	0.0000	0.0000	0.0001	0.0000	0.7325	0.0921	0.3252
Co	0.4191	0.5636	0.3488	0.7548	0.8707	0.9007	0.8685	1.0000	0.9141	0.5907	0.8417	0.0271	0.3796	0.1172
	0.0834	0.0149	0.1561	0.0003	0.0000	0.0000	0.0000	0.0000	0.0000	0.0098	0.0000	0.9151	0.1203	0.6432
Ni	0.4995	0.6919	0.2674	0.8888	0.9759	0.9189	0.9773	0.9141	1.0000	0.7508	0.9233	0.0560	0.3967	0.1804
	0.0348	0.0015	0.2835	0.0000	0.0000	0.0000	0.0000	0.0000	0.0000	0.0003	0.0000	0.8253	0.1031	0.4737
Cu	0.5579	0.5562	0.1985	0.6929	0.7635	0.7099	0.7992	0.5907	0.7508	1.0000	0.6633	0.3823	0.6556	0.6158
	0.0161	0.0165	0.4297	0.0014	0.0002	0.0010	0.0001	0.0098	0.0003	0.0000	0.0027	0.1174	0.0031	0.0065
Zn	0.4843	0.6100	0.2668	0.7999	0.9043	0.8435	0.9179	0.8417	0.9233	0.6633	1.0000	0.2060	0.3626	0.1584
	0.0417	0.0072	0.2845	0.0001	0.0000	0.0000	0.0000	0.0000	0.0000	0.0027	0.0000	0.4122	0.1392	0.5301
Pb	0.5728	-0.0084	0.1567	-0.0500	0.0347	0.0228	0.0866	0.0271	0.0560	0.3823	0.2060	1.0000	0.3626	0.1584
	0.0130	0.9736	0.5346	0.8437	0.8912	0.9284	0.7325	0.9151	0.8253	0.1174	0.4122	0.0000	0.1392	0.5301
As	0.7517	0.2929	0.3634	0.2882	0.4158	0.4210	0.4088	0.3796	0.3967	0.6556	0.3626	0.6858	1.0000	0.8316
	0.0003	0.2382	0.1383	0.2461	0.0861	0.0819	0.0921	0.1203	0.1031	0.0031	0.1392	0.0017	0.0000	0.0000
Au	0.6712	0.0575	0.1948	0.2807	0.2336	0.1208	0.2460	0.1172	0.1804	0.6158	0.1584	0.6534	0.8316	1.0000
	0.0023	0.8207	0.4386	0.2591	0.3509	0.6330	0.3252	0.6432	0.4737	0.0065	0.5301	0.0033	0.0000	0.0000

Coefficient
Significance Level

hydrothermal alteration front around the mineralized shear zone extended up to 10m from the CDQV.

The hydrothermal alteration halo around the unmineralized shear zone is far less extensive, and often not recognizable at all. Only in the case of K_2O and Na_2O has an antithetic relationship been observed. This is minor however and rarely extends more than 40cm away from the central quartz vein. The major difference between the mineralized and unmineralized shear zones, as far as the alteration halo is concerned, is that in the mineralized one the fluids have penetrated far deeper into the wallrock. A means of increasing the permeability of a rock is by shearing, and as a corollary to this, increased shearing will evoke a structurally controlled permeability (Boulter et al., 1987; Kerrich, 1986; Sibson et al., 1988). It is important to add that any shear zone will eventually reach a stage whereby the formation of new minerals in the conduits will eventually choke the system (Sibson et al., 1988; Vearncombe, 1989). At such a stage the fluid can either be (1) diverted into a new plumbing system, (2) hydraulic brecciation can occur if the pore fluid pressure can exceed the tensile strength of the host rock (Phillips, 1972; Vearncombe, 1989), or (3) reactivation of the shear zone can occur when the fluid pressure exceeds the lithostatic load (Sibson et al., 1988; Vearncombe, 1989). The relative age relationships between veins and sericitic fabric, as well as the hydraulic brecciation discussed in chapter 2 support the existence of a combination of the above.

2) It is possible to quantitatively estimate the individual element mobility during hydrothermal alteration of the shear zones, and to compare each element to another from within the same shear zone. The major elements mobility is dominated by large SiO_2 enrichments in both the mineralized and unmineralized shear zones. The trace element mobility is dominated by enrichments in Cr and As, as well as moderate enrichments in Rb, V, Ni, Zn and Pb within the mineralized shear zone. The unmineralized shear zone is characteristically depleted in these elements.

The chemistry of the fluid passing through the mineralized shear zone is markedly different to that passing through the unmineralized shear zone. Furthermore the close association between As, S and Au suggest that they were introduced simultaneously.

3) The geochemical trends and the presence of coupled elements suggest the formation of specific minerals as well as the pre-existence of several others. Due to the fact that fluid penetration of the wallrock in the unmineralized shear zone is limited, the background geochemical trends tend to indicate host rock minerals only, while alteration assemblages can be predicted for the mineralized shear zone. In both cases sodic feldspar is present in the host rock. In the case of the mineralized shear zone, primary muscovite within the host rock may also have been an important source of potassium. The main mineral formed directly from K-metasomatism appears to be sericite, which formed at the expense of sodic feldspar and chlorite. Other minerals associated with the quartz veining are dolomite and ankerite, while discrete calcite veins also occur. In the mineralized shear zone sulphidisation has been responsible for pyrite and arsenopyrite formation. Maximum gold solubility in sulphide-rich brines is dependent on the formation of a gold-thio complex, and maximum gold solubility in aqueous sulphide solutions will be reached at temperatures lower than 350 Celsius at neutral pH (Weissberg, 1970).

4) The alteration trends highlight the major difference between the two shear zones, viz. the difference in the size of the two shear zones, with the mineralized shear being at least 10m wide while the unmineralized one is less than 1m wide. The effect of this is that there is less fluid-wallrock interaction in the unmineralized shear zone. The fact that both shear zones show elevated element concentrations across their width, combined with the fact that only the wider of the two is mineralized, may suggest that the unmineralized shear did not have enough suitably "quiet" sites for mineralisation to occur, whereas the shear

induced-permeability in the mineralized shear zone was ideal for mineralisation.

CHAPTER 6

DISCUSSION

Previous research in the Barberton supracrustal remnant has emphasized the role played by pre-, syn-, and post-tectonic granitoid emplacement into and around the supracrustal remnant. In the light of recent advances in the understanding of crustal-forming processes and Archaean supracrustal remnant accretion, the "destructive" emplacement of granitoid masses is no longer ubiquitously accepted. However, rather than being drawn into a discussion of the exact role played by the granitoid masses this discussion will be limited to placing the shear zones into a regional geometric model. From that regional model inferences can be drawn as to the driving mechanisms behind deformation.

A summary of the currently accepted deformational history in the north-western portion of the Barberton supracrustal remnant is given in Table 4 and outlined below.

D_1 - formation of regional scale folds along east-north-east to west-south-west axes and associated north-west directed thrusting;
D_2 - regional cleavage development;
D_3 - arcuation of the synclines about a north-west to south-east trending fold axis.

Other suggested modifications include pre-D_1 deformation as recognized from folded bands in chert pebbles within conglomerates, and reactivation of pre-existing thrust faults as wrench faults. Evidence cited as support for the latter includes the presence of horizontal to sub-horizontal lineations on fault planes and the existence of conjugate fault sets in orientations compatible with a regional strike-slip system (Anhaeusser, 1965; Robertson, 1989).

A wide range of movement directions have been documented along the major east-north-east trending faults within the Barberton belt. The Sheba Fault, for example, is reported to have initiated as a north-westerly directed thrust (Ramsay, 1963; Roering, 1965; Anhaeusser, 1976; Robertson, 1989) and been reactivated as a right lateral strike-slip fault in the Sheba Hills area (Anhaeusser, 1976), and as a left lateral strike-slip fault in the Fairview Gold Mine area (Visser et al., 1956). In the most recent study of the Sheba Gold Mine area, Robertson (1989) recognized the space problem such movements would produce and suggested that the lateral movement along the Sheba Fault should in fact be opposite to that suggested by Visser et al., (1956) and Anhaeusser (1976), namely left lateral east of Sheba Mine and right lateral at Fairview Mine. This latter suggestion simply reverses rather than alleviates the space problem. Both these scenarios will be discussed later in this chapter, but firstly the local deformation environment around the Eureka, Mamba and Cat's Cave Shear Zones needs to be discussed.

These shears all exhibit identical deformation styles and movements, namely north block over south block reverse movement. Individual shears typically bifurcate up dip while linking down dip to produce characteristic thrust imbricate patterns. The deformation styles described from each shear zone are best classified within the brittle-ductile field. The similar progressive deformation history, similar deformation styles, alteration haloes, and mineralisation styles all suggest that the Margaret Section shear zones form part of the same linked thrust fault system. In keeping with the geometry of such systems it is proposed that the Eureka, Mamba and Cat's Cave structures are linked at depth along a sole thrust as indicated in Figure 32. This linked system will hereafter be referred to as the Margaret Section thrust imbricate. Two possible scenarios are envisaged for the development of this thrust imbricate: viz. a discrete deformation event resulting from southerly directed thrusting, or as an integral part of the larger regional deformation pattern. An important time constraint is that individual thrusts within the imbricate

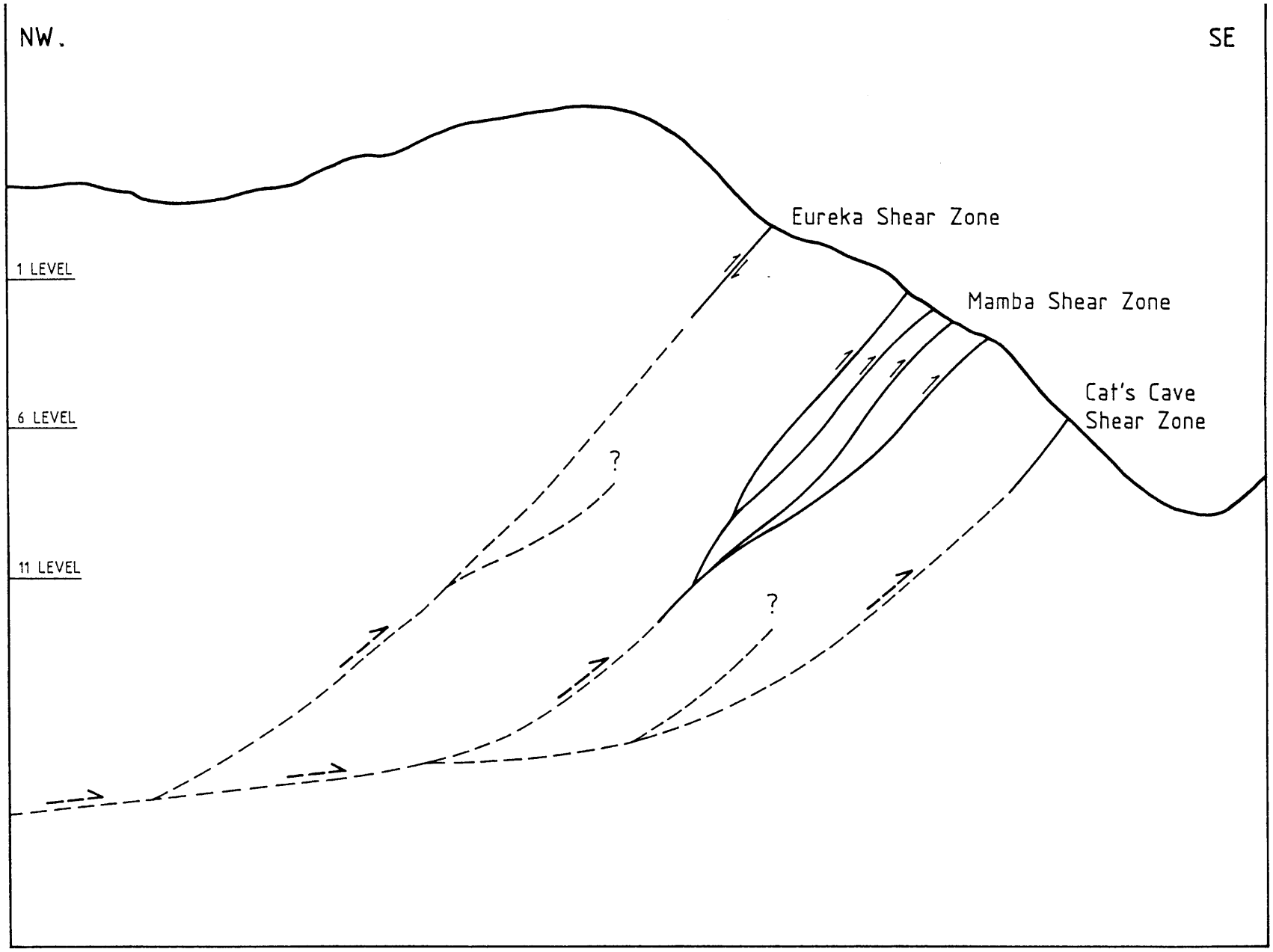

FIGURE 32 SCHEMATIC NW-SE CROSS SECTION THROUGH THE SOUTHERN LIMB OF THE EUREKA SYNCLINE

(not to scale)

system clearly crosscut the bedding within the overturned southern limb of the Eureka Syncline, thereby making them younger.

1. The implication is therefore that if, as the first proposal suggests, the southward thrusting relates to a previously unrecognised deformation event, this event must have occurred after overturning of the southern limb of the Eureka Syncline but prior to the last deformation event along the Sheba Fault. This would require exceptional timing as the overturning of the southern limb of the Eureka Syncline and the development of the Sheba Fault Zone are seen as a continuous event (Ramsay, 1963; Anhaeusser, 1976). The lack of a regional pattern of north over south thrusting further detracts from the feasibility of this model.

2. The second model suggests the formation of these thrust imbricates as an integral part of the regional deformation event. It has long been recognized that faults, shear systems and other structural criteria form in set geometrical patterns in response to the prevailing stress regime. The Margaret Section thrust imbricate system should therefore relate to a larger dominant stress regime. Within the study area the dominant deformation features are the overturned and arcuated Eureka Syncline, and the Sheba Fault Zone. It is logical therefore to try to relate the formation of the Margaret Section thrust imbricate to the event/s responsible for the regional deformation pattern. The same time constraints obviously apply, suggesting the development of the Margaret Section thrust imbricate synchronous with the development of the Sheba Fault.

Ramsay (1963) suggested that the initial folding of the Eureka and Ulundi synclines about a north-east to south-west trending fold axis, as well as the initiation of the Sheba Fault represents the earliest deformation event (D_1) seen in the Barberton supracrustal remnant, and formed in response to a north-westerly directed compression. The vast majority of faults formed during this initial phase would therefore have a thrust geometry. The Margaret thrust imbricate system

developed in the footwall of the Sheba Fault zone, which is itself a thrust zone. Geometrical models which can accommodate local thrust sets of opposite vergence in association with regional thrust system have been documented and are referred to as back thrusts (Butler, 1982). Two methods for the development of back thrusts have been proposed, namely as (1) pop-up back thrusts or as (2) antithetic back thrusts (Butler, 1982). Back thrusts which are developed by layer parallel shortening prior to frontal ramp formation are termed pop-up back thrusts (Elliott, 1981). Antithetic back thrusts are considered to result from the rotation of the hangingwall above the frontal footwall ramp (Butler, 1982).

An important consideration when dealing with a back thrust environment, is the fact that back thrusts do not propagate into the footwall of an existing thrust, instead they propagate from an existing thrust plane backwards into the hangingwall of that thrust. If the Margaret Section thrust imbricates are ascribed to a back thrust environment then the existence of at least one or more thrust planes in the footwall of the Sheba Fault Zone is implied. A number of possibilities exist as to the location of such a fault. The first is that the thrust plane (a single event is assumed for simplicity only) is in fact a blind thrust, i.e. does not intersect the earth's surface at the present erosion level. Secondly, the thrust may intersect the present erosion surface north of the New Consort Gold Mine (Figure 33) and has not been recognized. A third option is that the thrust coincides with the granitoid-greenstone boundary.

The first is difficult to either prove or disprove, while the second is unlikely due to the fact that the area north of the New Consort Gold Mine exhibits a totally different style of deformation, with no documented evidence for north-westerly directed thrusting (M..Tomkinson pers. comm., 1990). Support for the third possibility comes from Fripp et al., (1980) who recognised a zone of north directed thrusting in mylonites at the granite-greenstone contact exposed in Honey Bird Creek (Figure 33). This zone dips south at between 25 and 40 and lies along strike from an important structural break

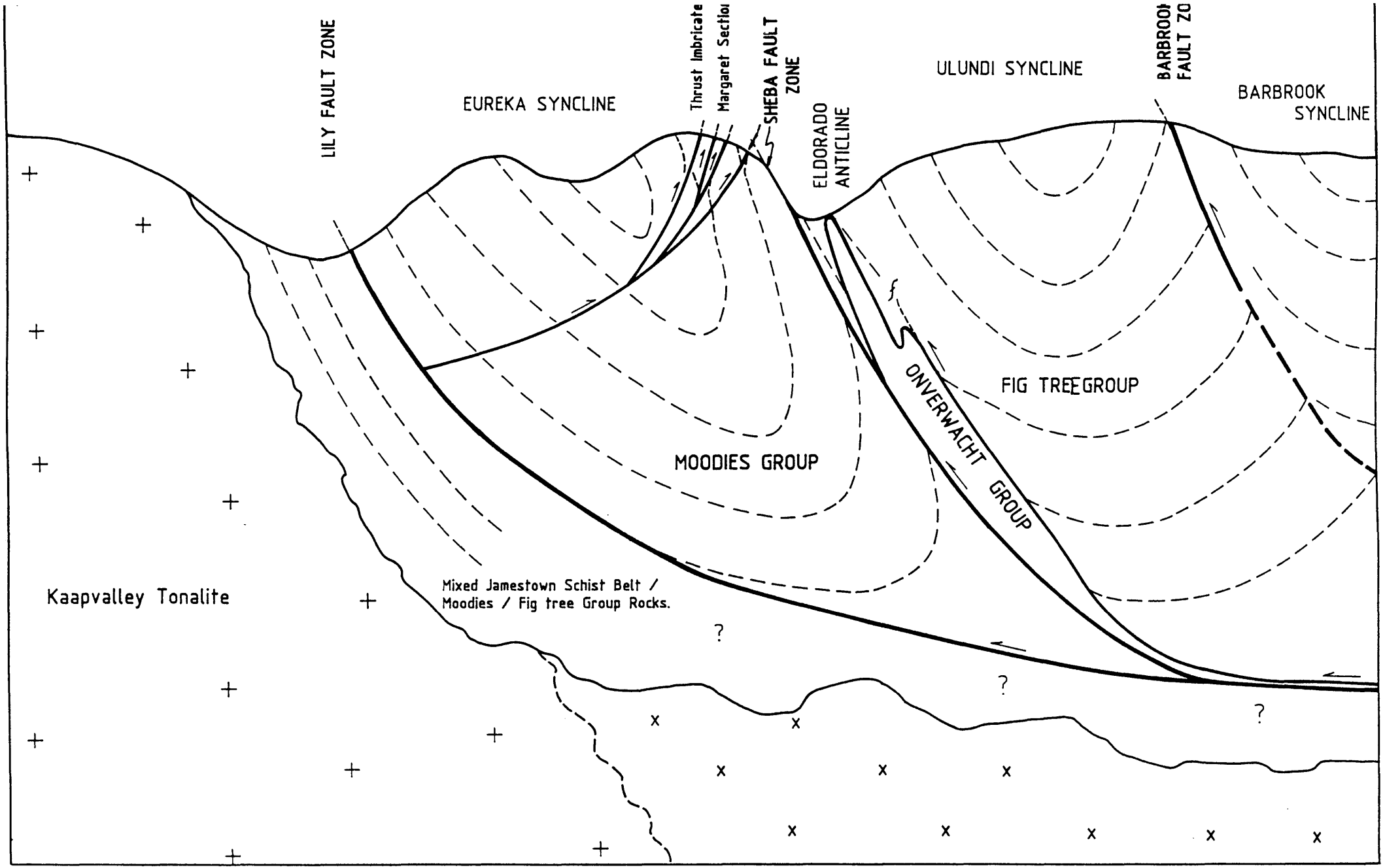

FIGURE 33

SCHEMATIC NW-SE CROSS SECTION FROM THE KAAPVALLEY TONALITE TO THE BARBROOK SYNCLINE

(not to scale)

within the supracrustal remnant, namely the Lily Fault zone (Figures 1).

It is therefore suggested that the Margaret Section imbricate set is a set of back thrusts within the larger north verging Sheba-Lily thrust system (Figure 34).

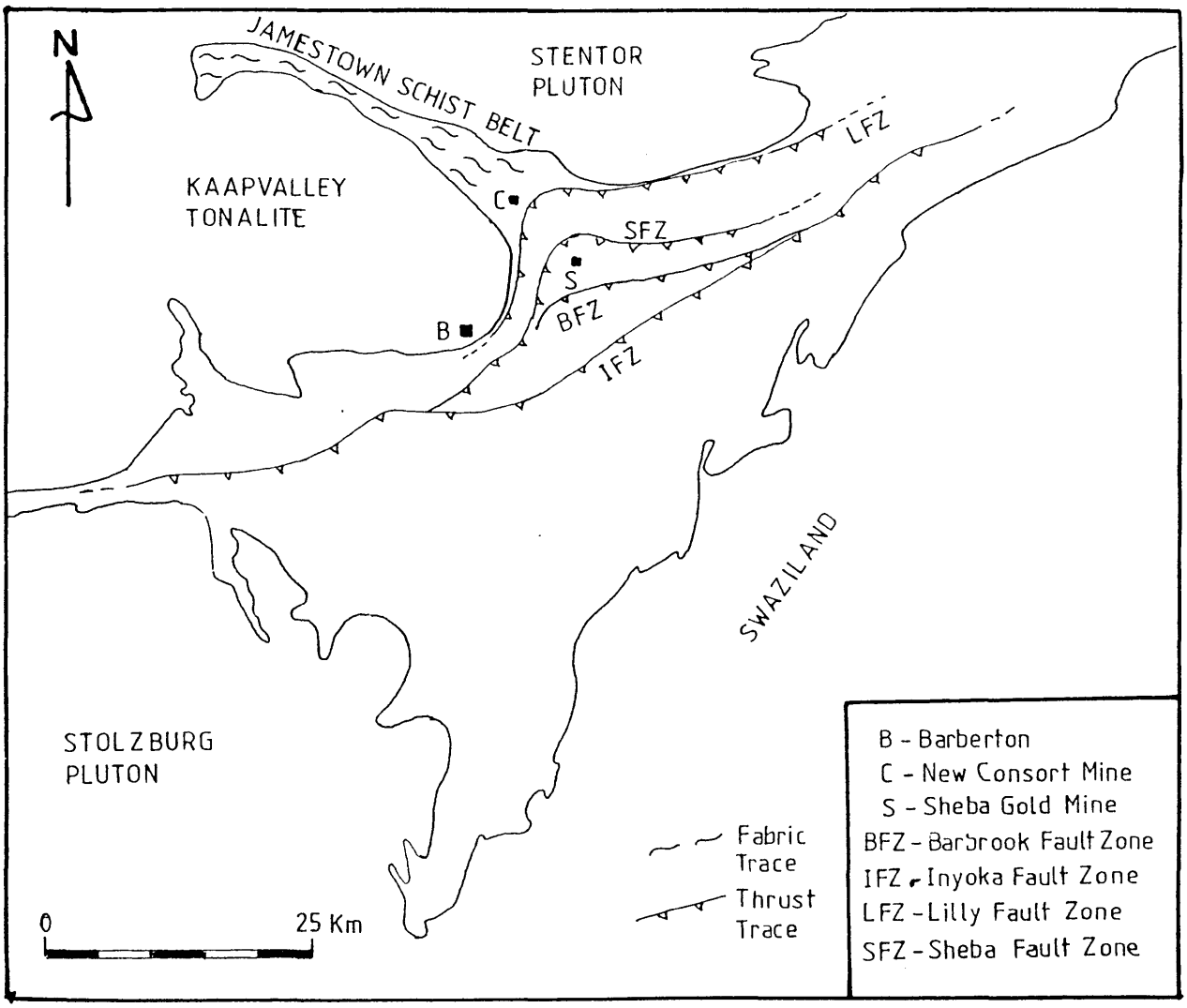

Figure 34. Simplified plan of the major shear zones of the north western Barberton supracrustal remnant (thrust plane triangles are on the overthrown block; modified after de Wit, 1991).

In the light of these facts a single progressive deformation sequence for the northern portion of the Barberton Mountain Land is proposed. In this system the first event (D_1) involved the deformation of sedimentary basins, due to crustal shortening directed along a north-west to south-east axis. This period of crustal shortening resulted in the folding and overturning of the sedimentary succession, and the development of regional scale ENE/WSW trending anticlines and synclines (eg. the Ulundi and Eureka Synclines). Continued crustal shortening led to the development of space problems in the fold belt and the eventual formation of large scale northward verging thrust faults now recognised as the Sheba Fault Zone, Barbrook Fault Zone etc. Deformation along these thrusts led to the elimination of anticlines within the fold pile and the development of the current back-to-back syncline geometry. It is also thought to have been responsible for the development of the south dipping regional cleavage.

A geometrical consequence of this northward directed thrusting was the Margaret Section imbricate fan as back thrusts in the footwall of the Sheba Fault Zone.

Differential displacement within this regional north verging thrust system is considered to have been accommodated by arcuation of the Eureka/Ulundi fold pair, resulting in regional flexural slip parallel to bedding and apparent strike slip motion east and west of the axis of arcuation.

Progressive simple shear is also responsible for the rotation of structures associated with the Eldorado Anticline into parallelism with the prominent mineral lineation seen in the ductile section of the Sheba Fault Zone as exposed at the Royal Sheba Mine.

As has already been demonstrated the Sheba Fault Zone does not exhibit similar deformation styles along its entire course. The two most prominent deformation styles are an early age of ductile deformation, observed at the Royal Sheba Mine, and a later truncating brittle deformation age, as observed at the Eldorado and Golden Quarry outcrops. It is suggested that

the strain rate and/or the orientation of the maximum compressive stress changed during deformation, resulting in brittle failure along a new course, which truncated the earlier ductile event.

With a model for the Moodies Group structure thus proposed it is important to test it against existing ideas on deformation within the Sheba Mine area and to see if it can accommodate them. The Sheba Fault has featured prominently in all deformation models for the Sheba Mine area, hence a test of the previous findings along the Sheba Fault Zone against those predicted by the modified model is appropriate. Firstly the major evidence presented in support of an age of wrench faulting along the Sheba Fault is the existence of horizontal to sub-horizontal lineations within the ductile shear zones and along bedding planes, as well as the presence of a conjugate fault set.

These features are accommodated within the new model by suggesting that they developed in response to flexural slip processes along steeply dipping bedding planes, and as oblique slip processes along the Sheba Fault Zone. Flexural slip would have occurred during the progressive arcuation of the synclines, predominantly within the well bedded greywacke and shale units of the Fig Tree Group sediments. During progressive north-westerly directed thrusting, prior to the cataclastic event on the Sheba Fault, oblique slip movement directions would be generated along the sidewall ramp portion of the thrust zone (Figure 35). Therefore thrust movement directed toward the north-west would result in an apparent wrench component along the sidewall ramp zones. It is thus suggested that these apparent wrench movements recorded along the Sheba Fault trace are more accurately classified as oblique slip movements related to thrusting. The movement directions proposed by Visser et al., (1956) and Anhaeusser (1976) for the Sheba Fault west and east of the axis of arcuation, namely left and right lateral movements respectively, can be accommodated by the oblique slip component associated with the sidewall ramp area of a north-westerly directed thrust (Figure 35). To generate the opposite sense of movement as

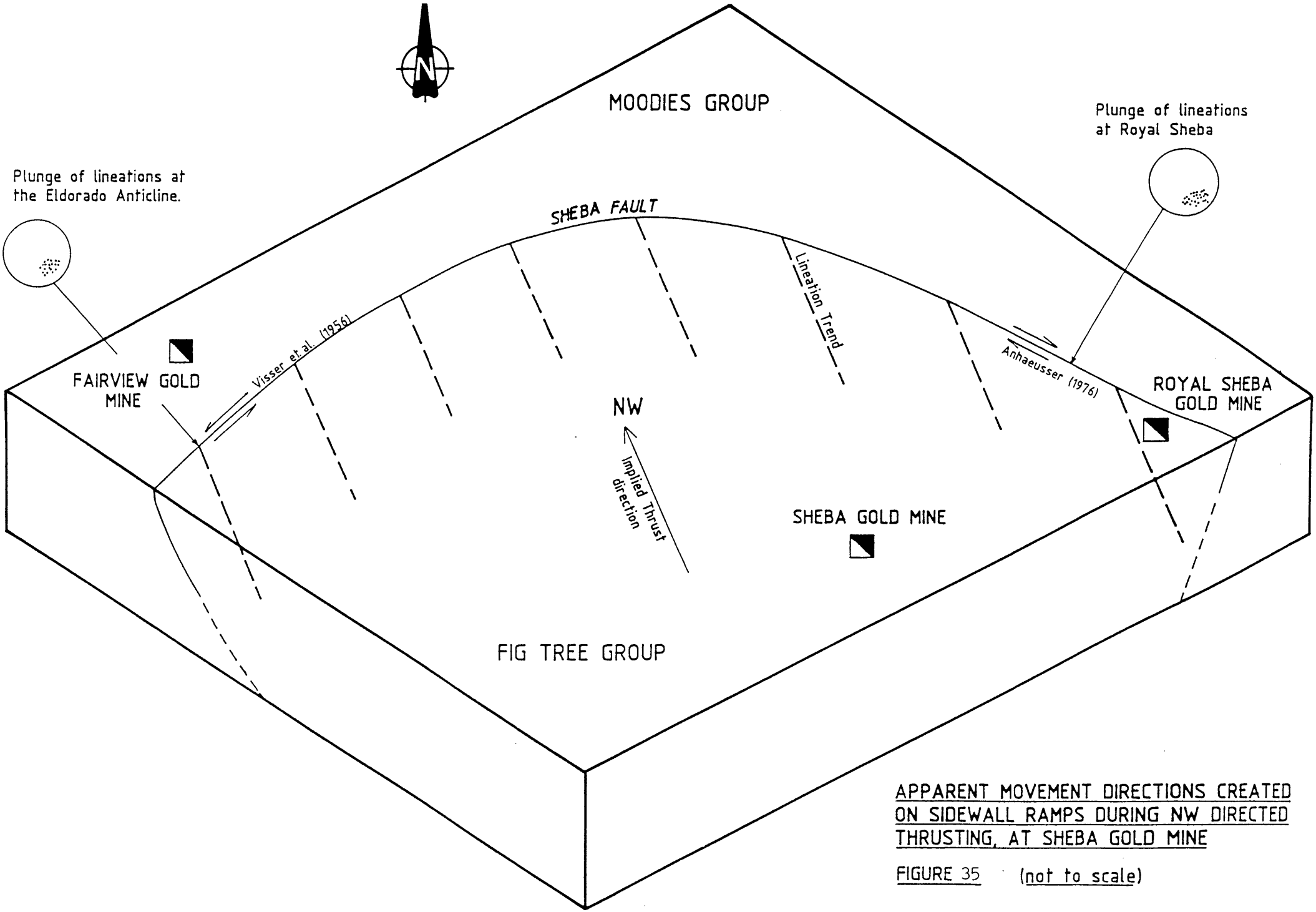

APPARENT MOVEMENT DIRECTIONS CREATED ON SIDEWALL RAMPS DURING NW DIRECTED THRUSTING, AT SHEBA GOLD MINE

FIGURE 35 (not to scale)

suggested by Robertson (1989), namely right and left lateral west and east of the axis of arcuation respectively, would require a normal movement component along the Sheba Fault zone. The stratigraphic relationship however indicates that older sediments are emplaced on top of younger sediments, a geometry which cannot be produced by normal faulting.

The regional cleavage documented by Ramsay (1963), Roering (1965), Anhaeusser (1976) and Robertson (1989) is of particular significance in testing this model. Folding is recorded during various stages in the deformation history of the north-western mountainland by all the above authors. However, they all record a conspicuous absence of folding associated with the cleavage-forming event. In the proposed model the cleavage is suggested to be related to simple shear rather than pure shear, and need not be assigned to a single deformation event.

An attempt to apply this thrust-dominated model to the remainder of the northern portion of the Barberton supracrustal remnant is difficult due to the lack of personal experience in the area; however, a number of important observations deserve documentation:

Firstly, the obvious duplication of stratigraphy south-east of the Sheba Mine area.

Secondly, the clear spatial relationship between the duplicated stratigraphy and regional persistent east-north-east faults (e.g. the Barbrook Fault) sub-parallel to the Sheba Fault zone.

Thirdly, the fact that all these major faults have the effect of juxtaposing Zwartkoppie Formation rocks against younger sediments in thrust relationship. It is therefore tentatively suggested that the entire north-western portion of the Barberton supracrustal remnant has been affected by a north-westerly directed crustal shortening event, which manifests itself primarily by ductile deformation in the form of folding followed by the development of predominantly northward verging thrust imbricates.

CHAPTER 7

CONCLUSIONS

The following conclusions can be made as a result of the present investigation into the relationship between gold mineralization and shear zone occurrence in the Moodies Group arkoses, at Sheba Gold Mine.

1) Deformation within the Mamba Shear Zone is dominated by a dip-slip movement component, with a reverse sense of motion;

2) The deformation style is consistent with that of a brittle-ductile shear environment;

3) The auriferous mineral phases are dominated by pyrite and arsenopyrite, of which several generations exist;

4) The presence of elevated gold values and sulphide concentrations in association with tourmaline mineralization suggests a late stage granitic fluid influence in the shear zones;

5) The Mamba Shear Zone has undergone hydrothermal alteration which has been dominated by the breakdown of feldspar to sericite, and an enrichment in silica, arsenic and gold within the shear zones;

6) The Eureka and Cat's Cave Shear Zones exhibit similar deformation environments, movement directions, mineralization styles and hydrothermal alteration to that seen in the Mamba Shear Zone;

7) The Eureka, Mamba and Cat's Cave Shear Zone form a north dipping thrust imbricate pile;

8) The Sheba Fault Zone in the study area exhibits a north-westerly directed thrust sense of movement;

9) The Eureka, Mamba and Cat's Cave thrust imbricate pile formed as back thrusts to the Sheba Fault Zone;

10) The deformation history of the Sheba Gold Mine area of the Barberton Mountainland can be summarised into a single progressive simple shear event.

ACKNOWLEDGEMENTS

The author would like to thank the following people and organizations for valuable contributions made to this project.

Anglovaal Limited for financing this project, through Eastern Transvaal Consolidated Mines Ltd. Capital Vote No. 3023.

Mr. J.S.Mostert, Consulting Geologist for Anglovaal, who went out of his way to promote this project.

Dr's. S.McCourt and M.J.Tomkinson for their valuable suggestions and advice in the field, as well as their endless enthusiasm.

My colleagues Simon Pepper and Peter Haworth, who without complaining, supervised my underground sections of Sheba Gold Mine in my absence.

Messrs. H.G.Philpot and G.M.van Aswegen for making the computing facilities at Anglovaal Exploration (Barberton) available to me.

The management of Barberton Mines Ltd, for allowing me to visit and publish information on Fairview Mine.

And most importantly my wife Jane, who despite being on the receiving end of my frustration was still prepared to proof read this project.

References

Allsopp, H.L., Ulrych, .J., and Nicolaysen, L.O. (1968). Dating Some Significant Rocks in the History of the Swaziland System by the Rb-Sr Isochron Method. **Canadian Journal of Earth Sciences** 5: 605-619.

Andrews, A.J., Hugon, H., Corfu, F., and Lavigne, M.J. (1986). The Anatomy of a Gold-Bearing Greenstone Belt: Red Lake, Northwest Ontario, Canada. **In**. Gold'86. Macdonald, A.J. (ed). PDM Digital Publication Management, Toronto.

Anhaeusser, C.R. (1965). Wrench Faulting and its Relationship to Gold Mineralization in the Barberton Mountain Land. **Economic Geology Research Unit**. Information Circular No. 24.

---------- (1969). **The Stratigraphy and Gold Mineralization of the Sheba Hills Area of the Barberton Mountain Land**. Ph.D. thesis (unpub.), Witwatersrand University, 332p.

---------- (1975). The Geological Evolution of the Primitive Earth: Evidence from the Barberton Mountain Land. **Information Circular Economic Geology Research Unit**. University of the Witwatersrand 98: 22p.

---------- (1976b). The Geology of the Sheba Hills Area of the Barberton Mountain Land, South Africa, with particular reference to the Eureka Syncline. **Transaction of the Geological Society of South Africa** 79: No. 2 253-280.

---------- (1986). Archaean Gold Mineralization in the Barberton Mountain Land. **In**. Anhaeusser, C.R.and Maske, S., eds., **Mineral Deposits of Southern Africa, Vol. 1.** Geological Society of South Africa., 1020p.

Anhaeusser, C.R. and Viljoen, M.J. (1965). The Base of the Swaziland System in the Barberton-Noordkaap-Louw's Creek Area, Barberton Mountain Land. **Economic Geology Research Unit**. Information Circular No. 25: 23p.

Barley, M.E. (1987). Hydrothermal Alteration of Archaean Supracrustal Sequences in the Central Norseman-Wiluma Belt, Western Australia: a Brief Review. In. Ho, S.E. and Groves, D.I. Eds., **Recent Advances in Understanding Precambrian Gold Deposits.** University of Western Australia, Publ. 2.

Barley, M.E., Eisenlohr, B.N., Groves, D.I., Perring, C.S. and Vearncombe, J.R. (1989). Late Archaean Convergent Margin Tectonics and Gold Mineralization: A New Look at the Norseman-Wiluma Belt, Western Australia. **Geology** 17: 826-829.

Barnes, H.L. (1979). **Geochemistry of Hydrothermal Ore Deposits**. John Wiley and Sons, New York, 798p.

Beach, A. (1974). A Geochemical Investigation of Pressure Solution and the Formation of Veins in a Deformed Greywacke. **Contributions to Mineralogy and Petrology** 46: 61-68.

Beach, A. (1979). Pressure Solution as a Metamorphic Process in Deformed Terrigenous Sedimentary Rocks. **Lithos** 12: 51-58.

Best, M.G. (1982). **Igneous and Metamorphic Petrology**. W.H.Freeman and Co. San Francisco, 630p.

Boulter, C.A., Fotios, M.G., and Phillips, G.N. (1987). The Golden Mile, Kalgoorlie: A Giant Gold Deposit Localized in Ductile Shear Zones by Structurally Induced Infiltration of an Auriferous Metamorphic Fluid. **Economic Geology** 82: No. 7. 1661-1677.

Butler, W.H. (1982). The Terminology of Structures in Thrust Belts. **Journal of Structural Geology** 4: No. 3 239-245.

Deer, W.A., Howie, R.A., and Zussman, J. (1966). **An Introduction to the Rock Forming Minerals**. Commonwealth Press Ltd., Hong Kong, 528p.

de Wit, M.J. (1981). Gliding and Overthrust Nappe Tectonics in the Barberton Greenstone Belt. **Journal of Structural Geology** 4: No. 2. 117-136.

de Wit, M.J. (1991). Archaean greenstone belt tectonism and basin development: some insights from the Barberton and Pietersburg greenstone belts, Kaapvaal Craton, South Africa. **Journal of African Earth Sciences** 13: No. 1. 45-64.

de Wit, M.J., Armstrong, R., Hart, R.J., and Wilson, A.H. (1987). Felsic Igneous Rocks within the 3.3- to 3.5- Ga Barberton Greenstone Belt: High Crustal Equivalents of the Surrounding Tonalite-Trondhjemite Terrane, Emplaced During Thrusting. **Tectonics** 6: No. 5. 529-549.

Eriksson, K.A. (1977). Tidal Deposits from the Archaean Moodies Group, Barberton Mountain Land, South Africa. **Sedimentary Geology** 18: 257-281.

Eriksson, K.A. (1978). Marginal Marine Depositional Processes from the Archaean Moodies Group, Barberton Mountain Land, South Africa: Evidence and Significance. **Precambrian Research** 8: 153-182.

Eriksson, K.A. (1980). Transitional Sedimentation Styles in the Moodies and Fig Tree Groups, Barberton Mountain Land, South Africa: Evidence Favouring an Archaean Continental Margin. **Precambrian Research** 12: 141-160.

Elliott, D. (1981). The Strength of Rocks in Thrust Sheets. **EOS** 62: 397.

Fripp, R.E.P., Van Nierop, D.A. Callow, M.J., Lilly, P.A. and du Plessis, L.U. (1980). Deformation in Part of the Archaean Kaapvaal Craton, South Africa. **Precambrian Research** 13: p 241-251.

Grant, J.A. (1986). The Isocon Diagram: Simple Solution to Greisen's Equation for Metasomatic Alteration. **Economic Geology** 81: 1976-1982.

Grathier, J.P. (1983). Estimation of the Volume Changes by Comparitive Chemical Analysis in Heterogeneously Deformed Rocks (Folds With Mass Transfer). **Journal of Structural Geology** 5: No. 3/4 329-339.

Gribnitz, K.H. (1964). Notes on the Barberton Goldfield. **In.** Haughton, S.H. ed., **The Geology of Some Ore Deposits in Southern Africa.** Geological Society of South Africa 2: 77-90.

Groves, D.I., Ho, S.E., McNaughton, N.J., Meuller, A.G., Perring, C.S. and Rock, N.M.S. (1988). Genetic Models for Archaean Lode-Gold Deposits in Western Australia. **In.** Ho, S.E. and Groves, D.I. eds., **Advances in Understanding Precambrian Gold Deposits.** The University of Western Australia, Publication No.12. 1-22.

Hall, A.L. (1918). The Geology of the Barberton Gold Mining District. **Geological Survey of South Africa, Memoir 9.**

Hamilton, J.V. and Hodgson, C.J. (1986). Mineralization and Structure of the Kolar Gold Field, India. **In.** Macdonald, A.J. eds., **Gold'86.** PDM Digital Publishing Management, Toronto.

Harris, L.B. (1987). A Tectonic Framework for the Western Australian Shield and its' Significance to Gold Mineralization: a Personal View. **In.** Ho, S.E. and Groves, D.I. eds., **Recent Advances in Understanding Precambrian Gold Deposits.** University of Western Australia, Publication No.11.

Hatch, F.H. and Corstorphine, G.S. (1905). **The Geology of South Africa:** 2nd ed., MacMillian and Co., London.

Haynes, S.J. (1987). Classification of Quartz Veins in Turbidite Hosted Gold Deposits, Greenschist Facies, Eastern Nova Scotia. **CIM Bulletin** 90: 37-51.

Hearn, M.G. (1943). **A Study of the Working Properties of the Chief Gold Producers of the Barberton District, Eastern Transvaal**. D.Sc. thesis (unpub.), University of the Witwatersrand, 334p.

Ho, S.E. and Groves, D.I. (1987). **Recent Advances in Understanding Precambrian Gold Deposits**. University of Western Australia, Publication 11.

Hobbs, B.E., Means, W.D. and Williams, P.F. (1976). **An Outline of Structural Geology.** John Williams and Sons, Inc. 571p.

Kerrich, R. and Allison, I. (1978). Vein Geometry and Hydrostatics during Yellow-Knife Mineralization. **Canadian Journal of Earth Sciences** 15: 1653-1660.

Kroner, A. and Compston, W. (1988). Ion Microprobe Ages of Zircons From Early Archaean Granite Pebbles and Greywacke, Barberton Greenstone Belt, Southern Africa. **Precambrian Research** 38: 367-380.

Kroner, A. and Todt, W. (1988). Single Zircon Dating Constraining the Maximum Age of the Barberton Greenstone Belt, Southern Africa. **Journal of Geophysical Research** 93: B 12 15,329-15,337.

Kroner, A., Compston, W. and Williams, I.S. (1989). Growth of the Early Crust in the Ancient Gneiss Complex of Swaziland as Revealed by Single Zircon Dating. **Tectonophysics** 161: 271-298.

Lister, G.S. and Snoke, A.W. (1984). S-C Mylonites. **Journal of Structural Geology** 6: No. 617-638.

Meyer, C. and Hemley, J.J. (1967). Wallrock Alteration, 167-235. **In**. Barnes, H.l. ed., **Geochemistry of hydrothermal ore deposits.** Holt, Reinehart and Winston, Inc., New York, 670p.

Meuller, A.G. and Harris, l.B. (1987). An Application of Wrench Tectonic Models to Mineralized Structures in the Golden Mile District, Kalgoorlie, Western Australia. **In**. Ho, S.E. and Groves, D.I. eds., **Recent Advances in Understanding Precambrian Gold Deposits.** University of Western Australia.

Miyashiro, A. (1981). **Metamorphism and Metamorphic Belts.** George Allen and Unwin, London. 492p.

Mollengraaf, G.A.F. (1898). Report of the State Geologist of the South African Republic for the year 1897. **Transactions of the Geological Society of South Africa** 4: 119-147.

Nesbitt, B.E. (1988). Gold Deposition Continuum: A Genetic Model for Lode Au Mineralization in the Continental Crust. **Geology** 16: 1044-1048.

Oosthuizen, E.J. (1976). **The Geochronology of a Suite of Rocks from the Granitic Terrain Surrounding the Barberton Mountain Land**. Ph.D. thesis, (unpubl.), University of the Witwatersrand.

Phillips, W.J. (1972). Hydraulic Fracturing and Mineralization. **Journal of The Geological Society of London** 128: 337-359.

Phillips, W.R. and Griffen, D.T. (1981). **Optical Mineralogy: the nonopaque minerals.** W.H.Freeman and Co. San Francisco. 677p.

Platt, J.P. (1984). Secondary Cleavage in Ductile Shear Zones. **Journal of Structural Geology** 6: No. 4 439-422.

Price, N.J. and Hancock, P.L. (1972). Development of Fracture Cleavage and Kindred Structures. **24th IGC Section 3**.

Ramsay, J.G. (1963). Structural Investigation in the Barberton Mountain Land, Eastern Transvaal. **Transaction of the Geological Society of South Africa** 66: 353-401.

Robb, L.J. (1977a). **The Geology and Geochemistry of the Archaean Granite-Greenstone Terrane between Nelspruit and Bushbuckridge, Eastern Transvaal**. M.Sc. thesis (unpubl.). University of the Witwatersrand.

---------- (1977b). A General Geological Description of the Archaean Granitic Terrane between Nelspruit and Bushbuckridge, Eastern Transvaal. **Information Circular. Economic Geology Research Unit**. University of the Witwatersrand 11, 12p.

Roering, C. (1965). The Tectonics of the Main Gold Producing Areas of the Barberton Mountain Land. **Information Circular Economic Research Unit**. 23: 23p.

Robertson, M. (1989). **The Structural Controls on Gold Mineralization in the Main Reef Complex: Sheba Gold Mine, Barberton**. M.Sc. thesis, (unpubl.), University of the Witwatersrand. 123p.

Rutter, E.H. (1976). The Kinematics of Rock Deformation by Pressure Solution. **Philosophical Transactions of the Royal Geological Society London** 283: 203-219.

Sang, J. and Ho, S.E. (1987). A Review of Gold Deposits in China. **In**. Ho, S.E. and Groves, D.I. eds., **Recent Advances in Understanding Precambrian Gold Deposits.** University of Western Australia. Publication 11.

Sango, P.M. (1988). Structural and Lithological Controls of Gold Mineralization in the Lupa Goldfield, Tanzania. **In**. Ho S.E. and Groves, D.I. eds., **Recent Advances in Understanding Precambrian Gold Deposits.** University of Western Australia. Publication 12: 99-110.

Schouwstra, R.P. (1988). Mineralogical Investigation of the Zwartkoppie Type Ore, Sheba Gold Mine. **South African Council for Mineral Technology. MINTEK Communication No. C1120**M: 1-32.

Schenk, A. (1888). Die Geologiesche Entwickelung Sudafrikas: Petermanns Mitt. **In**. South African Council for Stratigraphy (SACS), (1980). **Stratigraphy of South Africa**. Part 1 (Comp. L.E.Kent). Lithostratigraphy of the the Republic of South Africa, South West Africa/Namibia, and the Republics of Bophuthatswana, Transkei and Venda: Handb. 8., Geol. Surv. S.Afr: 29-43. SACS (1981).

Sibson, R.H., Robert, F. and Poulsen, K.H. (1988). High Angle Reverse Faults, Fluid Pressure Cycling, and Mesothermal Gold-Quartz Deposits. **Geology** 16: 551-555.

Sibson, R.H. (1987) Earthquake Rupturing as a Mineralizing Agent in Hydrothermal Systems. **Geology** 15: 701-705.

South African Council for Stratigraphy (SACS), (1980). **Stratigraphy of South Africa**. Part 1 (Comp.L.E.Kent). Lithostratigraphy of the the Republic of South Africa, South West Africa/Namibia, and the Republics of Bophuthatswana, Transkei and Venda: Handb. 8., Geol. Surv. S.Afr: 29-43.

Steyn, M van R. (1976). **Die Stratigrafie, Die Struktuur en die Mineralisasie van die Fairview-myngebied, Distrik Barberton, Oos-Transvaal.** D.Sc. (ongepub.), Universitiet van Pretoria.

Truswell, J.F. (1967). A Critical Review of Stratigraphic Terminology as Applied in South Africa. **Transactions of the Geological Society of Southern Africa** 70: 81-116.

Truter, F.C. (1950). A Review of Volcanism in the Geological History of South Africa. **Proceedings of the Geological Society of South Africa** 52: 29-139.

Turner, J.F. and Verhoogen, J. (1960). **Igneous and Metamorphic Petrology.** McGraw-Hill Beck Co. U.S.A. 694p.

Van Eeden, O.R. (1941). Die Geologie van die Shebarante en Omstreke, Distrik Barberton. D.Sc. (unpub.),. University of Stellenbosch. **In**. SACS 1980. **Stratigraphy of South Africa**. Part 1 (Comp.L.E.Kent). Lithostratigraphy of the Republic of South Africa, South West Africa/Namibia, and the Republics of Bophuthatswana, Transkei and Venda: Handb. 8., Geol. Surv.S.Afr: 29-43.

Vearncombe, J.R. (1989). **Structural Processes of Epigenetic Gold Mineralization.** Unpublished Course notes.

Viljoen, M.J. and Viljoen, R.P. (1969a). An Introduction to the Geology of the Barberton Granite-Greenstone Terrain. **In**. Upper Mantle Project. **Special Publication of the Geological Society of South Africa** 2: 9-28.

---------- (1969b). The Geology and Geochemistry of the Lower Ultramafic Unit of the Onverwacht Group and a Proposed New Class of Igneous Rock. **In**. Upper Mantle Project. **Special Publication of the Geological Society of South Africa** 2: 55-85.

---------- (1979). Reassessment of Part of the Barberton Type Section Area, South Africa- a comment. **Precambrian Research** 9: 349-352.

Visser, D.J.L., Van Eeden, O.R., Joubert, G.K., Sohnge, A.P.G., Van Zyl, J.S., Rossouw, P.J., and Taljaard, J.J. (1956). The Geology of the Barberton Area. **Special Publication of the Geological Survey of South Africa** 15: 242p.

Wagener, J.H.F. and Wiegand, J. (1986). The Sheba Gold Mine, Barberton Greenstone Belt, 155-161. **In**. Anhaeusser, C.R. and Maske, ., eds., **Mineral Deposits of Southern Africa,1. Geological Society of South Africa.**, 1020p.

Weissberg, B.C. (1970). Solubility of Gold in Hydrothermal Alkaline Sulphide Solutions. **Economic Geology,** 65: 551-556.

Williams, D.A.C. and Furnell, R.G. (1979). Reassessment of Part of the Barberton Type Area, South Africa. **Precambrian Research** 9: 325-347.

Wise, D.H., Dunn, D.E., Engelder, J.T.,Geiser, P.A., Hatcher,.D., Kish, S.A., Odom, A.L., and Schamel, S. (1984). Fault Related Rocks: Suggestions for Terminology. **Geology** 12: 391-394.

Appendix 1

EASTERN TRANSVAAL CONSOLIDATED MINES LIMITED

SHEBA (MAMBA) Mine BH No. 11M30 Sheet 1 Date: 17/10/1989 Logged by: G.B.SNOW

Drilling Commenced: 3/5/1989 Farm Name: X = Y = Z =
Drilling Completed: 15/5/1989 Farm No. SYSTEM:

GEOLOGICAL LOG — MINERALIZED BOREHOLE — SAMPLING

FROM	TO	M,I	ROCKTYPE	CONTACTS	CA=0°	Grainsize	COLOUR	STRUCTURE	KEY FEATURES	MINERALIZATION	Alteration/Description	FROM	TO	No.
0.00	45.74	M	Arkosite		39	fine	grey	sedimentary structures	crude banding	minor pyrite	local zones of intense carbonate alteration	000	17	
												17	50	
												50	76	
												76	106	
0.00	2.02	I	Arkosite	sheared		fine	dark	bedding parallel chloritic shears			minor chloritic	106	137	
								truncate carbonate veins; bedding				137	167	
								steepens into fracture; irregular				167	191	
								quartz-carbonate veins				191	220	
												220	228	
1.80	1.90	P	Irregular									228	250	
			quartz									250	260	
			vein									260	290	
												290	324	
2.02	2.27	M	Arkosite	sheared		fine	pale	crude bedding	crude banding	euhedral pyrite &	minor carbonate &	324	357	
								micro-shears		ascicular arseno-	silicification	357	384	
										pyrite associated		384	415	
										with quartz veins		415	445	
												445	478	
2.27	2.53	M	Arkosite	sheared		fine	pale	brecciated	carbonate filled	euhedral pyrite	carbonate and	478	507	
								veins; chlorite	bounding shears;		silicification	507	538	
								shears	ptygmatic veining			538	568	
									silicious fragments			568	601	
									in carbonate matrix			601	635	
												635	665	
2.53	2.53	2.71	M	Arkosite	sheared	37.5	fine	pale	bedding parall		ascicular arseno-	minor carbonate	665	694	
								-el chloritic		pyrite and fine		694	725	
								shears		euhedral pyrite		725	751	

EASTERN TRANSVAAL CONSOLIDATED MINES LIMITED

SHEBA (MAMBA) Mine BH No. 11M30 Sheet 2 Date: 17/10/1989 Logged by: G.B.SNOW

Drilling Commenced: 3/5/1989 Farm Name :
Drilling Completed : 15/5/1989 Farm No.

X = Y = Z =
SYSTEM:

MINERALIZED BOREHOLE

GEOLOGICAL LOG

SAMPLING

FROM	TO	M.I	ROCKTYPE	CONTACTS	CA=0°	Grainsize	COLOUR	STRUCTURE	KEY FEATURES	MINERALIZATION	Alteration/Description	FROM	TO	No.
					40			minor cross-	pyrite smears on					
								cutting quartz	shear planes			751	780	
								carbonate veins				780	812	
												812	840	
2.71	45.74	M	Arkosite	sheared	45	fine	grey	minor chloritic	well bedded: pristine		minor chloritic	840	890	
								bedding parallel				890	995	
								shears				995	1095	
												1095	1195	
3.00	3.22	P	hydraulic brecciation									1195	1310	
												1310	1410	
42.55	42.71	P	dark quartz								minor carbonate	1410	1510	
			vein									1510	1610	
												1610	1710	
END OF HOLE AT 45.74m												1710	1810	
												1810	1910	
												1910	2010	
												2010	2110	
												2110	2595	
												2595	3095	
												3095	3595	
												3595	4095	
												4095	4574	

EASTERN TRANSVAAL CONSOLIDATED MINES LIMITED

SHEBA (MAMBA) Mine BH No. 11M29 Sheet 2 Date: 17/10/1989 Logged by: G.B.SNOW

Drilling Commenced: 20/4/1989 Farm Name: X = Y = Z =
Drilling Completed: 2/5/1989 Farm No. SYSTEM:

GEOLOGICAL LOG — UNMINERALIZED BOREHOLE — SAMPLING

FROM	TO	M,I	ROCKTYPE	CONTACTS	CA=0°	Grainsize	COLOUR	STRUCTURE	KEY FEATURES	MINERALIZATION	Alteration/Description	FROM	TO	No.
1.76	2.00	I	chloritic shearing					chloritic shears and microfractures			chloritic			
	2.00		Iron Oxide joint		34									
2.00	5.56	M	Arkosite	sharp		fine		thin zones of hydraulic brec-ciation; bedd-ing parallel chloritic shears	crude colour band-ing; thin shale bands; folding in bedding; iron oxide joints	disseminated pyrite	chloritis alterat-ion about shears			
END OF HOLE AT 5.56m														

EASTERN TRANSVAAL CONSOLIDATED MINES LIMITED

SHEBA (MAMBA) Mine BH No. 11M29 Sheet 1 Date: 17/10/1989 Logged by: G.B.SNOW

Drilling Commenced: 20/4/1989 Farm Name : X = Y = Z =
Drilling Completed : 2/5/1989 Farm No. SYSTEM:

GEOLOGICAL LOG — UNMINERALIZED BOREHOLE — SAMPLING

FROM	TO	M,I	ROCKTYPE	CONTACTS	CA=0°	Grainsize	COLOUR	STRUCTURE	KEY FEATURES	MINERALIZATION	Alteration/Description	FROM	TO	No.
0.00	5.56	M	Arkosite	sharp	23.5	fine	pale	numerous quartz carbonate veins	intense bleaching; transposed veins		intense carbonate			
								chloritic and sericitic shears				00	36	
												36	66	
												66	96	
												96	126	
0.00	1.26	I	Arkosite	gradational		fine	pale	quartz-carbonate veins cut by irregular late carbonate veins; sericitis and chloritic shears cross all	crude colour banding	fine euhedral pyrite	carbonate and silicification; locally chloritic		166	
												166	174	
												174	200	
												200	233	
												233	263	
												263	293	
												293	313	
												313	345	
1.10	1.20	P	Stockwork veins									345	375	
												375	405	
1.26	1.66	M	Dark quartz vein	sharp	88	v.fine	dark	lower contact sheared; micro-fracturing; irregular calcite veining	inclusions of arkosite in vein	minor pyrite with micro-fracturing	dark quartz replacing light quartz in vein	405	429	
												429	460	
												460	485	
												485	521	
												521	556	
1.66	2.00	M	Arkosite	sheared		fine	pale	intense sericitis shearing; cross cutting calcite veins		minor pyrite	intense carbonate & silicification			

Appendix 2

Element	Tube	KV	Ma	Analytical Line	Analysing Crystal	Collimator	Counter	Peak 2θ	Count Time Sec.	Background 2θ	Count Time Sec.	Standard	Blanks	Detection Limits	Analytical Accuracy
SiO_2	Cr	50	50	Ka	Pet	Coarse	Flow	109.165	60	106.000	30	SiO_2 100% NIMD 37.02%		0.004%	0.2%
Al_2O_3	Cr	50	50	Ka	"	"	"	145.040	60	139.160	30	NIML 13.90%	SiO_2	0.005%	0.5%
Fe_2O_3	Au	50	50	Ka	Lif200	Fine	"	57.525	40	Blank standards used to calibrate background.		NIML 10.28%	SiO_2 and $60CaO+40SiO_2$	0.001%	0.5%
MnO	Au	50	50	Ka	Lif200	"	"	62.990	40			NIML 0.78%	SiO_2 and $60CaO+40SiO_2$	0.001%	0.5%
MgO	Cr	50	50	Ka	PX-1	Coarse	"	23.300	60	25.300	30	W-1 6.55%	SiO_2	0.011%	0.3%
CaO	Cr	50	50	Ka	pet	Fine	"	45.240	40	Blank standards		NIML 3.32%	SiO_2 and $40Fe_2O_3 60SiO_2$	0.0003%	0.2%
K_2O	Cr	50	50	Ka	Pet	"	"	50.720	40	used to calibrate		W-1 0.65%	SiO_2 and $60CaO+40SiO_2$	0.0003%	0.2%
TiO_2	Cr	50	50	Ka	Pet	"	"	36.720	40	background		W-1 1.05%	SiO_2 and $60CaO+40SiO_2$	0.0004%	0.2%
P_2O_5	Cr	50	50	Ka	Ge	Coarse	"	141.040	60	138.000 143.000	30 30	BR 1.10%	SiO_2	0.001%	0.2%
Na_2O	Cr	50	50	Ka	PX-1	Fine	"	28.170	60	30.000	30	BR 3.12%	SiO_2	0.018%	2%
Sc	Cr	50	50	Ka	Lif200	"	"	97.730	60	95.850 98.555	30 30	BCR 33 ppm	SiO_2 and $CaCO_3$	0.3 ppm	10%
Ba	Cr	50	50	La	Lif220	"	"	115.275	60	114.500 116.500	30 30	W-1 160 ppm	SiO_2 and MgO	1 ppm	± 20%
Zn	Au	50	50	Ka	Lif200	"	"	41.795	60	39.65 46.70	30 30	NIMP 100 ppm	SiO_2 and $CaCo_3$	0.3 ppm	± 10%
Cu	Au	50	50	Ka	Lif200	"	"	45.040	60	39.65 46.70	30 30	W-1 110 ppm	SiO_2 and $CaCo_3$	0.2 ppm	± 10%
Ni	Au	50	50	Ka	Lif200	"	"	48.690	60	46.70 50.00	30 30	BR 260 ppm	SiO_2 and $CaCo_3$	0.1 ppm	± 10%
Cr	Au	50	50	Ka	Lif200	"	"	69.375	60	68.10 70.80	30 30	JB1 400 ppm	SiO_2	0.6 ppm	10%
V	Au	50	50	Ka	Lif220	"	"	123.220	60	117.10 123.80	30 30	W-1 260 ppm	SiO_2	0.5 ppm	± 10%
La	Au	50	50	Ka	Lif220	"	"	138.920	60	132.60 141.80	30 30	BR 80 ppm	SiO_2	1.5 ppm	15%
Zr	Rh	50	50	Ka	Lif220	"	Scint	32.045	60	29.30 34.89	30 30	AGV 230 ppm	SiO_2	0.3 ppm	3%
Sr	Rh	50	50	Ka	Lif220	"	"	35.830	60	34.89 36.90	30 30	W-1 190 ppm	SiO_2	0.2 ppm	3%
Nb	Rh	50	50	Ka	Lif220	"	"	30.420	60	29.45 34.80	30 30	GSP 23 ppm	SiO_2	0.1 ppm	3%
Y	Rh	50	50	Ka	Lif220	"	"	33.855	60	29.45 34.80	30 30	NIMG 145 ppm	SiO_2	0.3 ppm	3%
Rb	Rh	50	50	Ka	Lif220	"	"	37.960	60	34.80 41.10	30 30	NIMG 320 ppm	SiO_2	0.4 ppm	2%
U	Rh	50	50	Ka	Lif220	"	"	37.300	100	36.90 41.10	30 30	NIMG 15 ppm	SiO_2	0.1 ppm	20%
Th	Rh	50	50	Ka	Lif220	"	"	39.250	100	36.90 41.10	30 30	GSP 105 ppm	SiO_2	0.5 ppm	20%
Pb	Au	50	50	Ka	Lif220	"	Flow/ Scint	40.225	60	39.80 41.50	30 30	GSP 54 ppm	SiO_2	1 ppm	± 10%
Ga	Au	50	50	Ka	Lif220	"	"	56.165	60	55.50 57.20	30 30	GSP 23 ppm	SiO_2	0.2 ppm	10%
Co	Au	50	50	Ka	Lif220	"	"	77.890	60	77.40 79.00	30 30	NIMD 210 ppm	SiO_2	1 ppm	± 10%

12 May 1989
/br

Appendix 3

row	Samno	Si	DELTA_Si	Al	Fe	DELTA_Fe	Mn	DELTA_Mn	Mg	DELTA_Mg	Ca	DELTA_Ca	Na	K
1	MC1	70.03	-0.180	14.16	4.25	0.780	0.04	-0.104	2.82	0.316	0.98	-0.430	1.72	5.30
2	MC2	69.62	-0.195	14.33	4.16	0.721	0.05	0.107	2.80	0.291	1.21	-0.304	1.58	5.39
3	MC3	69.80	-0.210	14.66	3.94	0.594	0.03	-0.351	2.62	0.181	0.67	-0.623	2.60	5.27
4	MC4	70.08	-0.209	14.70	3.86	0.557	0.03	-0.353	2.58	0.160	0.70	-0.608	2.63	5.10
5	MC5	69.01	-0.210	14.49	4.03	0.649	0.05	0.095	2.95	0.346	1.25	-0.289	2.55	5.06
6	MC6	69.59	-0.176	14.01	3.97	0.680	0.06	0.359	2.83	0.335	1.53	-0.100	2.38	4.61
7	MC7	71.26	-0.153	13.96	3.69	0.567	0.04	-0.091	2.54	0.203	1.30	-0.233	0.47	5.49
8	MC8	70.42	-0.189	14.40	3.43	0.412	0.05	0.102	2.81	0.290	2.04	0.167	0.00	5.24
9	MC9	72.45	-0.013	12.17	4.36	1.124	0.05	0.303	2.05	0.113	2.16	0.463	0.00	4.37
10	MC10	83.51	1.376	5.83	3.19	2.245	0.06	2.265	1.57	0.780	2.28	2.223	0.08	2.25
11	MC11	67.88	-0.369	17.84	3.70	0.230	0.03	-0.467	1.87	-0.307	0.93	-0.570	0.02	6.46
12	MC12	67.73	-0.978	14.86	4.86	0.939	0.06	0.281	3.11	0.383	1.96	0.087	0.00	5.27
13	MC13	74.45	0.028	12.01	4.00	0.975	0.04	0.057	2.29	0.260	1.37	-0.060	0.00	4.44
14	MC14	72.74	-0.105	13.48	3.37	0.482	0.04	-0.059	1.99	-0.024	1.18	-0.279	1.08	5.28
15	MC15	72.32	-0.108	13.44	3.21	0.416	0.04	-0.056	1.94	-0.046	1.20	-0.264	1.79	5.11
16	MC16	70.20	-0.120	13.23	3.30	0.479	0.10	-0.760	2.73	0.364	2.54	0.582	2.39	4.85
17	MC17	70.64	-0.155	13.86	3.94	0.686	0.04	-0.084	2.40	0.144	0.74	-0.560	2.33	5.26
18	MC18	72.30	-0.116	13.57	3.14	0.372	0.03	-0.299	1.92	-0.065	0.75	-0.545	2.61	5.07
19	MC19	70.48	-0.185	14.34	3.83	0.584	0.03	-0.336	2.19	0.009	0.66	-0.621	2.47	5.61
20	MC20	70.62	-0.125	13.39	3.29	0.457	0.09	1.132	2.50	0.234	2.22	0.366	2.48	4.94
21	MC21	70.63	-0.167	14.06	3.81	0.607	0.04	-0.097	2.28	0.072	0.96	-0.437	2.58	5.21
22	MC22	70.53	-0.183	14.31	3.72	0.542	0.03	-0.335	2.23	0.030	0.65	-0.626	2.30	5.25
23	MC23	71.29	-0.169	14.22	3.46	0.443	0.03	-0.331	2.03	-0.056	0.71	-0.589	2.53	5.19
24	MC24	71.73	-0.148	13.96	3.15	0.338	0.04	-0.091	1.93	-0.086	0.87	-0.486	3.03	5.07
25	MC25	69.91	-0.227	15.00	3.69	0.459	0.03	-0.366	2.17	-0.044	0.56	-0.692	2.57	5.75
26	MC26	71.37	-0.162	14.12	3.21	0.348	0.04	-0.101	1.93	-0.097	0.81	-0.527	2.74	5.18
27	MC27	72.35	-0.132	13.82	3.23	0.386	0.04	-0.082	1.90	-0.091	0.76	-0.547	2.70	4.95
28	MC28	70.44	-0.162	13.94	3.54	0.506	0.05	0.138	2.26	0.072	1.35	-0.202	2.96	5.07
29	MC29	69.79	-0.189	14.40	3.79	0.561	0.05	0.102	2.38	0.092	1.19	-0.319	2.65	5.11
30	MC30	70.34	-0.188	14.37	3.79	0.564	0.03	-0.338	2.17	-0.002	0.77	-0.558	2.52	5.45
31	MC31	71.74	-0.119	13.51	3.63	0.593	0.03	-0.296	2.00	-0.022	0.81	-0.506	2.31	5.29
32	MC32	71.84	-0.139	13.84	3.38	0.448	0.03	-0.312	1.92	-0.083	0.70	-0.583	2.58	5.26
33	MC33	70.35	-0.163	13.94	3.48	0.480	0.07	0.593	2.30	0.090	1.58	-0.066	2.53	5.64
34	MC34	71.92	-0.153	14.08	3.30	0.390	0.03	-0.324	1.85	-0.132	0.69	-0.596	2.73	5.20
35	MC35	70.96	-0.170	14.18	3.48	0.455	0.03	-0.329	2.02	-0.058	0.74	-0.570	2.70	5.24
36	MC36	71.61	-0.175	14.40	3.05	0.256	0.04	-0.119	1.77	-0.188	0.92	-0.474	2.59	4.99
37	MC37	70.99	-0.193	14.58	3.19	0.297	0.04	-0.130	1.91	-0.134	1.18	-0.333	2.35	4.95
38	MC38	70.37	-0.187	14.36	3.59	0.482	0.04	-0.116	2.18	0.003	1.12	-0.357	2.73	5.15
39	MC39	70.84	-0.169	14.13	3.37	0.414	0.05	0.123	2.09	-0.022	1.27	-0.259	2.92	5.11
40	MC40	70.71	-0.158	13.92	3.30	0.406	0.06	0.367	2.09	-0.008	1.52	-0.100	2.86	4.95
41	MC41	71.92	-0.124	13.61	3.05	0.329	0.05	0.166	1.94	-0.058	1.33	-0.195	2.82	4.93
42	MC42	72.32	-0.149	14.10	2.89	0.215	0.03	-0.325	1.75	-0.180	0.89	-0.480	2.99	4.96
43	MC43	70.11	-0.203	14.58	3.75	0.525	0.04	-0.130	2.19	-0.007	0.96	-0.457	2.89	5.08
44	MC44	71.68	-0.174	14.39	3.04	0.253	0.03	-0.339	1.83	-0.159	0.63	-0.639	3.32	4.86
45	MC45	72.04	-0.157	14.17	3.21	0.343	0.02	-0.552	1.81	-0.156	0.68	-0.605	3.02	5.04
46	MC46	73.62	-0.047	12.81	2.75	0.273	0.05	0.238	1.84	-0.051	1.28	-0.177	2.40	4.93
47	MC47	76.52	0.000	12.69	2.14	0.000	0.04	0.000	1.92	0.000	1.54	0.000	0.00	4.55
48	MC48	71.55	-0.131	13.66	3.51	0.524	0.05	0.161	2.32	0.123	1.19	-0.282	2.15	4.61

File DELTA4 1/ 7/91

row	DELTA_K	Ti	DELTA_Ti	P	DELTA_P	DISTANCE	SLOPE
1	0.044	0.4004	0.473	0.07	0.568	8.5	1.116
2	0.049	0.3966	0.442	0.06	0.328	33.5	1.129
3	0.003	0.4023	0.430	0.06	0.298	63.0	1.155
4	-0.032	0.4405	0.561	0.08	0.727	91.0	1.158
5	-0.026	0.3959	0.423	0.06	0.314	121.5	1.142
6	-0.082	0.3761	0.398	0.05	0.132	152.0	1.104
7	0.097	0.3701	0.381	0.06	0.364	179.0	1.100
8	0.015	0.3411	0.234	0.05	0.102	205.5	1.135
9	0.001	0.4256	0.822	0.12	2.128	224.0	0.959
10	0.076	0.1434	0.281	0.08	3.353	239.0	0.459
11	0.010	0.5503	0.607	0.08	0.423	255.0	1.406
12	-0.011	0.4551	0.595	0.06	0.281	275.0	1.171
13	0.031	0.3247	0.408	0.04	0.057	307.0	0.946
14	0.092	0.3111	0.202	0.05	0.177	340.5	1.062
15	0.060	0.3078	0.193	0.05	0.180	370.5	1.059
16	0.022	0.3230	0.272	0.05	0.199	399.5	1.043
17	0.058	0.3900	0.466	0.05	0.144	430.0	1.092
18	0.042	0.3435	0.319	0.05	0.169	461.5	1.069
19	0.091	0.3683	0.338	0.04	-0.115	492.5	1.130
20	0.029	0.3262	0.269	0.05	0.185	522.5	1.055
21	0.033	0.3833	0.420	0.05	0.128	553.0	1.108
22	0.023	0.3640	0.325	0.05	0.108	584.5	1.128
23	0.018	0.3518	0.289	0.05	0.116	618.0	1.121
24	0.013	0.3322	0.240	0.05	0.136	650.0	1.100
25	0.069	0.3797	0.319	0.05	0.057	679.5	1.182
26	0.023	0.3299	0.217	0.05	0.123	709.5	1.113
27	-0.001	0.3161	0.192	0.05	0.148	738.0	1.089
28	0.014	0.3483	0.302	0.04	-0.090	765.5	1.099
29	-0.010	0.3758	0.359	0.05	0.102	796.0	1.135
30	0.058	0.3871	0.403	0.05	0.104	826.0	1.132
31	0.092	0.3766	0.452	0.05	0.174	865.0	1.065
32	0.060	0.3671	0.382	0.05	0.146	942.5	1.091
33	0.128	0.3459	0.293	0.05	0.138	1045.0	1.099
34	0.030	0.3473	0.285	0.05	0.127	1145.0	1.110
35	0.031	0.3563	0.309	0.04	-0.105	1252.5	1.117
36	-0.034	0.3201	0.158	0.04	-0.119	1352.5	1.135
37	-0.053	0.3465	0.238	0.05	0.088	1452.5	1.149
38	0.000	0.3621	0.314	0.05	0.105	1552.5	1.132
39	0.009	0.3700	0.364	0.05	0.123	1652.5	1.113
40	-0.008	0.3481	0.303	0.05	0.140	1752.5	1.097
41	0.010	0.3215	0.231	0.05	0.166	1852.5	1.072
42	-0.019	0.3536	0.306	0.05	0.125	1952.5	1.111
43	-0.028	0.3876	0.385	0.05	0.088	2052.5	1.149
44	-0.058	0.3259	0.180	0.05	0.102	2352.5	1.134
45	-0.008	0.3448	0.268	0.04	-0.104	2845.0	1.117
46	0.073	0.2849	0.159	0.04	-0.009	3345.0	1.009
47	0.000	0.2436	0.000	0.04	0.000	3845.0	1.000
48	-0.059	0.3247	0.238	0.05	0.161	4335.0	1.076

row	Samno	Si	DELTA_Si	Al	Fe	DELTA_Fe	Mn	DELTA_Mn	Mg	DELTA_Mg	Ca	DELTA_Ca	Na	DELTA_Na	K
1	MC49	71.98	0.02	13.59	3.31	-0.31	0.03	-0.41	2.05	-0.37	0.92	-0.34	2.19	0.13	5.28
2	MC50	74.15	0.15	12.44	2.72	-0.38	0.03	-0.35	1.67	-0.44	1.22	-0.05	2.33	0.31	4.86
3	MC51	71.69	-0.02	14.00	3.18	-0.36	0.03	-0.42	1.81	-0.46	0.97	-0.33	2.02	0.01	5.71
4	MC52	71.79	-0.01	13.93	2.55	-0.48	0.04	-0.23	1.56	-0.53	1.70	0.18	1.50	-0.25	6.13
5	MC53	96.18	19.10	0.92	1.25	2.86	0.02	4.85	0.33	0.50	0.90	8.47	0.04	-0.70	0.40
6	MC54	74.51	0.59	9.02	3.07	-0.03	0.07	1.09	2.08	-0.04	5.27	2.64	1.32	0.03	4.30
7	MC55	71.59	0.04	13.18	3.70	-0.20	0.04	-0.18	2.54	-0.20	1.25	-0.08	2.80	0.49	4.73
8	MC56	75.25	0.13	12.78	3.48	-0.23	0.05	0.05	2.49	-0.19	1.57	0.19	2.10	0.15	4.60
9	MC57	71.49	0.04	13.20	3.36	-0.28	0.07	0.43	2.64	-0.16	1.82	0.33	2.24	0.19	4.79
10	MC58	72.66	0.11	12.59	3.61	-0.19	0.07	0.50	2.65	-0.12	2.01	0.54	1.57	-0.13	4.51
11	MC59	72.25	0.03	13.48	3.56	-0.25	0.03	-0.40	2.38	-0.26	0.74	-0.47	2.29	0.19	4.73
12	MC60	69.75	-0.05	14.10	3.98	-0.20	0.04	-0.24	2.68	-0.21	1.15	-0.21	2.66	0.32	4.99
13	MC61	68.89	-0.10	14.72	4.22	-0.19	0.04	-0.27	2.75	-0.22	0.82	-0.46	2.37	0.13	5.14
14	MC62	71.94	0.06	13.05	3.18	-0.31	0.07	0.44	2.43	-0.22	1.96	0.45	2.74	0.47	4.37
15	MC63	67.02	-0.07	13.87	5.65	0.16	0.07	0.36	3.77	0.14	1.73	0.21	2.11	0.07	4.80
16	MC64	67.47	-0.09	14.24	5.96	0.19	0.05	-0.06	3.91	0.15	0.99	-0.33	1.71	-0.16	4.92
17	MC65	66.88	-0.12	14.55	5.80	0.13	0.05	-0.08	3.81	0.09	1.23	-0.18	1.84	-0.11	5.09
18	MC66	69.96	0.00	13.45	4.74	0.00	0.05	0.00	3.22	0.00	1.39	0.00	1.92	0.00	4.86
19	MC67	71.33	0.00	13.41	4.08	0.00	0.04	0.00	2.65	0.00	0.82	0.00	2.06	0.00	5.06

row	DELTA_K	Ti	DELTA_Ti	P	DELTA_P	DISTANCE	SLOPE	Au
1	0.08	0.3532	-0.07	0.05	-0.18	18.0	1.01	0.15
2	0.08	0.2499	-0.28	0.04	-0.28	51.0	0.92	0.10
3	0.13	0.3448	-0.12	0.05	-0.20	81.0	1.04	0.25
4	0.22	0.3101	-0.21	0.05	-0.20	111.0	1.04	0.45
5	0.20	0.0277	0.07	0.02	3.87	146.0	0.07	0.65
6	0.32	0.1850	-0.27	0.16	2.98	170.0	0.67	0.10
7	-0.01	0.3323	-0.10	0.07	0.19	187.0	0.98	0.10
8	0.00	0.3136	-0.13	0.06	0.05	216.5	0.95	0.30
9	0.00	0.2895	-0.22	0.05	-0.15	248.0	0.98	0.10
10	-0.01	0.2889	-0.18	0.05	-0.11	278.0	0.94	0.25
11	-0.03	0.3347	-0.11	0.05	-0.17	303.0	1.00	0.10
12	-0.02	0.5133	0.30	0.09	0.43	329.0	1.05	0.08
13	-0.03	0.5206	0.26	0.09	0.37	360.0	1.09	0.10
14	-0.07	0.3318	-0.09	0.06	0.03	390.0	0.97	0.08
15	-0.04	0.4173	0.07	0.06	-0.03	417.0	1.03	0.08
16	-0.04	0.4630	0.16	0.06	-0.06	444.5	1.06	0.08
17	-0.65	0.4528	0.11	0.06	-0.08	474.5	1.08	0.08
18	0.00	0.3773	0.00	0.06	0.00	505.0	1.00	0.08
19	0.00	0.3485	0.00	0.05	0.00	538.5	1.09	0.10

row	Samno	Sc	DELTA_Sc	Ba	DELTA_Ba	Cr	DELTA_Cr	V	DELTA_V	La	DELTA_La	Zn	DELTA_Zn
1	MC1	12.5	0.62	764.9	-0.32	355.1	0.76	72.3	0.55	9.6	-0.29	54.9	1.89
2	MC2	13.5	0.73	816.8	-0.28	344.2	0.68	71.3	0.51	9.5	-0.31	48.7	1.54
3	MC3	12.8	0.61	750.9	-0.36	367.3	0.75	74.2	0.53	16.8	0.19	46.9	1.39
4	MC4	13.2	0.65	716.7	-0.39	414.8	0.98	78.1	0.61	10.5	-0.26	49.6	1.52
5	MC5	12.6	0.60	699.0	-0.39	352.0	0.70	73.5	0.54	10.3	-0.26	45.7	1.35
6	MC6	12.1	0.59	697.0	-0.37	335.4	0.68	66.2	0.43	10.2	-0.24	57.2	2.05
7	MC7	11.5	0.52	810.4	-0.27	306.8	0.54	63.4	0.38	3.5	-0.74	28.6	0.53
8	MC8	9.1	0.16	697.2	-0.39	277.0	0.35	62.8	0.32	6.9	-0.50	23.0	0.19
9	MC9	6.9	0.04	600.8	-0.38	309.0	0.78	44.9	0.12	5.6	-0.52	18.1	0.11
10	MC10	5.1	0.61	336.3	-0.27	118.5	0.42	19.9	0.03	-0.6	0.00	33.8	3.33
11	MC11	15.9	0.64	863.8	-0.39	480.4	0.88	90.9	0.54	10.7	-0.38	19.0	-0.20
12	MC12	12.4	0.53	646.0	-0.45	379.8	0.79	76.7	0.56	17.6	0.23	31.3	0.57
13	MC13	9.1	0.39	621.7	-0.35	257.3	0.50	57.5	0.45	14.6	0.26	94.6	4.88
14	MC14	8.4	0.15	774.4	-0.28	226.3	0.18	50.4	0.13	9.3	-0.28	38.5	1.13
15	MC15	8.2	0.12	789.0	-0.26	225.0	0.17	50.1	0.13	11.2	-0.13	28.7	0.59
16	MC16	9.1	0.27	691.7	-0.34	228.7	0.21	51.9	0.19	9.7	-0.24	36.5	1.06
17	MC17	11.4	0.51	759.5	-0.31	313.4	0.58	65.0	0.42	9.5	-0.29	47.1	1.54
18	MC18	9.8	0.33	779.5	-0.28	256.1	0.32	54.0	0.21	7.3	-0.44	37.3	1.05
19	MC19	11.1	0.42	831.8	-0.27	289.4	0.41	68.1	0.44	16.5	0.20	52.1	1.71
20	MC20	10.4	0.43	739.4	-0.30	258.7	0.35	57.4	0.30	15.5	0.20	38.6	1.51
21	MC21	11.3	0.48	769.2	-0.31	298.1	0.48	67.0	0.44	7.6	-0.44	61.2	2.25
22	MC22	11.6	0.49	787.0	-0.31	300.4	0.47	64.1	0.36	11.6	-0.16	52.2	1.72
23	MC23	10.2	0.32	768.5	-0.32	280.1	0.38	59.4	0.27	8.5	-0.38	40.8	1.14
24	MC24	9.6	0.26	771.5	-0.30	264.7	0.33	57.0	0.24	12.5	-0.07	41.8	1.24
25	MC25	11.5	0.41	850.2	-0.29	297.1	0.39	68.8	0.39	11.1	-0.23	61.7	2.07
26	MC26	9.2	0.20	829.5	-0.26	265.0	0.31	57.7	0.24	12.7	-0.06	37.8	1.00
27	MC27	9.4	0.25	822.7	-0.25	234.7	0.19	60.2	0.32	10.4	-0.22	45.4	1.45
28	MC28	9.3	0.23	747.3	-0.33	247.3	0.24	56.1	0.22	4.7	-0.65	40.2	1.15
29	MC29	11.0	0.40	793.4	-0.31	288.0	0.40	63.7	0.34	8.4	-0.39	62.3	2.23
30	MC30	11.3	0.45	806.0	-0.29	286.3	0.39	66.9	0.41	14.9	0.08	45.4	1.36
31	MC31	10.1	0.37	746.0	-0.30	264.7	0.37	60.1	0.35	5.3	-0.59	47.5	1.62
32	MC32	8.8	0.17	705.2	-0.36	266.2	0.35	57.6	0.26	10.9	-0.18	47.9	1.58
33	MC33	10.4	0.35	658.5	-0.45	236.8	0.19	54.0	0.18	7.7	-0.43	47.6	1.55
34	MC34	8.3	0.08	691.7	-0.38	244.7	0.22	58.3	0.25	6.6	-0.51	49.5	1.62
35	MC35	10.1	0.31	701.3	-0.38	252.0	0.24	60.1	0.28	12.0	-0.12	45.5	1.40
36	MC36	8.7	0.11	833.5	-0.27	206.6	0.00	56.7	0.19	10.3	-0.26	36.4	0.89
37	MC37	9.6	0.21	855.1	-0.26	237.8	0.14	60.8	0.26	9.9	-0.29	39.8	1.04
38	MC38	10.1	0.29	777.8	-0.32	266.7	0.30	58.6	0.24	13.4	-0.03	41.1	1.14
39	MC39	9.3	0.21	741.8	-0.34	276.4	0.37	58.0	0.24	10.3	-0.24	46.1	1.41

29	98.9	0.55	14	0.37	0.0616459	-0.82	73.4547	-0.39	6.8	3.4	0.07
30	96.3	0.51	17	0.67	0.0670182	-0.79	61.1786	-0.49	6.1	5.5	0.73
31	95.5	0.59	11	0.15	0.0795210	-0.75	39.7914	-0.65	6.8	4.3	0.44
32	94.9	0.55	13	0.32	0.0433198	-0.88	37.7098	-0.68	6.8	4.6	0.51
33	84.7	0.37	10	0.00	0.0263879	-1.01	32.8336	-0.72	6.3	3.9	0.05
34	89.8	0.44	8	-0.20	0.0300415	-0.91	35.5811	-0.70	6.2	4.2	0.35
35	89.7	0.43	12	0.19	0.1432520	-0.58	53.7962	-0.55	5.9	3.3	0.05
36	68.2	0.07	10	-0.02	0.4480740	0.32	31.8413	-0.74	5.5	4.0	0.26
37	71.2	0.10	9	-0.13	0.4282110	0.25	35.4104	-0.71	5.8	2.5	-0.22
38	89.2	0.40	15	0.47	0.1513440	-0.56	67.9788	-0.44	5.7	4.0	0.26
39	96.7	0.54	15	0.50	0.0594427	-0.82	41.8221	-0.65	5.6	5.8	0.86
40	86.9	0.41	14	0.42	0.0448526	-0.88	28.5410	-0.76	6.5	2.8	-0.09
41	80.8	0.34	8	-0.17	0.0385667	-0.88	18.3012	-0.85	5.4	2.7	-0.10
42	80.2	0.28	13	0.30	0.0503198	-0.85	15.4808	-0.87	6.9	5.7	0.83
43	103.5	0.60	15	0.45	0.0325963	-0.91	16.7264	-0.86	6.3	3.7	0.15
44	83.6	0.31	14	0.37	0.0235990	-0.94	18.1793	-0.85	5.5	4.5	0.42
45	85.6	0.36	8	-0.20	0.0348897	-0.92	15.2946	-0.87	6.0	3.9	0.25
46	77.7	0.37	13	0.43	0.0995729	-0.67	20.9868	-0.81	4.9	3.8	0.34
47	56.3	0.00	9	0.00	0.2976980	0.00	106.7976	0.00	4.0	2.8	0.00
48	97.1	0.60	16	0.65	0.4658840	0.46	29.4277	-0.74	5.0	3.2	0.06

File DELTATR1 1/ 7/91

row	DELTA_Nb	Y	DELTA_Y	Rb	DELTA_Rb	Zr	DELTA_Zr	Sr	DELTA_Sr	U
1	0.25	8.7	-0.18	124.2	0.04	78.2	0.02	118.8	0.08	1.0
2	0.57	8.8	-0.18	127.0	0.05	82.0	0.05	127.1	0.14	0.3
3	0.43	8.9	-0.19	127.9	0.04	88.6	0.11	132.5	0.16	0.2
4	0.38	8.6	-0.22	124.3	0.00	105.0	0.31	141.6	0.24	0.1
5	0.40	9.9	-0.09	121.9	0.00	81.1	0.03	160.9	0.43	1.1
6	0.18	10.1	-0.04	108.2	-0.08	73.1	-0.04	163.7	0.50	0.0
7	0.23	9.2	-0.12	124.4	0.06	78.4	0.03	93.7	-0.14	1.1
8	0.10	8.2	-0.24	124.5	0.03	71.1	-0.09	104.7	-0.07	0.0
9	1.19	7.4	-0.19	97.6	-0.05	88.0	0.33	120.8	0.28	0.0
10	0.47	5.4	0.24	47.8	-0.03	30.8	-0.03	113.9	1.51	0.0
11	0.56	9.9	-0.26	146.9	-0.02	113.0	0.16	49.5	-0.64	0.3
12	0.37	8.8	-0.21	136.9	0.09	83.8	0.04	113.4	-0.02	0.0
13	0.40	6.9	-0.23	114.1	0.13	71.1	0.09	84.3	-0.10	0.0
14	0.13	8.0	-0.21	114.8	0.01	72.3	-0.01	103.1	-0.02	0.0
15	0.06	7.8	-0.22	105.6	-0.07	73.0	0.00	134.5	0.29	0.1
16	0.39	11.8	0.19	100.8	-0.09	73.8	0.03	186.2	0.81	0.6
17	0.44	8.5	-0.18	129.2	0.11	87.3	0.16	136.2	0.26	0.0
18	0.40	8.0	-0.21	113.7	0.00	80.2				

19	0.35	8.2	-0.24	133.8	0.11	81.7	0.05	134.3	0.20	0.0
20	0.21	10.7	0.07	105.5	-0.06	83.1	0.14	180.4	0.73	1.5
21	0.74	8.6	-0.18	125.0	0.06	79.5	0.04	143.0	0.31	0.0
22	0.37	10.4	-0.03	118.7	-0.01	80.2	0.03	133.6	0.20	1.7
23	0.20	9.4	-0.12	120.4	0.01	82.5	0.07	135.3	0.22	0.0
24	0.39	9.2	-0.12	111.6	-0.05	79.1	0.04	142.7	0.31	1.0
25	0.31	8.9	-0.21	137.2	0.09	83.7	0.03	128.8	0.10	0.0
26	0.17	9.3	-0.12	115.9	-0.02	78.9	0.03	148.2	0.35	0.1
27	0.31	8.0	-0.23	104.7	-0.10	74.7	-0.01	133.6	0.24	0.1
28	0.18	8.8	-0.16	116.9	0.00	76.3	0.01	169.3	0.56	0.9
29	0.50	9.2	-0.15	116.1	-0.04	80.4	0.03	151.8	0.36	0.0
30	0.35	8.9	-0.17	132.7	0.10	84.3	0.08	145.2	0.30	0.5
31	0.60	7.2	-0.29	124.9	0.10	80.8	0.10	128.6	0.22	1.6
32	0.56	7.9	-0.24	104.9	-0.10	83.1	0.10	128.1	0.19	0.0
33	0.33	9.8	-0.07	97.5	-0.17	81.5	0.08	133.5	0.23	0.0
34	0.40	8.3	-0.21	117.6	-0.01	78.5	0.03	127.1	0.16	0.4
35	0.32	9.0	-0.15	123.1	0.03	79.2	0.03	135.7	0.23	0.0
36	0.25	7.1	-0.34	105.5	-0.13	77.0	-0.02	130.6	0.17	0.3
37	0.26	7.3	-0.33	109.2	-0.11	85.8	0.08	148.8	0.31	0.0
38	0.11	8.7	-0.19	118.3	-0.02	82.8	0.06	148.7	0.33	0.2
39	0.26	8.7	-0.18	106.8	-0.10	91.9	0.20	141.8	0.29	0.4
40	0.48	9.3	-0.11	103.7	-0.11	83.5	0.10	147.2	0.36	0.2
41	0.26	7.9	-0.22	101.9	-0.11	77.2	0.04	146.5	0.38	0.3
42	0.55	8.3	-0.21	108.6	-0.08	91.5	0.19	142.3	0.30	0.0
43	0.37	8.6	-0.21	121.7	-0.01	88.2	0.11	132.2	0.17	0.0
44	0.21	7.1	-0.34	107.0	-0.12	78.9	0.01	139.9	0.25	0.1
45	0.34	8.0	-0.25	116.3	-0.02	84.5	0.10	135.7	0.23	0.9
46	0.21	8.6	-0.10	104.9	-0.03	72.8	0.05	142.0	0.43	0.7
47	0.00	9.5	0.00	106.8	0.00	69.0	0.00	98.7	0.00	0.0
48	0.16	11.6	0.13	108.7	-0.05	76.7	0.03	150.7	0.42	0.9

row	Samno	Sc	DELTA_Sc	Ba	DELTA_Ba	Cr	DELTA_Cr	V	DELTA_V	La	DELTA_La	Zn	DELTA_Zn
1	MC49	9.2	-0.25	1024.5	0.24	281.7	-0.18	60.0	-0.18	11.3	-0.38	23.6	-0.58
2	MC50	7.2	-0.36	980.5	0.29	195.1	-0.38	47.5	-0.29	10.7	-0.36	23.9	-0.54
3	MC51	10.0	-0.21	1158.3	0.36	275.1	-0.22	58.6	-0.22	13.9	-0.26	31.7	-0.45
4	MC52	8.6	-0.32	1471.1	0.73	244.4	-0.31	57.5	-0.23	11.2	-0.40	23.1	-0.60
5	MC53	1.9	1.28	146.9	1.62	41.1	0.77	8.4	0.70	-2.3	0.00	7.3	0.92
6	MC54	4.8	-0.41	1163.2	1.12	178.5	-0.22	32.7	-0.32	8.3	-0.31	24.2	-0.35
7	MC55	9.2	-0.23	1025.8	0.28	274.3	-0.18	60.5	-0.14	15.1	-0.15	63.2	0.16
8	MC56	9.4	-0.19	894.1	0.15	257.3	-0.20	58.0	-0.15	7.8	-0.55	38.6	-0.27
9	MC57	9.7	-0.19	939.0	0.17	233.5	-0.30	52.9	-0.25	12.9	-0.27	26.5	-0.52
10	MC58	10.5	-0.08	863.1	0.13	237.9	-0.25	50.6	-0.25	12.4	-0.27	46.9	-0.10
11	MC59	10.1	-0.17	882.7	0.07	283.1	-0.17	60.4	-0.17	18.7	0.03	41.3	-0.26
12	MC60	12.1	-0.05	898.7	0.05	493.2	0.39	74.0	-0.02	11.9	-0.37	36.4	-0.38
13	MC61	13.2	-0.01	887.1	-0.01	496.2	0.34	86.0	0.09	16.6	-0.16	39.7	-0.35
14	MC62	8.9	-0.25	779.9	-0.02	276.8	-0.16	57.8	-0.17	15.2	-0.13	28.8	-0.47
15	MC63	13.9	0.10	766.0	-0.09	399.8	0.14	79.1	0.06	18.2	-0.02	66.5	0.16
16	MC64	16.8	0.30	790.2	-0.09	472.9	0.32	91.3	0.19	21.0	0.10	65.8	0.12
17	MC65	15.8	0.20	823.4	-0.07	459.2	0.25	88.0	0.13	21.6	0.10	62.1	0.03
18	MC66	12.2	0.00	819.4	0.00	339.6	0.00	72.2	0.00	18.1	0.00	55.7	0.00
19	MC67	12.6	0.00	818.3	0.00	323.5	0.00	65.4	0.00	18.7	0.00	45.1	0.00

row	Ni	DELTA_Ni	Co	DELTA_Co	S	DELTA_S	As	DELTA_As	Nb
1	83.4	-0.30	13.0	-0.32	0.4330790	1.04	50.8459	-0.30	5.1
2	65.6	-0.40	8.0	-0.54	0.4005650	1.06	43.4563	-0.35	3.4
3	79.6	-0.35	10.0	-0.49	0.5877520	1.68	103.5423	0.38	6.0
4	65.7	-0.46	10.0	-0.49	0.5476480	1.51	74.2283	-0.01	4.4
5	10.7	0.33	0.5	-0.62	0.2602900	17.07	403.6568	80.72	0.3
6	53.5	-0.32	13.0	0.02	0.1214870	-0.14	51.3041	0.06	2.4
7	81.9	-0.29	12.0	-0.36	0.2254010	0.09	59.9907	-0.15	4.7
8	87.6	-0.22	12.0	-0.34	0.1394400	-0.30	85.4678	0.25	5.2
9	81.8	-0.29	12.0	-0.36	0.1163700	-0.44	68.2381	-0.04	4.9
10	83.7	-0.24	11.0	-0.38	0.0951575	-0.52	82.9531	0.23	4.4
11	86.8	-0.26	13.0	-0.32	0.1485100	-0.30	70.5775	-0.02	5.6
12	95.1	-0.23	20.0	0.00	0.1966910	-0.11	73.5678	-0.03	9.4
13	97.7	-0.24	22.0	0.06	0.2056470	-0.11	77.8028	-0.02	9.1
14	77.2	-0.32	11.0	-0.40	0.1163370	-0.43	59.0628	-0.16	4.8
15	145.0	0.20	19.0	-0.03	0.3134410	0.44	73.6453	-0.01	6.2
16	154.1	0.24	20.0	-0.01	0.3360880	0.51	83.2430	0.09	7.8
17	163.3	0.28	24.0	0.17	0.3273940	0.44	85.7681	0.10	7.1
18	117.6	0.00	19.0	0.00	0.2105810	0.00	72.2168	0.00	5.6
19	102.9	0.00	17.0	0.00	0.2046060	0.00	57.2278	0.00	4.6

row	DELTA_Nb	Y	DELTA_Y	Rb	DELTA_Rb	Zr	DELTA_Zr	Sr	DELTA_Sr	U	Th	DELTA_Th
1	-0.10	10.9	-0.01	118.1	0.07	87.8	0.11	146.0	0.00	0.8	4.0	4.66
2	-0.34	7.9	-0.22	93.8	-0.07	67.2	-0.07	153.6	0.15	0.0	2.6	0.65
3	0.03	9.6	-0.15	118.8	0.05	87.3	0.07	125.5	-0.17	1.4	4.3	1.43
4	-0.24	10.2	-0.10	111.9	-0.01	81.3	0.00	167.2	0.11	0.0	2.4	0.36
5	-0.22	2.0	1.68	6.2	-0.17	6.4	0.19	48.4	3.89	0.0	0.8	5.88
6	-0.36	5.7	-0.22	69.1	-0.05	53.1	0.01	260.9	1.69	0.6	1.4	0.23
7	-0.14	10.9	0.02	83.1	-0.22	80.3	0.04	171.7	0.21	0.1	3.5	1.10
8	-0.02	9.7	-0.06	98.5	-0.05	78.2	0.05	148.5	0.08	0.4	4.0	1.48
9	-0.11	10.5	-0.02	96.1	-0.10	69.5	-0.10	177.6	0.25	0.0	1.3	-0.22
10	-0.16	10.5	0.03	87.2	-0.14	64.4	-0.32	146.9	0.08	0.0	0.4	-0.75
11	0.00	10.6	-0.03	96.2	-0.12	82.2	0.04	133.1	-0.08	0.0	3.0	0.76
12	0.60	21.5	0.88	108.0	-0.05	155.3	0.89	169.8	0.12	0.6	11.0	5.17
13	0.48	21.6	0.81	118.1	-0.01	150.4	0.75	152.3	-0.04	1.6	11.3	5.07
14	-0.12	9.3	-0.12	80.3	-0.24	89.5	0.18	190.6	0.36	1.9	6.3	2.82
15	0.07	11.2	0.00	119.3	0.06	85.2	0.05	162.1	0.09	1.9	6.1	2.48
16	0.32	14.3	0.24	135.9	0.18	90.4	0.09	107.5	-0.30	1.2	7.0	2.89
17	0.17	15.0	0.27	137.8	0.17	95.2	0.12	127.1	-0.19	0.7	5.6	2.05
18	0.00	10.9	0.00	108.8	0.00	78.5	0.00	144.8	0.00	0.0	1.7	0.00
19	0.00	10.0	0.00	106.2	0.00	81.8	0.00	135.6	0.00	0.4	3.8	0.00